ADAPTIVE FAULT DETECTION AND

CONDITION MONITORING OF

INDUCTION MOTOR

LU WENJING

NATIONAL UNIVERSITY OF SINGAPORE
2011

0

ADAPTIVE FAULT DETECTION AND

CONDITION MONITORING OF

INDUCTION MOTOR

LU WENJING
(B.ENG NUS)

A THESIS SUBMITTED FOR THE DEGREE OF MASTER OF
ENGINEERING
DEPARTMENT OF ELECTRICAL AND COMPUTER
ENGINEERING
NATIONAL UNIVERSITY OF SINGAPORE
2011

Acknowledgment

First of all, I sincerely thank my supervisor, Prof. Chang Che Sau for his patient guidance on me. It has always been his invaluable advice and trust that encouraged me throughout my research. I believe that both the scientific knowledge and the life philosophies that I learnt from Prof. Chang will benefit me for the entire life.

I am deeply grateful to research fellow Dr. Wang Zhaoxiao, for her vital provision of her experiment data and recommendation of readings to further my understanding in the domain of motor fault detection.

I wish to thank Prof. Jirutitijaroen Panida, for her vital recommendation during my final year project of bachelor's degree which forms part of the graduate research.

I am also thankful to my research partner Zhang Yifan with whom the difficulties encountered in research are always been discussed. Moreover, I really appreciate Xiong Peng and Shu Zhen for their generous help in my work. I equally thank my labmates: Zhao Xinjie, Tan Sicong, Quan Hao, Chao Jun for their kind encouragement when I was frustrated, and for the laughter that we have had together.

In addition, I would like to acknowledge the technologist-in-charge of the Power Systems Laboratory, Mr. Seow Hung Cheng, for his assistance.

I felt obliged to thank my best friends, Ye Yan, Jiang Yanwen, my beloved husband Yue Chao and my parents for their encouragement and consolation whenever I feel demoralized.

Finally, thank Lord for sustaining me throughout all the challenges I faced.

Table of Contents

Summary

Condition monitoring and fault diagnosis of induction motor are of great interest for the purpose of improving overall industrial system reliability. Since a few years ago, our project group has been developing various algorithms for fault detection and diagnosis of induction motors. A database containing time-domain measurements of stator currents on three 1-kW laboratory motors (one normal, one with broken bar and one with fault bearing) was created by our group before the candidate's project.

This research is focused upon the investigation of the two specific types of induction motor faults: broken rotor bar fault and bearing fault, which are measured on two laboratory motors. They are also the most frequently occurring faults in industries. The goal of this research is to develop appropriate algorithms for the perspective of on-line detection and diagnosis of these laboratory motor faults.

In the framework of the present thesis, faults occurring on these motors have been studied in details both theoretically and numerically. Although fault-related features can be observed directly on the frequency spectrum derived from time-domain measurements of stator currents, a good feature extraction strategy and quantification method will reduce the human effort and surely improve the reliability and convenience of online fault detection. Hence, the candidate proposes two techniques namely Adaptive Centered Wavelet Technique (ACWT) and Adaptive Wavelet Packet Technique (AWPT) to achieve an adaptive feature extraction for stator currents of motors under different inverter frequencies. The capability of ACWT for reliable detection of broken rotor bar fault under various inverter frequencies is proven numerically robust but is less-convincing in bearing fault detection. In order to improve on the shortcoming of ACWT, AWPT is proposed to narrow down the window size of extraction while maintaining the adaptability for different inverter frequencies. In addition, several statistic indices are studied to quantify the extracted features. It is proposed to employ Shannon entropy's great predictability of fault-related features and its consistent performance, which will make the method a generally accepted index in the present thesis for different inverter frequencies. Finally, the goal of the reliable motor fault detection under various inverter frequencies based on prior knowledge of a few normal operating conditions is achieved by employing both AWPT with Shannon entropy index. A two-dimensional fault detection graph is developed in the end to visualize the results.

List of Figures

List of Tables

List of Symbols

Symbols used in Section 2

ir	Rotor loop currents
ie	Circulating end ring current
Lb	Rotor bar leakage inductance
Le	Rotor end ring leakage inductance
rb	Rotor bar resistance
re	End ring segment resistance
f_s	Inverter frequency
f_{br}	Broken rotor bar characteristic frequency in stator current
f_b	Bearing fault characteristic frequency in stator current
f_v	Bearing fault characteristic frequency in vibration
f_o	Outer race bearing fault characteristic frequency in vibration
f_{in}	Inner race bearing fault characteristic frequency in vibration
f_{ball}	Ball defect bearing fault characteristic frequency in vibration
f_r	Mechanical rotor frequency
s	Per-unit slip
p	Number of poles pairs;
Nb	Number of balls in bearing
Db	Ball diameter
Dc	Pitch or cage diameter
β	Contact angle

Symbols used in Section 3 and 4

$\psi(t)$	Mother wavelet
$\psi_{a,b}(t)$	Wavelet family of scaling parameter a and translation parameter b
$w(t, f_i)$	Morlet wavelet of center frequency f_i

$W(f, f_i)$ Frequency spectrum of morlet wavelet of center frequency f_i

$WT_x(t, f_i)$ Continuous wavelet transform of signal x by $w(t, f_i)$

f_{sample} Sampling frequency

f_{sl} Lowest possible inverter frequency

f_s^* Estimated inverter frequency

M   Mean of absolute value

STD   Standard deviation of absolute value

E   Shannon entropy

$\mathcal{F}$ Wavelet center placement for bearing fault detection

R   Resampling ratio

ccfsH   Coefficients of normal motor after extraction

ccfsB   Coefficients of bearing fault motor after extraction

ccfsBR   Coefficients of broken rotor bar motor after extraction motor

H   Stator current signal of normal motor

B   Stator current signal of bearing fault motor

BR   Stator current signal of broken rotor bar motor

Symbols used in Section 5

$\psi_{j,k}(t)$ Wavelet coefficient at level j, packet k

$\phi_{j,k}(t)$ Scaling coefficients at level j, packet k

g   High-pass filter for wavelet packet decomposition

h   Low-pass filter for wavelet packet decomposition

d_j^p Coefficient at level j packet p, node [j, p]

$\overline{d_j^p}$ Normalized coefficient at level j packet p, node [j, p]

f_R Resampling frequency

α   Slope of $E(\overline{d_8^1})$ against f_s

Chapter 1

Introduction

1.1   Motivation and Objectives

During the last twenty years, condition monitoring and fault diagnosis of induction motor have become a great interest for the purpose of improving overall industrial system reliability [1]. Undetected machine break-down could be avoided to the greatest possible extent since most of the early faults could be detected on-line. Moreover, the more reliable information of machine conditions helps to make a better decision on the issue of maintenance. Excessive inspection and maintenance could be avoided. As a result, the annual cost of machine maintenance could be cut down which brings economic benefits to industries.

Since last year our project group has been developing various algorithms for the fault detection and diagnosis of induction motors. Dr. Wang, a leading researcher in our group, set up the experimental equipment and collected stator currents from three 1-kW laboratory motors (one normal, one with broken bar and one with faulty bearing). A database containing these measurements was created.

This research is focused upon the investigation of two specific types of motor faults namely the broken rotor bar fault and bearing fault, which are the most frequently occurring faults in industries. The goal of this research is to propose appropriate

methods and develop algorithms for the perspective of on-line detection and diagnosis of these two types of laboratory motor faults.

1.2   Earlier Work and Contribution of this Thesis

During the past decade, many methods have been developed in the research area of condition monitoring and fault diagnosis of induction motor [2]-[4]. Various techniques utilized differ from each other in terms of the following four aspects:

1) Choice of measurement signal: The motor condition should be measurable from the motor's vibration signal, stator current signal, acoustic signal, etc. [5]-[9]

2) Choice of motor operating state: There is a choice between motor operating states, either steady state or transient state, during the conduction of measurement.[10]-[12]

3) Choice of feature to be extracted: There exist a few methods which extract the features from signals. They reflect the time domain characteristics or/and the frequency domain characteristics of measured signals.[12]-[14],[16],[18]

4) Classification Criterion: Based on feature properties, various methods, such as Mahalanobis distance, SVM and neural network, are developed to classify features into different groups representing different motor conditions. [16][21]

This thesis will target at online condition monitoring and diagnosis of motor fault by developing a feasible and reliable technique by addressing the following issues for real-case applications:

1) whether the technique is generally applicable to motors under various operating conditions, including different inverter frequency , different load condition and different installation;

2) whether the faulty condition in local environment needs to be known a prior by the diagnosis system for the subsequent stage of motor condition identification;

3) whether there exist some tolerance of this technique to deal with certain degree of errors in measurement; and

4) whether the fault thresholds can be easily built;

Thus, by taking into the above considerations, the stator current of motor is chosen as the measurement signal for the following two reasons. Firstly, the main advantage of stator current signal is that the noise level to the input is less subjective to the environmental conditions as compared to vibration signal and acoustic signal [1]. Hence, the accuracy of fault detection is less affected by noisy external environment which may vary in time in industries. Secondly, the measurement of stator current is easy to be implemented for an online system. The feasibility study of detecting motor fault via stator current is presented in details in [5]-[6].

In terms of feature extraction, the wavelet transform (WT) is used in this thesis as a preprocessor to extract the signal feature in the time-frequency domain. Fault detection based on motor current relies on interpretation of the frequency components that are related to rotor or bearing asymmetries [1]. Thus, many studies use Fourier transform as a preprocessor to directly represent those components in the frequency

domain [7], [12]-[14]. However, stator currents measured from industrial motors are best modeled as a non-stationary signal or piece-wise stationary signal because of its dependency on electric supply, static and dynamic load conditions, noise and fault conditions which are subject to time variation [2]. Fourier transform (FT) is not appropriate to be used to analyze a signal that has a transitory characteristic such as drifts, abrupt changes, and frequency trends [15]. Its weakness and the practical disadvantage of frequency method in analyzing non-stationary or transient signals are discussed in [16]. Hence, compared with the frequency domain analysis by FFT, the time-frequency analysis is more appropriate for online motor condition monitoring and fault detection system. Among the time-frequency analysis techniques, wavelet transform (WT) becomes more and more popular for its better time and frequency resolution property as compared with short Fourier transform (SFT) [2]. Wavelet transform is further divided into three types: Continuous Wavelet Transform (CWT), Discrete Wavelet Transform (DWT) and Wavelet Packet Decomposition (WPD). Each of them has its pros and cons in signal processing [17]. The proposed techniques in this thesis make use of CWT and WPD.

So far, many methods based on wavelet transform as a preprocessor for motor fault detection have been explored, such as [18]-[22]. These techniques all reveal the capability of multiple resolution representation and the applicability to non-stationary signals of wavelet transform. However, a generally applicable method still remains as a challenge for fault detection under various operating conditions because of the

dependency of motor fault feature on the operating condition. Most of the papers limit their scopes to specific motor fault detection under one constant operating condition such as a constant inverter frequency. Some other papers intend to achieve a more general application by building a neural network to recognize various operating conditions [21]-[22]. The main disadvantage of using neural network is the strong dependency of detection accuracy on the training data. In the case of not trained normal operating condition in subsequent testing stage, the false warning may occur. In addition, like other blind separation methods, neural network also gives a blind separation of different conditions. Thus, only when the specific motor fault in local condition is encountered in training stage and used as a benchmark in testing stage, the test motor condition revealed by subsequent signal can be identified by its feature location to the benchmarks of the predefined conditions. In online application, where various factors affect stator current, it is not possible to simulate all normal operating conditions as well as all faulty conditions. Thus, the fault type is usually unable to be addressed by neural network and a false warning is likely to occur. Hence, a reliable detection technique is needed for the online condition monitoring and fault detection of motor with limited prior knowledge of normal operating conditions and applicable to motor under various operating modes.

Therefore, new techniques have been proposed in the present thesis for more reliable motor condition monitoring and fault detection. These techniques take into consideration of motors running under various inverter frequencies. They only require

prior knowledge of local normal operating conditions to achieve specific fault detection. The first method is named Adaptive Centered Wavelet Technique (ACWT) which uses CWT to detect motor faults. Based on the numerical result, this method shows its capability in detecting broken rotor bar fault. However, it also reveals the weakness in detecting bearing fault. In order to improve on the shortcoming of ACWT, Adaptive Wavelet Packet Technique (AWPT) is proposed to narrow down the window size of feature extraction while maintaining the adaptability for different inverter frequencies. In addition, several statistic indices are studied to quantify the extracted features and build the threshold for motor condition classification. Shannon entropy's predictability of fault-related features and its consistent performance in the case of different inverter frequencies make it a generally accepted index in the present thesis. Finally, the goal of reliable motor fault detection under various inverter frequencies based on prior knowledge of local normal operating conditions is achieved by combining AWPT with Shannon entropy index.

1.3   Background Information

In Power System laboratory, there are three motors of the same design (3 phase, 4 pole, 1.1kw). The structure of the laboratory motor is shown in Figure 1.On these three motors we are able to create two different motor faults and keep one unchanged as a reference of motor's healthy condition in the local environment. Hence, three motors of different conditions: one normal, one with broken rotor bar and one with faulty bearing

are prepared for experiment.
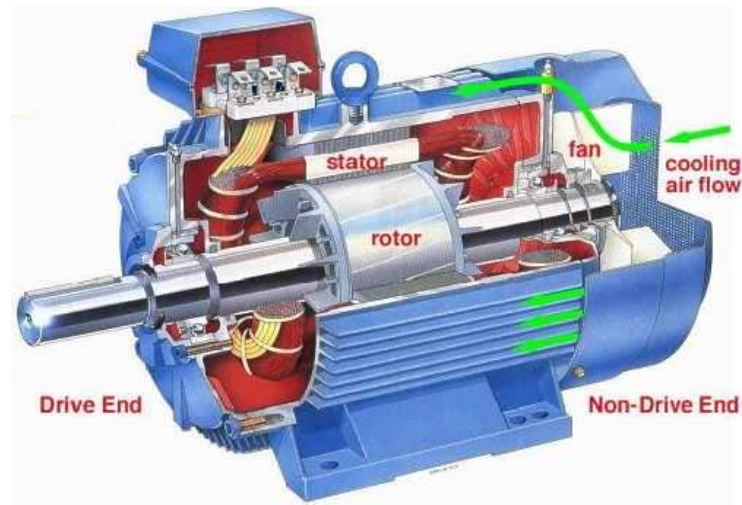
Figure 1 Motor structure

The broken rotor bar fault is one of the most common electrical faults of industrial motors and certainly worth looking at. Hence, it is realized on a laboratory motor by drilling a hole on one rotor bar.

Bearing faults are the primary cause of three phase induction motor failure. In the scope of this study, only localized bearing fault is concerned. It is realized by a man-made dent on one side shield of the bearing.
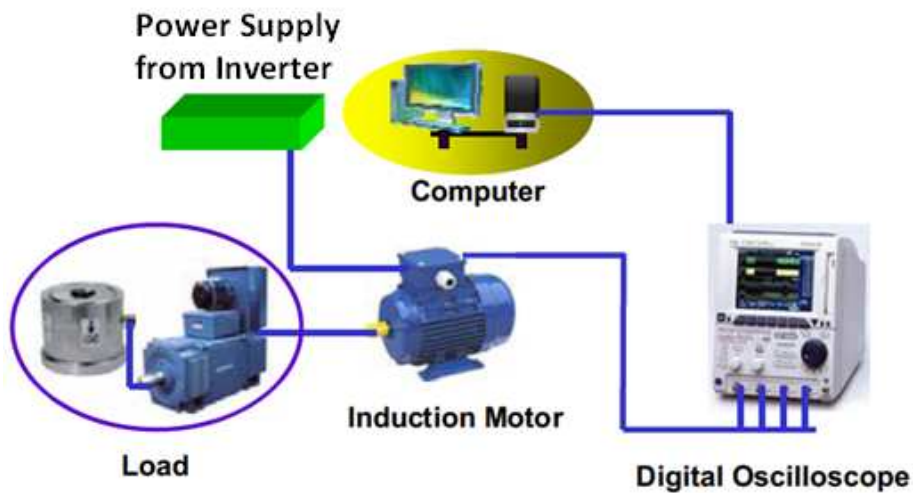
Figure 2 Experiment setup

After the preparation of the laboratory motors, the experiment is set up as shown in Figure 2. The induction motor is connected with a DC generator which acts as a load in this system. The load is set to be 41% loading from the rating motor throughout the experiment. The formula is provided in Appendix A. The intension of using a light load here is to increase the difficulty of fault detection because generally the effect of motor fault on the system becomes more pronounced when the load is heavier. A three phase inverter, which powers up the motor, is connected to the motor stator. Based on the experimental setting, the output inverter frequency is adjustable at six different levels which are 20, 25, 31.5, 37.5, 43.5 and 50 Hz. Hence there are six different operating conditions available for each motor.

During the experiment, the stator current data is collected under steady state operation of a motor. The signal is sampled by an oscilloscope at a frequency of 50 kHz and sent to computer. Each measurement lasts 20.04s hence every set of collected stator

current data consists of 1002000 sampling points. Five sets of measurement of one phase stator current are carried out for each operating condition. Meanwhile, the rotor speed is recorded for each operating condition. The details of the experiment are shown in Appendix A.

1.4   Thesis Organization

The rest of the present thesis is organized as follows. In Chapter 2, the nature of broken rotor bar fault and bearing fault, and their current signature analysis are studied. After the introduction of general concepts of these two faults, the two cases of faults: broken rotor bar fault and bearing fault on laboratory motors are examined and some predictions on the specific fault related features in stator current are made based on the theoretical study. Chapter 3 presents the first method ACWT with its application on broken rotor bar detection. Three indices, STD index, R index and Shannon entropy index, are used to quantify the information. The ACWT capability of reliable detection of broken rotor bar fault under various operating conditions is demonstrated. On top of the success of ACWT on broken rotor bar fault detection, ACWT is further extended for bearing fault detection in Chapter 4. Unlike the previous success, ACWT reveals its weakness in bearing fault detection. Two reasons are addressed for this result. The fault feature of bearing fault generated in our laboratory motor only shows the appearance of some characteristic frequencies instead of all as predicted in the theoretical study in Chapter 2. In addition, the window size of feature extraction in AWCT for bearing fault

detection is too large to focus only on the determined fault-related feature and exclude other disturbances. Thus, although the Shannon entropy agrees with the prediction and STD agrees with other researchers' experimental results, the application of AWCT is less convincing on bearing fault detection. In order to make an improvement, another method named AWPT is proposed in Chapter 5 to narrow down the window size while maintaining the adaptability in various inverter frequencies. In this chapter, the goal of fault detection under various operating modes based on prior knowledge of local normal operating conditions is achieved. Chapter 6 concludes the present work completed and proposes further work by extending the application of AWPT for more types of motor faults and local conditions.

Chapter 2

Motor Faults and Current Signature Analysis

Motor Current Signature Analysis (MCSA) represents a group of methods for motor fault detection based on analyzing the effect of motor fault on stator current [6]. Motor fault adds extra frequency components to stator current under operation. The specific locations of these frequencies are determined by operating mode, fault mode and physical construction of motor. Thus, the stator current can be used as an information source to estimate the motor condition. In this chapter, the general concepts of broken rotor bar fault and bearing fault are discussed. Their effects on stator current are illustrated. Based on the experimental setup, predictions of fault-related information in the local environment are made for these two cases.

2.1 Broken Rotor Bar Fault

2.1.1 General Concepts

Rotor faults (such as broken or cracked rotor bars and end rings), which all bring about a rotor asymmetry, give rise to fault specific patterns in electrical electromagnetic and mechanical quantities. Broken rotor bar as an electrical fault can be represented as an asymmetry circuit as below:
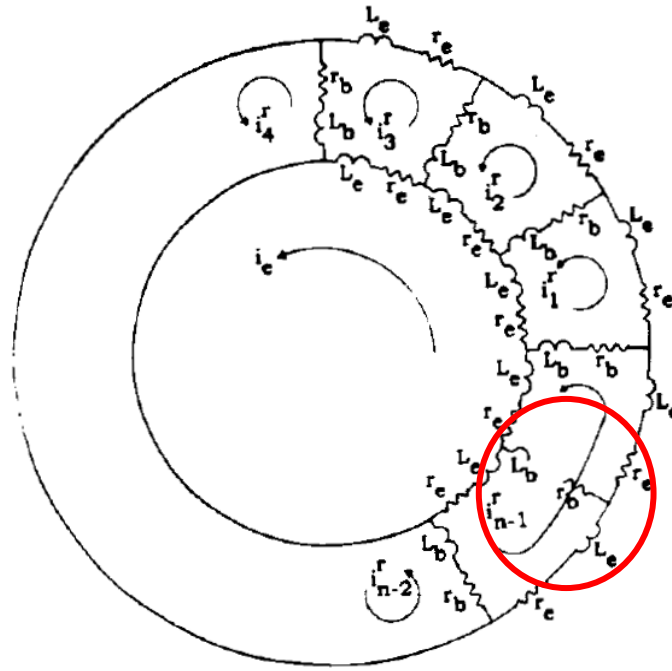
Figure 3 Electrically equivalent circuit of broken rotor bar

Where

i^r rotor loop currents

i_e circulating end ring current

L_b rotor bar leakage inductance

L_e rotor end ring leakage inductance

r_b rotor bar resistance

r_e end ring segment resistance

As can be seen in Figure 3, broken rotor bar results in the change of electrical circuit. It can be detected by monitoring the motor current frequency components produced by the magnetic field anomaly induced by the broken rotor bars [1]-[3]. These specific frequencies of interest are given in equation (1) by Kliman *et al.*[6]

$$f_{br} = f_s \times \left[k \left(\frac{1-s}{p} \right) \pm s \right] \quad (1)$$

where

f_{br} broken rotor bar characteristic frequencies

f_s inverter frequency;

s   per-unit slip;

p   number of poles pairs;

k   = 1, 2, 3,...;

Due to the normal winding configuration, we have k/p = 1,3,5... for the detectable f_{br} [6].

Two prominent characteristic frequencies (sideband frequencies) in the stator current are identified from a broken rotor bar by Kliman *et al.*[6] and Filippetti *et al.*[23]. They are located on the two sides of the inverter frequency f_s. The amplitude of left sideband frequency component $f_s(1 - 2s)$ is a special case of f_b when k/p =1 (1). It is proportional to the number of broken rotor bars [1]. The more rotor bars are broken the more significant the characteristic frequency is. The right sideband component $f_s(1 + 2s)$ is due to consequent speed oscillation and could also be used in monitoring fault severity. Its importance is clearly demonstrated in [23]. Some experimental studies suggest that when the amplitude of these characteristic frequencies is within 50dB smaller than the fundamental frequency component amplitude, the rotor should be considered unhealthy [24]. Thus, extracting the information on these two main components is usually sufficient to differentiate

broken rotor bar motor from other motors conditions such as the healthy motor and the motor with faulty bearing.

In this study, the analysis is limited for the motors of the same model and with a light load. Thus, the slip value is estimated in training stage using healthy motor and assumed to remain fairly constant in subsequent testing stage for all three motors.

2.1.2 Laboratory Model
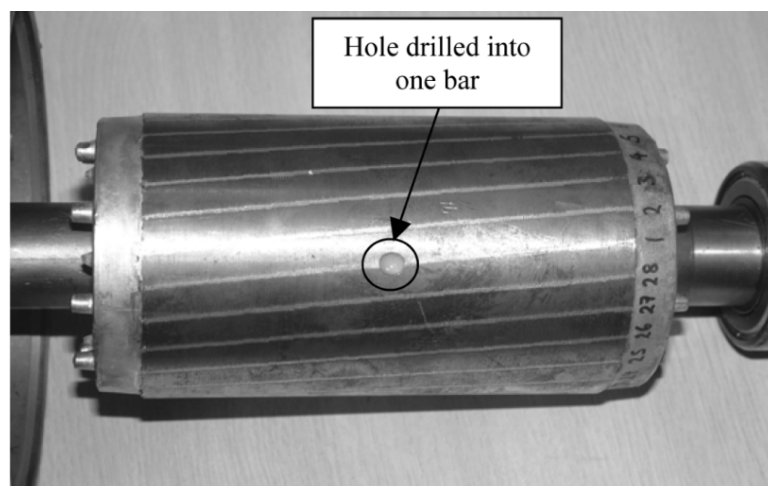
Figure 4 Broken rotor bar fault

In our experiment, the broken rotor fault is made by drilling a hole into one rotor bar as shown in Figure 4. Based on the experimental measurement, slip s is measured to be 0.026 in local condition. Hence, the two prominent characteristic frequencies of broken rotor bar fault $f_s(1 \pm 2s)$ at different inverter frequencies are shown in Table 1.

$f_{br(Hz)}$ ⟍ $f_{s(Hz)}$	20	25	31.5	37.5	43.5	50
$f_s(1-2s)$	18.96	23.70	29.86	35.55	41.24	47.40
$f_s(1+2s)$	21.04	26.30	33.14	39.45	45.76	52.60

Table 1 Broken rotor bar characteristic frequencies

2.2 Bearing Fault

2.2.1 General Concepts

Bearing faults are the most frequent faults in induction motors (41%) according to an IEEE motor reliability study for large motors [25]. Bearing faults can be categorized into distributed and localized faults [5]. Distributed faults, such as general roughness, influence the whole region and cannot be characterized by distinct frequencies. In contrast, single point defects are localized and have corresponding characteristic frequencies. They can be further classified according to the following affected element:

- Outer raceway defect

- Inner raceway defect

- Ball defect

A single point defect could be imagined as a missing piece of material on the corresponding element, such as a small hole, a pit, or a local deformation of the element, such as a dent.

In fact, f_v represents the periodicity by which an anomaly appears due to the

existence of defect. For example a hole on the outer raceway, as the rolling elements move over the defect, they are regularly in contact with the hole and produce an effect on the machine at a given frequency. f_v is a function of the bearing geometry and the mechanical rotor frequency f_r, whose detailed calculation is found in [5]. f_v for different localized bearing fault is given in (2)-(4). 错误！未找到引用源。 gives a graphical illustration of general bearing structure.

Outer raceway:
$$f_o = \frac{N_b}{2} f_r \left(1 - \frac{D_b}{D_c} \cos \beta \right) \tag{2}$$

Inner raceway:
$$f_{in} = \frac{N_b}{2} f_r \left(1 + \frac{D_b}{D_c} \cos \beta \right) \tag{3}$$

Ball
$$f_{ball} = \frac{D_c}{D_b} f_r \left(1 - \frac{D_b^2}{D_c^2} \cos^2 \beta \right) \tag{4}$$

where

N_b number of balls

D_b ball diameter

D_c pitch or cage diameter

β contact angle
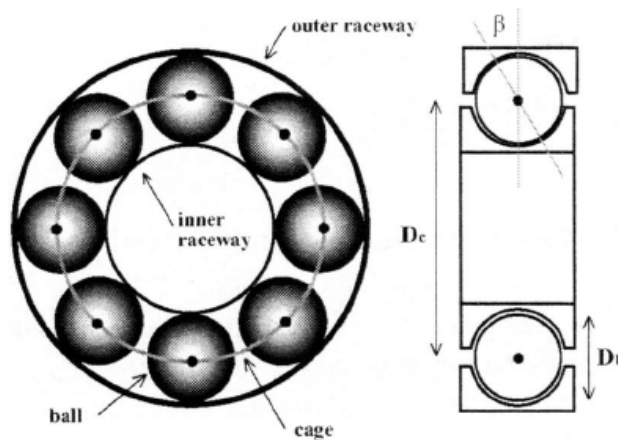
Figure 5 Bearing structure

16

These characteristic frequencies f_v can be further approximated for most bearings with 6 to 12 balls by (5) and (6)

$$f_o = 0.4 N_b f_r \tag{5}$$

$$f_{in} = 0.6 N_b f_r \tag{6}$$

The effect of bearing defect on the induction motor's stator current was firstly proposed by Schoen [5], who considered the generation of rotating eccentricities at frequency f_v. Mechanical vibrations caused by the bearing defect result in air gap eccentricity and oscillations in the air gap length. The latter in turn cause variations in flux density. Variations in flux density affect machine inductances, which produce sideband components of the fundamental frequency of stator current. Hence, two series of additional frequencies f_b are introduced in stator current

$$f_b = |f_s \pm k f_v| \tag{7}$$

where

k   = 1, 2, 3,…;

This model is widely applied in later work. However, it only includes the physical effect of radial movement of the rotor center caused by bearing defect. A recent work [26] takes into the consideration of the second physical effect of bearing defect, which is the load torque variation caused by bearing fault when the defect comes into contact with another bearing element. For example, each time a bearing ball passes by a hole of outer race, a mechanical resistance will appear when the ball tries to leave the hole. The consequence is a small increase of the load torque at each contact between the defect

and another bearing element. Load torque variations principally lead to phase modulations at f_v of the stator current fundamental frequency f_s. The phase modulation produces a characteristic signature which is given by the sideband components around fundamentals at $|f_s \pm k f_v|$. The result of the load variation approach coincides with Schoen's conclusion which is based on rotor eccentricity [5].

2.2.2   Laboratory Model

The shield type ball bearings (NTN 6205z) are used in experiment. The artificially damaged bearing is shown in Figure 6 and its structure is depicted in Figure 7. The metal shield plate is affixed to outside ring; inner ring incorporates a V-groove and labyrinth clearance. It has nine balls. In this study, we focus on one type of the single point fault. To realize such a bearing defect, a dent is made on one side shield as shown in Figure 6. The dent introduces a resistance when a bearing ball passes by. It causes the variation of load torque in rotation. The shield is fixed with the outer race. Hence, the frequency of physical contact between the bearings and the defect is as the same as the case of defect on outer race $f_v = f_o$.
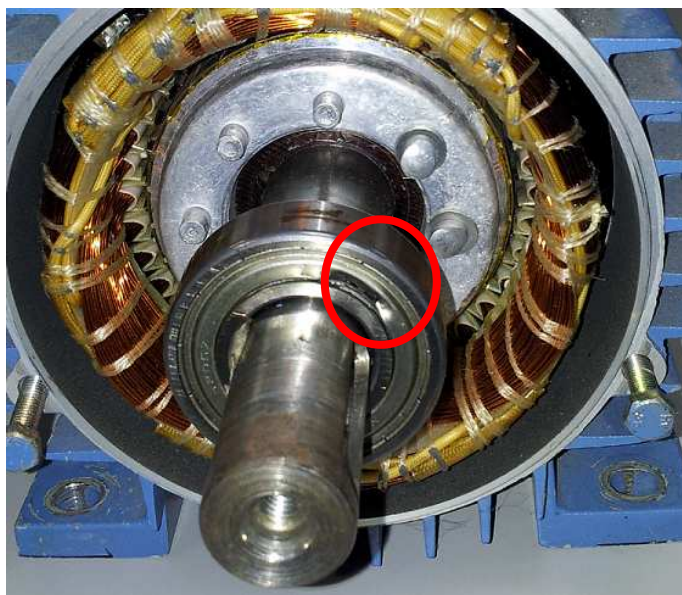
Figure 6 Faulty bearing with manmade dent on shield
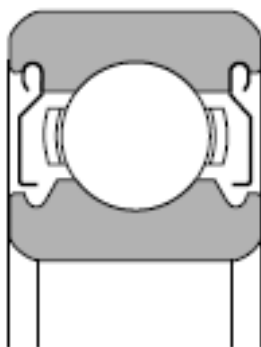
Figure 7 Shield bearing structure

Based on the previous study of bearing fault, the characteristic frequencies f_v in stator current are predicted by the formula (5) with the estimated slip 0.026. The detailed values of its two series of harmonics f_b calculated by the formula (7) are shown in Table 2 and Table 3. The existence of relatively significant components at these harmonics is an evidence for the outer raceway bearing fault.

f_s (Hz)	f_o (Hz)	f_b (Hz)										
		k=1	k=2	k=3	k=4	k=5	k=6	k=7	k=8	k=9	k=10	k=11
20	35.1	15.1	50.1	85.2	120.3	155.3	190.4	225.4	260.5	295.6	330.6	365.7
25	43.8	18.8	62.7	106.5	150.3	194.2	238.0	281.8	325.6	369.5	413.3	457.1
31.5	55.2	23.7	79.0	134.2	189.4	244.6	299.9	355.1	410.3	465.5	520.8	576.0
37.5	65.8	28.2	94.0	159.7	225.5	291.2	357.0	422.7	488.5	554.2	620.0	685.7
43.5	76.3	32.8	109.0	185.3	261.6	337.8	414.1	490.3	566.6	642.9	719.1	795.4
50	87.7	37.7	125.3	213.0	300.6	388.3	476.0	563.6	651.3	738.9	826.6	914.3

Table 2 Outer raceway bearing fault characteristic frequencies $|f_s - kf_o|$

f_s (Hz)	f_o (Hz)	f_b (Hz)										
		k=1	k=2	k=3	k=4	k=5	k=6	k=7	k=8	k=9	k=10	k=11
20	35.1	55.1	90.1	125.2	160.3	195.3	230.4	265.4	300.5	335.6	370.6	405.7
25	43.8	68.8	112.7	156.5	200.3	244.2	288.0	331.8	375.6	419.5	463.3	507.1
31.5	55.2	86.7	142.0	197.2	252.4	307.6	362.9	418.1	473.3	528.5	583.8	639.0
37.5	65.8	103.2	169.0	234.7	300.5	366.2	432.0	497.7	563.5	629.2	695.0	760.7
43.5	76.3	119.8	196.0	272.3	348.6	424.8	501.1	577.3	653.6	729.9	806.1	882.4
50	87.7	137.7	225.3	313.0	400.6	488.3	576.0	663.6	751.3	838.9	926.6	1014.3

Table 3 Outer raceway bearing fault characteristic frequencies $|f_s + kf_o|$

Chapter 3

Adaptive Centered Wavelet Technique for Broken Rotor Bar Detection

Adaptive Centered Wavelet Technique (ACWT) is proposed in this chapter to detect broken rotor bar fault. The methodology is developed in Section 4.1 followed by the result and discussion in Section 4.2. The methodology begins with the explanation of principal idea and the main procedures. The basic wavelet transform concept is briefly introduced and the proposed adaptive wavelet design for our experiment is illustrated. The main steps, such as inverter frequency estimation, feature extraction and feature evaluation, are explained separately. In Section 4.2, the performance of adaptive wavelet is firstly verified by experimental result and the feasibility of inverter frequency estimation is proven. The evaluation of extracted feature is conducted by the direct observation in time domain, the histogram observation and the quantification by statistic indices. It should be noted that all algorithms used in this thesis are carried out in time domain although many frequency spectrum graphs are used here to help readers understand the operations. At the end of Section 4.2, a comparison is made between ACWT and Short-Fourier Transform based algorithm [16] in order to justify the better performance of ACWT in the feature extraction stage.

3.1 Methodology

The key idea in the proposed method is to capture the time variation of a specific narrow frequency band where fault-related frequency components may reside and to analyze it statistically in order to distinguish the motor with broken rotor bar fault from the healthy motor and the faulty bearing motor under various inverter frequencies. Since the stator current of motor is affected by the connected power system, load condition and motor geometry, a supervised approach is developed to recognize the local normal operating conditions of motor priori to actual fault detection.

The proposed approach consists of three stages: training, testing and fault identification as illustrated in Figure 8.
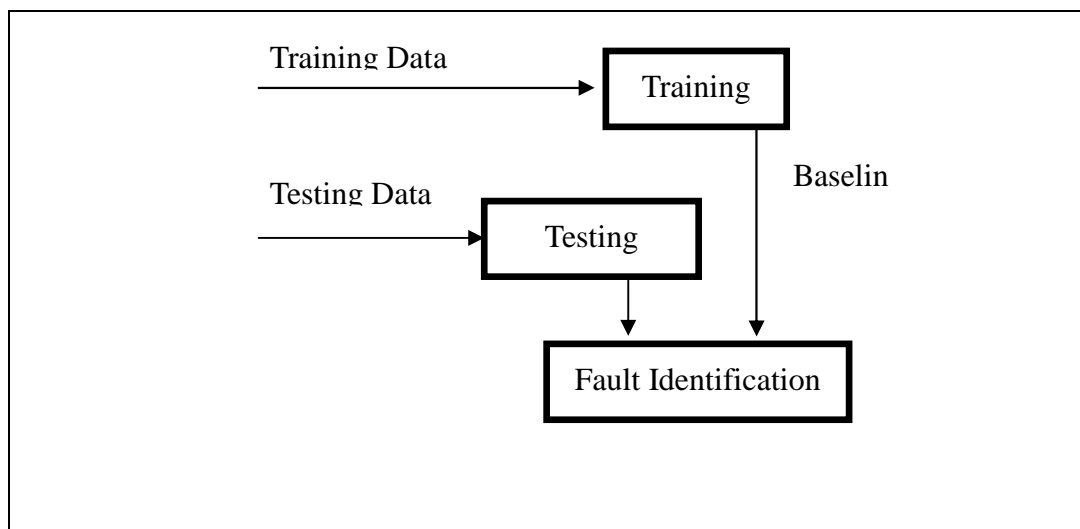

Figure 8 Block diagram of ACWT

During the training stage, shown in Figure 9, the stator current from healthy motor under various operating conditions is measured and processed to form a baseline for detecting broken rotor fault occurring in subsequent stages of motor operation. Since, the fault-related feature, which is outlined in Section 3.1, depends on the inverter

frequency, it is necessary to measure or estimate the inverter frequency. In online application, the motor is subject to various operating conditions. Hence, the estimation or measurement of inverter frequency is conducted periodically to ensure the correct association of measured signal with a specific operating condition. This could prevent false alarm at the switching of operating mode where mismatch may occur. ACWT includes the step of estimation of inverter frequency directly from stator current in order not to enroll excessive measurement facility for the perspective of convenience in online application. Once the inverter frequency is obtained, a specific wavelet function is selected to extract the potential broken rotor bar fault-related feature in this local condition. Later, several indices are proposed to quantify the resulting feature and build a baseline for broken rotor bar fault detection. The training is repeated a number of times and the baseline is built based on several measurements.
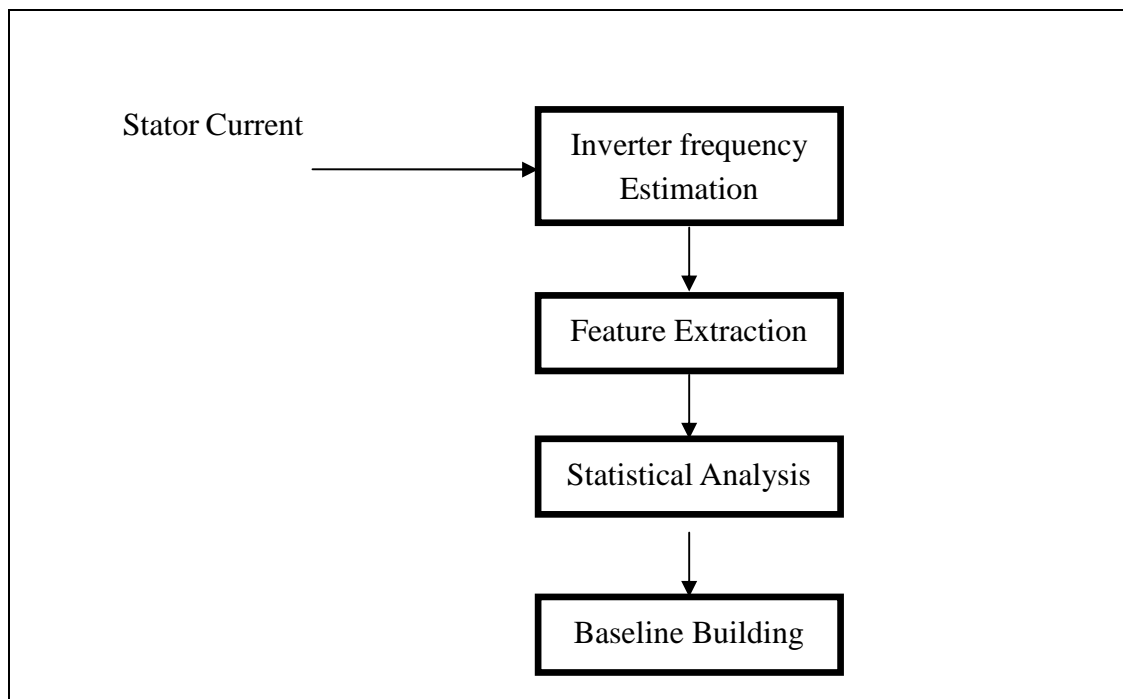

Figure 9 Training Stage of ACWT

During the test stage, shown in Figure 10, the signal's inverter frequency is measured or estimated to determine the operating mode of testing motor. The feature relevant to the broken rotor bar fault in the local condition is extracted and quantified. Next, the distance between the test feature and the baseline is computed. If the test feature is beyond the threshold of baseline at corresponding operating condition, it is tagged as a potential fault signal. Hence, the corresponding testing motor with this feature is diagnosed as a broken rotor bar motor.

Stator Current → Inverter frequency Estimation → Feature Extraction → Statistical Analysis →
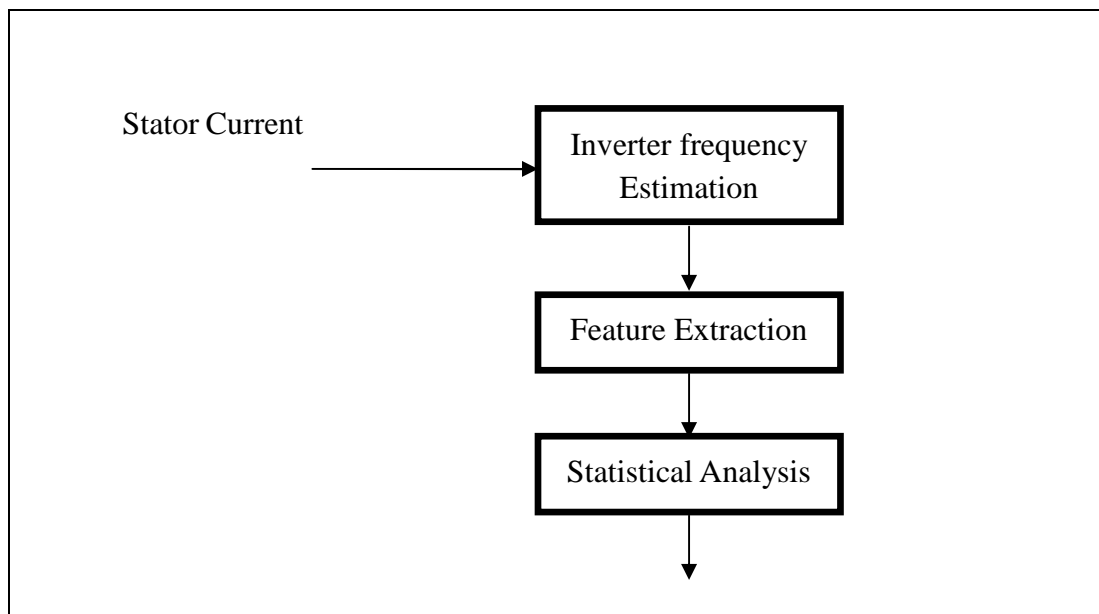
Figure 10 Testing stage of ACWT

3.1.1   Wavelet Transform

Wavelet transform is one of the tools used in time-frequency analysis. In this thesis, it is used to extract the time variation of a specified frequency band where broken rotor bar fault-related feature may reside. One of its inherent advantages is the good time resolution for the high-frequency transients and good frequency resolution for the low-frequency components. Morlet (1982a,b) first introduced the idea of wavelets as a

family of functions constructed from translation and dilation of a single function called the "*mother wavelet*" $\psi(t)$. They are defined by

$$\psi_{a,b}(t) = \frac{1}{\sqrt{|a|}} \psi\left(\frac{t-b}{a}\right), \quad a, b \in \mathbb{R}, a \neq 0, \tag{8}$$

where *a* is called a *scaling parameter* which measures the degree of compression or scale, and *b* a *translation parameter* which determines the time location of the wavelet. If $|a| < 1$, the wavelet is the compressed version (smaller support in time-domain) of the mother wavelet and corresponds mainly to higher frequencies. On the other hand, when $|a| > 1, \psi_{a,b}(t)$ has a larger time-width than $\psi(t)$ and corresponds to lower frequencies. Thus, wavelets have time-widths adapted to their frequencies. This is the main reason for the success of the Morlet wavelets in signal processing and time-frequency signal analysis. It may be noted that the resolution of wavelets at different scales varies in the time and frequency domains as governed by the Heisenberg uncertainty principle. At large scale, the solution is coarse in the time domain and fine in the frequency domain. As the scale *a* decreases, the resolution in the time domain becomes finer while that in frequency domain becomes coarser [17].

3.1.2   Adaptive Wavelet Design

A wavelet is a waveform of effectively limited duration that has an average value of zero. It is a wave-like oscillation with amplitude that starts out at zero, increases, and then decreases back to zero. The Morlet wavelet is chosen to be used for the convenience of center placement. It is a modulated Gaussian, shown in Figure 11.

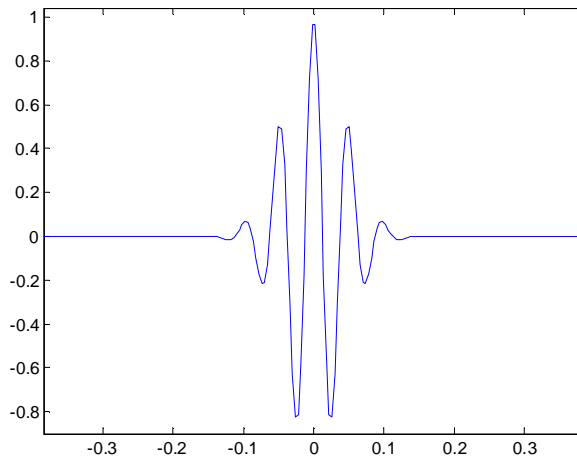Figure 11 Morlet wavelet

It is defined as below:

$$w(t, f_i) = exp\left(-\frac{t^2}{2b_i^2}\right)cos(2\pi f_i t) \tag{9}$$

where

f_i is the center frequency of wavelet

b_i is the standard deviation.

Its Fourier transform is shown below

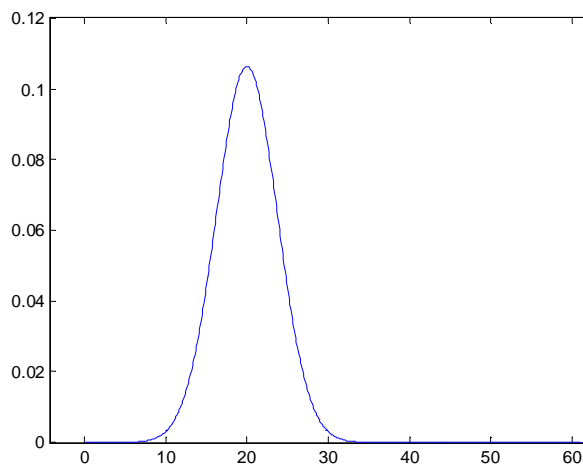$$W(f, fi) = b_i\sqrt{2\pi}exp(-2b_i^2\pi^2(f - f_i)^2) \tag{10}$$

Figure 12 Fourier transform of Morlet wavelet

26

Given a wavelet, the following admissibility should be satisfied:

$$0 < \int_{-\infty}^{+\infty} \frac{|W(f)|^2}{|f|} df < \infty \tag{11}$$

where $W(f)$ is the FT of $w(t)$.

Because $w(t)$ decays with time, the admissibility (8) is equivalent to the requirement $\int_{-\infty}^{+\infty} w(t)\, dt = 0$. Strictly speaking, the Morlet wavelet does not satisfy this zero-mean requirement. However, the mean can become infinitely small if the term f_i is sufficiently large. As f_i increases, the duration of the wavelet expands, and the time resolution will decrease correspondingly. As a result, the relationship between the standard deviation bi and the scaled center frequency f_i is kept as a constant in this thesis, e.g. $2\pi b_i f_i = 5$.

3.1.3   Inverter Frequency Estimation

A motor has finite operating modes. In other words, there are a limited number of inverter frequencies f_s feeding the motor based on the commands. In our experiment the measurement of stator current is conducted at the motors running at inverter frequency f_s determined by operation. In the steady state, the stator current at the inverter frequency f_s takes the majority of signal energy. A Morlet wavelet with center frequency placed at f_s will surely extract most energy from the signal as compared with the wavelets placed elsewhere at the same time. Thus, by placing a set of wavelets over those possible f_s and looking for the one where resides largest energy the inverter frequency of stator current can be estimated. The estimated inverter frequency is

27

denoted as f_s^*.

In this thesis, the wavelet centers are set to be [20 25 31.5 37.5 43.5 50] which covers all possible operating modes of motors in local environment. The Fourier transforms of these wavelets are shown in Figure 13. It is verified that the center frequency of each wavelet has the highest passing amplitude. In other words, a frequency component will be maximally extracted by a wavelet with the center frequency at its position. As can be seen in the figure, the blue dotted arrow and red solid arrow denote the passing amplitudes of 20Hz sinusoidal signal in wavelets centered 20 and 25 respectively. The energy of the feature extracted from this signal is higher by using wavelet centered at 20Hz instead of the one centered at 25Hz. The wavelets further away from 20Hz have decreasing passing amplitude for 20Hz frequency component. Hence, by finding which wavelet extracts the highest energy from stator current, the inverter frequency of the measured stator current can be determined.
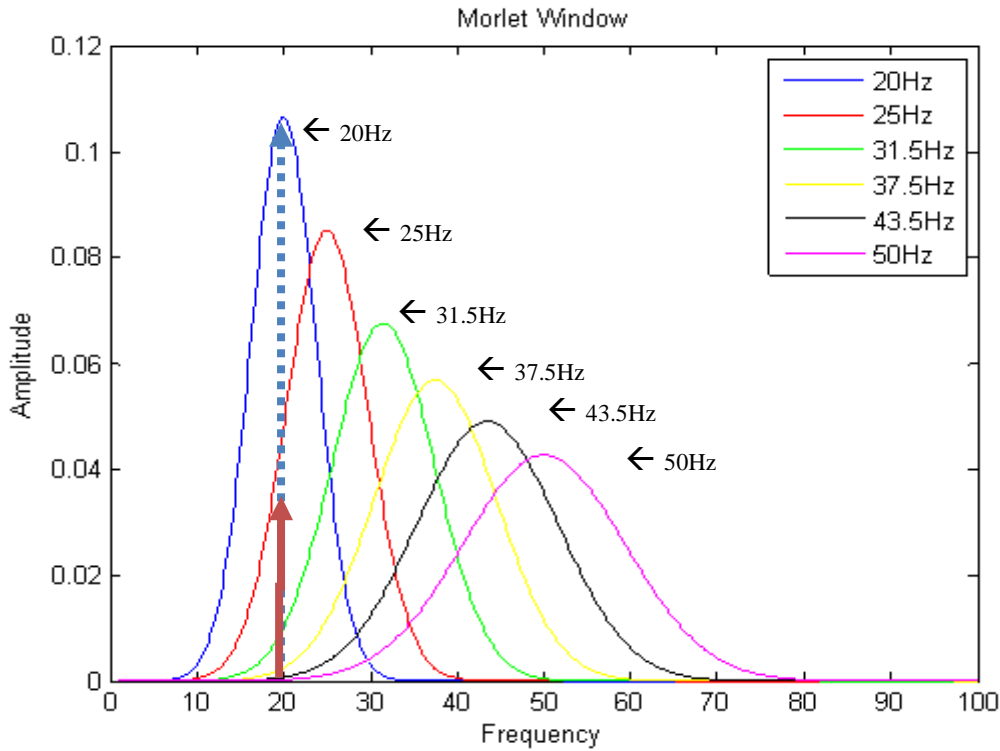
Figure 13 Fourier transforms of wavelets

Since the experiment is conducted on the motors running at the steady state, a small portion of one measurement data is enough to detect the inverter frequency of the measured stator current. In online detection, when motor is subjected to the switching of operating mode at unpredictable time instants, the inverter frequency should be frequently estimated in order to categorize measured data into a right group of a specific operating mode with reference to the corresponding benchmark. In addition, the energy value extracted by each wavelet can be compared with historical data of corresponding operating mode to differentiate the steady state data for ACWT from the transient state data.

In ACWT, the number of observation points of measured signal, which is used for inverter frequency detection, is calculated by the formula in (12):

$$N = f_{sample}/f_{sl} \tag{12}$$

Where

f_{sample} sampling rate,

f_{sl} lowest possible inverter frequency

A new signal is formed by using the first N sample points of the measured signal in order to reduce computational load while cover at least one period of the lowest possible inverter frequency to avoid the bias in the inverter frequency detection stage. In our measurement, each measured signal has 1002000 sampling points and its lowest possible inverter frequency is 20Hz in the scope of this thesis. Hence, N is calculated to be 2500.

The wavelet coefficients extracted from the signal $x(t)$ by the morlet wavelet $w(t, f_i)$ with a center frequency fi are given by the equation (13).

$$WT_x(t, f_i) = \int_{-\infty}^{+\infty} x'(\tau)w(-(t - \tau), f_i)d\tau \tag{13}$$

Where

x(t)   signal to be extracted

w(t,f$_i$)   morlet wavelet at center f_i

In the inverter frequency detection stage, x(t) is the new formed signal which is the first 2500 sampling point of the measured signal.

After obtained the wavelet coefficients of the new signal, its average energy is calculated as follow:

$$energy(f_i) = \frac{1}{L} \sum_{k=1}^{L} |WT_x(t_k, f_i)|^2 \tag{14}$$

Where

L   length of signal WTx

t_k kth sample point

f_i center frequency of wavelet

At last, the estimated inverter frequency f_s^* is determined by following equation

$$f_s^* = max\ (\{fi|energy(f_i)\}) \tag{15}$$

3.1.4   Feature Extraction

The wavelet with its center frequency f_i at estimated inverter frequency f_s^* is further used to extract the feature from the original stator signal. The feature is the wavelet coefficients obtained in the formula (13) by using original stator current signal as x(t). Aim to achieve a more precise analysis of the characteristics of feature, the use of full length original signal, which has 1002000 sampling points, helps to avoid the statistical bias in the extraction.

Figure 14 gives an example of wavelets centered at 25 and 50Hz. As can be seen, the window width and amplitude are automatically adapted to the center frequency. The frequency component located at the center is mostly conserved after extraction. The further the components are away from this center, the more they are discriminated in extraction. The window amplitude decreases to nearly zero for a frequency situated

beyond two times the center frequency. Thus, when it is applied to stator current, only information near inverter frequency is retained after extraction and other components including the harmonics of inverter frequency are excluded. The arrows in Figure 14 denote the magnitude of wavelet at center frequency f_i and sideband frequencies f_i *(1-2s)* and f_i *(1+2s)*. The adaptation of window width automatically takes into account of the increasing distance of characteristic frequencies from center frequency f_i. It allows a relatively constant ratio of extraction at f_i and f_i *(1±2s)* when f_i varies. Thus, it results in a relatively unbiased extraction along different f_i by remaining the proportionality of extraction.
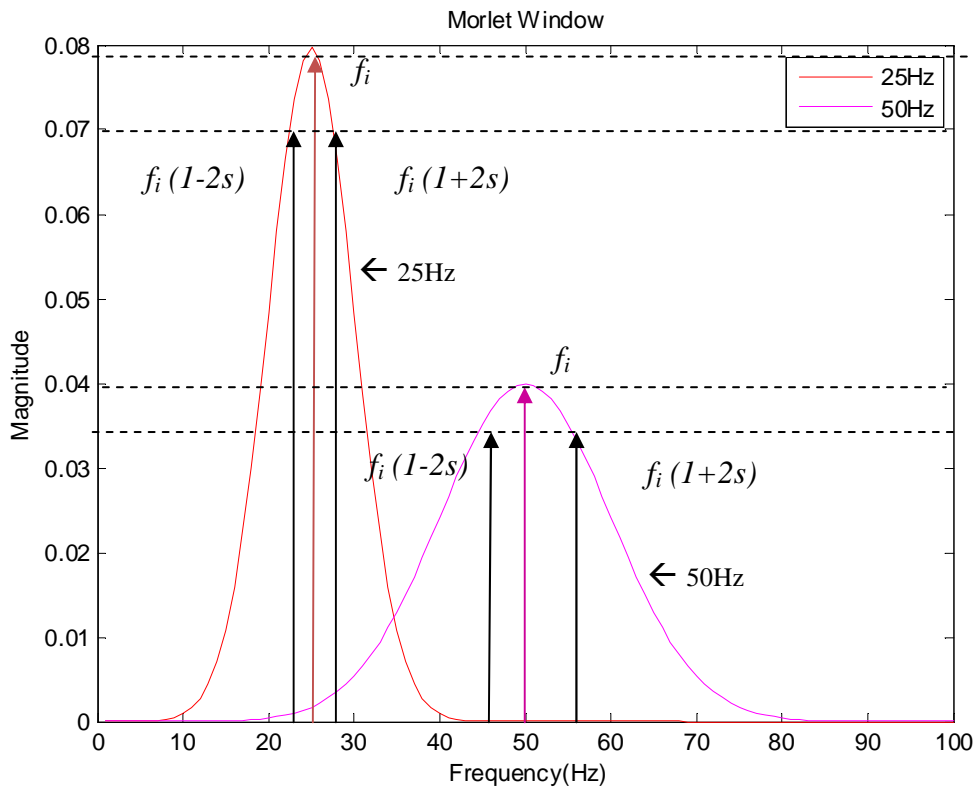

Figure 14 Spectrum of wavelet windows centered at 25 and 50Hz

3.1.5   Feature Evaluation

After the feature extraction, the time variation of the targeted frequency band, named broken rotor bar feature, is obtained, which can be observed in time domain and/or in frequency domain. In this thesis, several statistic indices are studied and compared to quantify the feature which reveals the motor rotor condition.

3.1.5.1   Mean and Standard Deviation Indices

Among various statistic measurements, the mean and standard deviations of absolute value of feature are among the most popular. They are also widely applied in the analysis of stator current [16], [18]-[22]. The equations of mean and standard deviation, denoted M and STD respectively, are given in (16) and (17).

$$M = \frac{1}{L} \sum_{k=1}^{L} |WT_x(t_k, f_s^*)| \tag{16}$$

$$STD(|WT_x|) = \frac{1}{L} \sum_{k=1}^{L} (|WT_x(t_k, f_s^*)| - M)^2 \tag{17}$$

Where

L : total sample points

$WT_x(t_k, f_s^*)$: broken rotor bar feature for operating mode f_s^*

3.1.5.2   Shannon Entropy

Entropy is a common concept in many fields, mainly in signal processing. It is a measure of the degree of uncertainty [27]. Shannon entropy (18), which is developed in [28], is used in this thesis as a statistic measure of feature.

$$E(x) = \sum_i x_i^2 \log x_i^2 \tag{18}$$

Where

xᵢ: ith sample point of signal x.

3.1.6   Fault Identification

After the features of normal operating motor are quantified by the statistic indices (16)-(18), the baseline is built for the comparison with subsequent signals which may be from faulty motors.

In testing stage, the further the STD index and M index of feature are above the baseline, the higher possibility of the presence of broken rotor bar fault [4][13][18]. The STD and M are important measurements of the statistical distribution of data. The higher M value implies wider distribution while higher STD implies heavier tail of distribution. The two prominent broken rotor bar characteristic frequencies $f_s(1 \pm 2s)$ are very close to the inverter frequency and of small amplitudes. They are retained after the feature extraction. These extra frequency components change the data distribution of the feature as compared to the healthy motor case and the bearing fault motor case where only one main inverter frequency is retained after extraction. Those extra frequency components extend the extreme values of the feature and smoothing its distribution by the superimposition effect.

With respect to Shannon entropy index, its lower value below the baseline implies a higher possibility of broken rotor bar fault. The measured stator current usually contains both the frequency components and background random noises. The

frequency components, which are the determined factors in the signal, reduce the randomness of signal. Since entropy is a measure of the degree of uncertainty [27], signals with more determined information are less random and have lower entropy values. The presence of broken fault relevant frequency components are the extra determined information in stator current. In analyzing the broken rotor bar fault, the wavelet extracts the information within a very narrow frequency band around the inverter frequency. The two prominent broken rotor bar relevant frequency components are retained in extracted feature and reduce the feature entropy value as compared with the healthy case. Based on the reasoning above, if the entropy index of a measured feature is smaller than the baseline built by healthy motor, there is a possibility of the presence of broken rotor bar fault.

3.2   Result and Discussion

3.2.1   Centered Wavelet Performance

Figure 15 shows the frequency spectrum observation of the extracted feature and the original stator current of the motor with broken rotor bar fault. As predicted by Section 4.1, the frequency band around inverter frequency is conserved after the feature extraction. The leveling off starts from 30Hz, which is 1.5 times inverter frequency. It is also observed that the broken rotor bar prominent characteristic frequencies are well conserved after feature extraction in a zoom-in version in Figure 16. The capability of

ACWT in extracting broken rotor bar fault feature is verified graphically here.
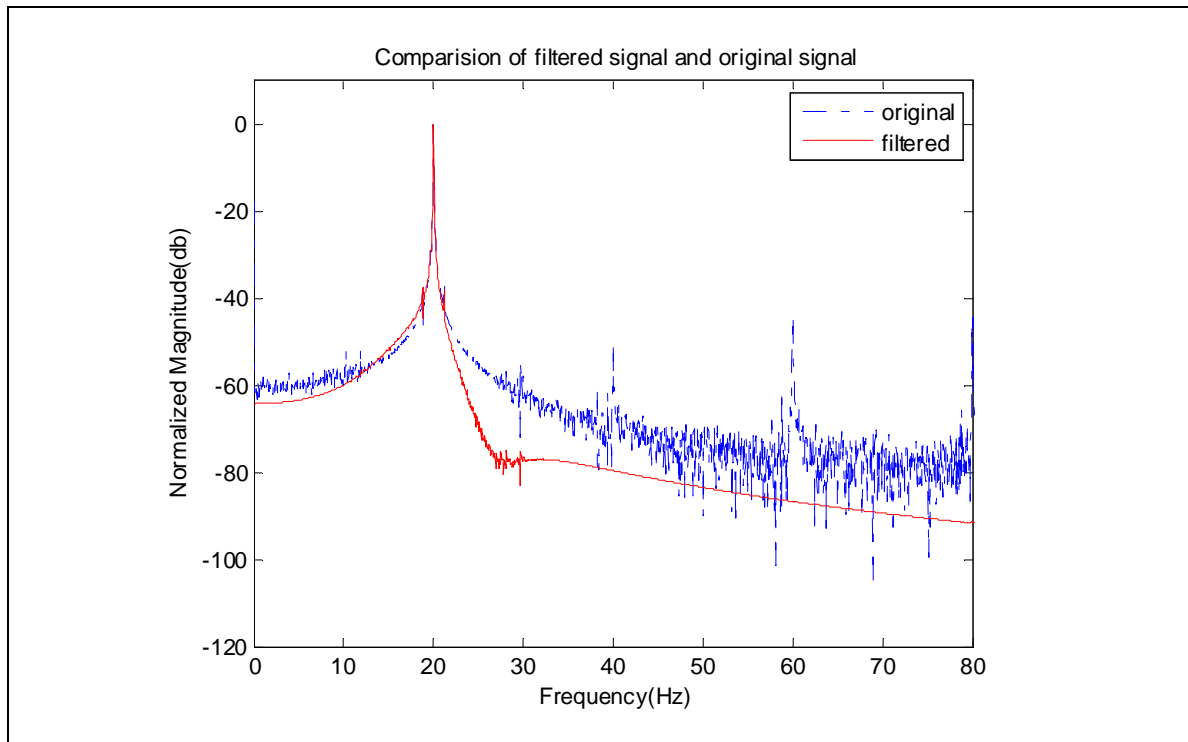

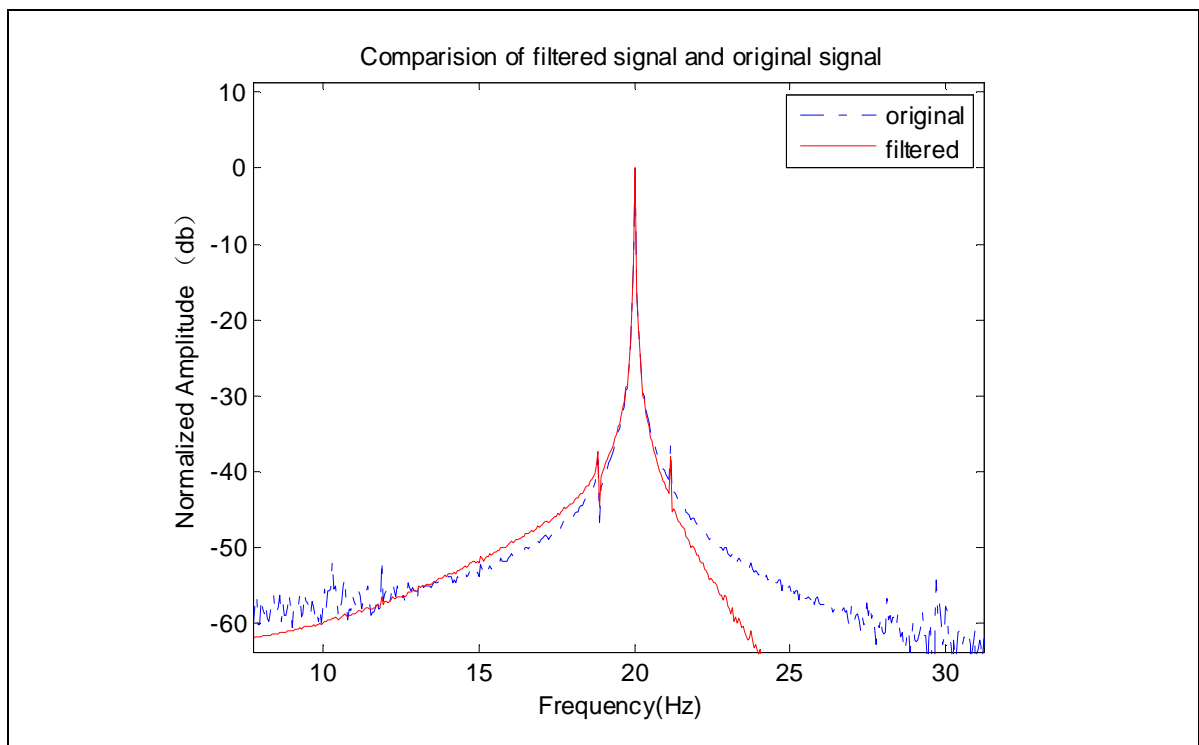Figure 15 Spectrums of feature and original signal

Figure 16 Zoom-in spectrums of feature and original signal

36

3.2.2   Inverter Frequency Estimation

Table 4.1 shows the energy of feature extracted from each normal operating condition by different centered wavelet. As can be seen in the comparison of energy among all wavelets in a specific operating condition, the largest energy is given by the wavelet adapted to the corresponding operating mode. It is proven experimentally the feasibility of the inverter frequency estimation algorithm developed in Section 4.1.

Wavelet Energy Signal \ Wavelet	1	2	3	4	5	6
20Hz	9704.76	1593.23	2.87	0.86	0.88	0.47
25Hz	3402.42	8449.72	1187.94	10.10	0.91	0.51
31.5Hz	287.14	2771.20	7221.85	2439.52	123.81	1.30
37.5Hz	30.55	446.51	3691.23	6482.87	2953.89	274.89
43.5Hz	4.84	70.18	971.43	3952.21	5869.95	2877.86
50Hz	1.19	11.46	190.91	1242.36	3768.04	5258.63

Table 4 Energy of features from healthy motor

3.2.3   Feature Evaluation

3.2.3.1   Direct Observation

Figure 17 and the zoom-in graphs in Figure 18 are examples of stator current signals from three motors at 20Hz inverter frequency: healthy, broken rotor bar and faulty bearing. Through directly observation there is significant noise presented in stator current for all three cases. In addition, the amplitude of stator current from bearing fault motor is smaller than other two cases. Other than this, no specific information of characteristic frequency can be read from them. Hence, no conclusion upon the motor fault can be drawn from direct observation of the original stator current.
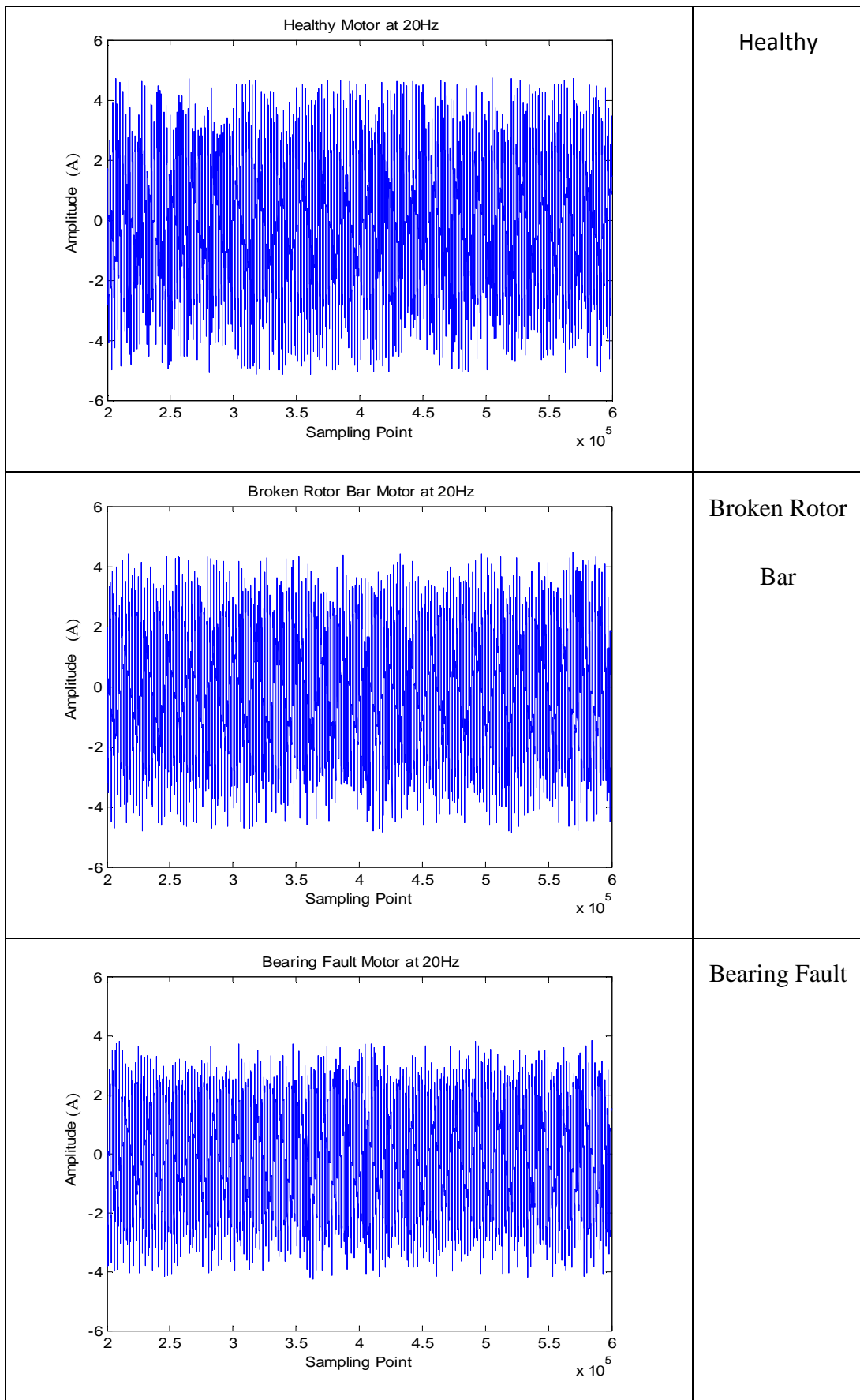
Figure 17 Stator current signals at f_s = 20Hz

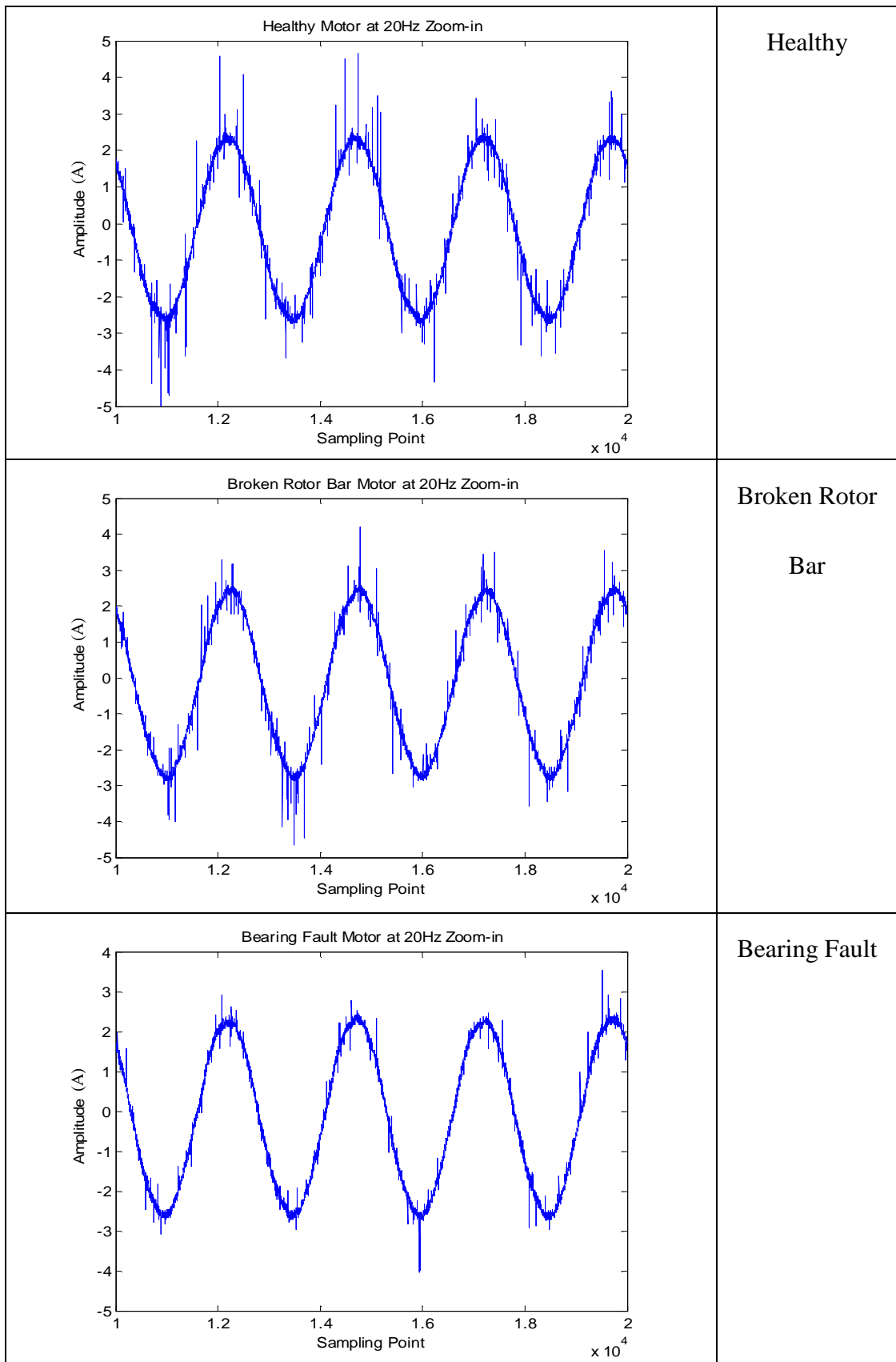|	
	Healthy
	Broken Rotor Bar
	Bearing Fault

Figure 18 Zoom-in stator current signals at f_s = 20Hz

The extracted features from three motors and their zoom-in version are shown in

40

Figure 19 and Figure 20 respectively. By direct observation, it is found that the extracted features have less noise than the original signals because the extraction concentrates only one limited frequency band where resides the inverter frequency as a determined sinusoidal signal component. The frequency components as well as the noise which fall outside the narrow band are automatically filtered out.

It should be noted that there is a difference between the broken rotor bar feature and other two cases. In Figure 19 the edges of feature in broken rotor bar case reflect another periodic characteristic. This may corresponds to the presence of extra frequency components around inverter frequency.
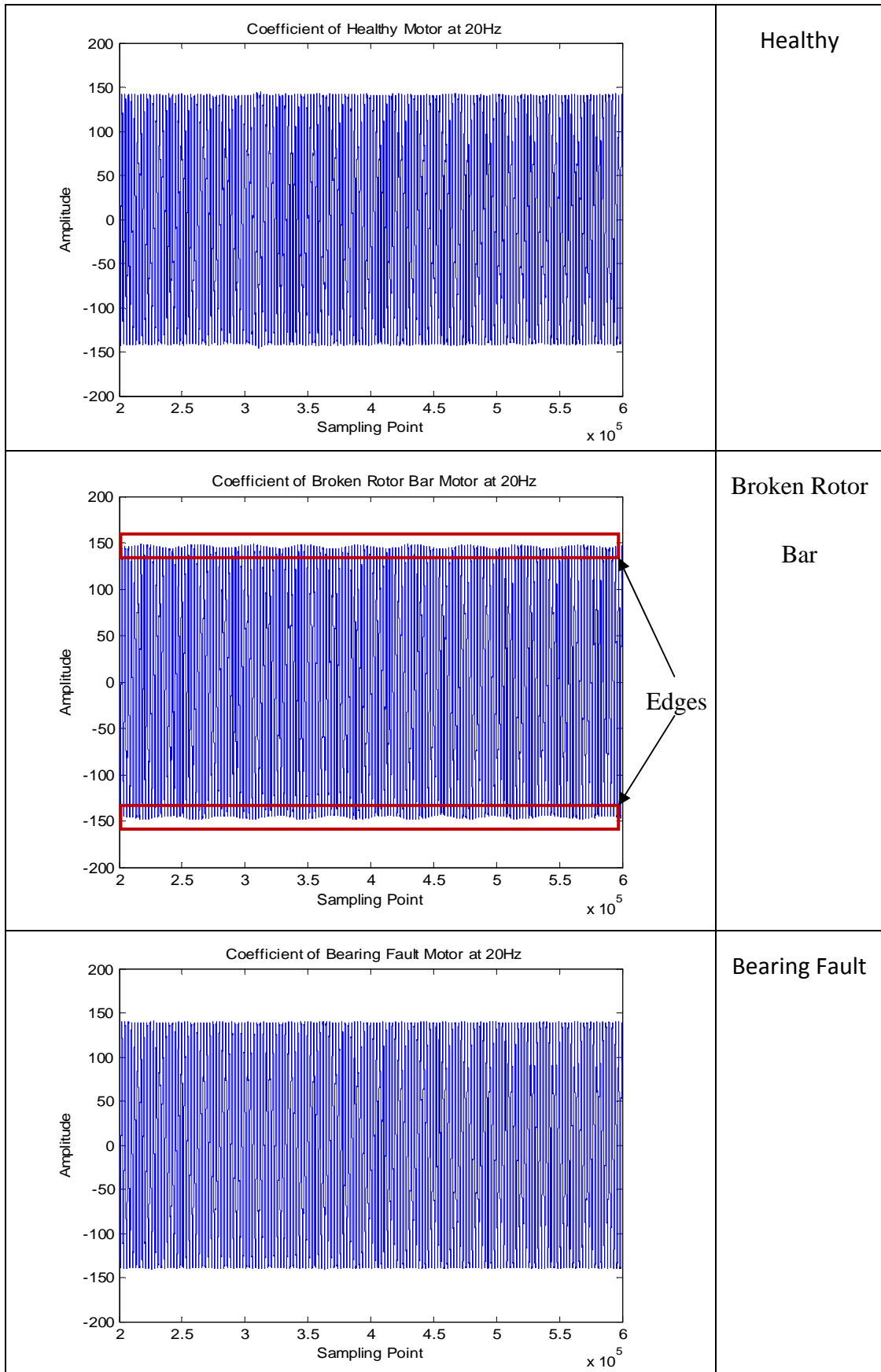
Figure 19 Extracted features from stator currents at f_s = 20Hz

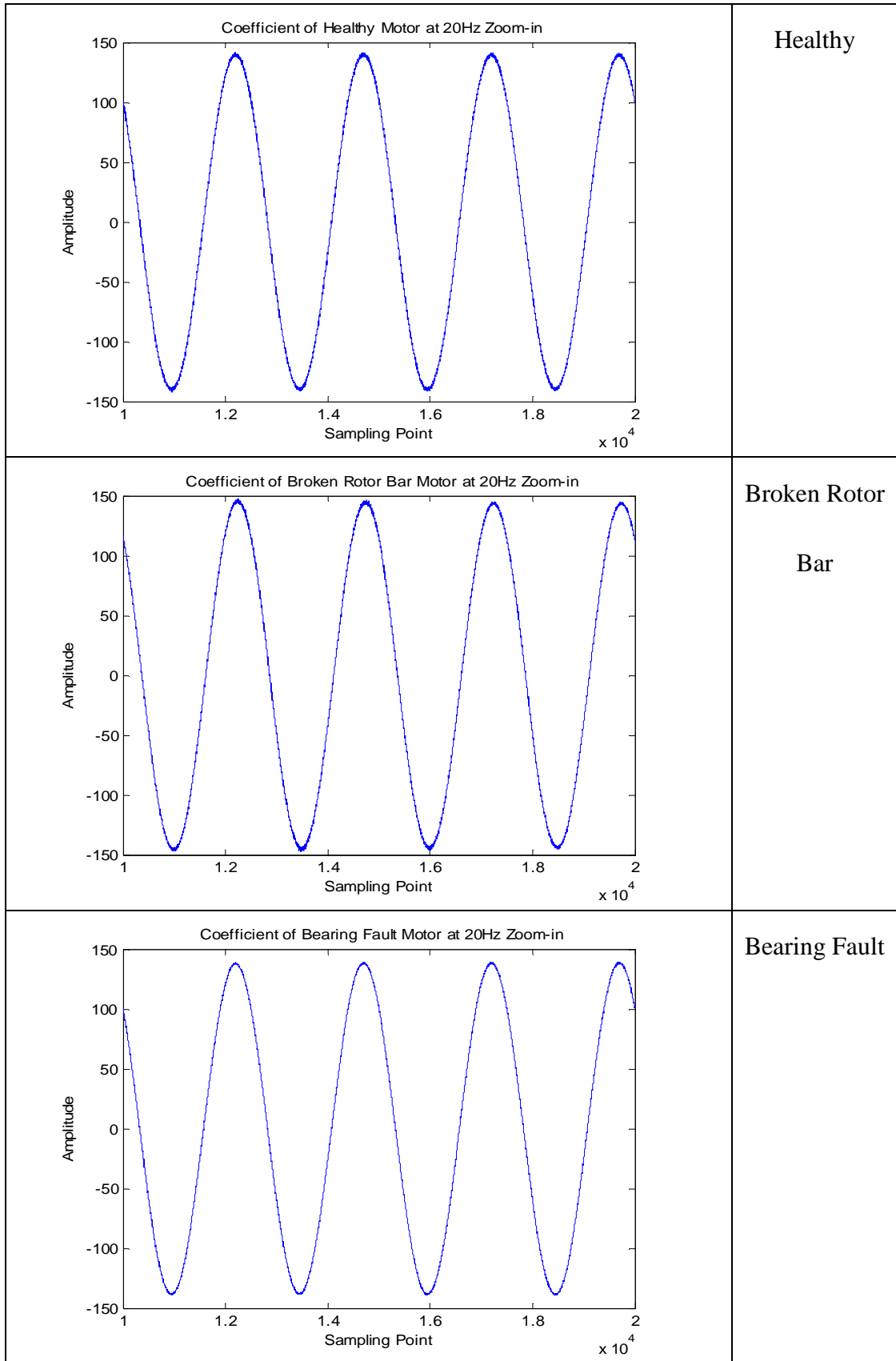|	
Coefficient of Healthy Motor at 20Hz Zoom-in	Healthy
Coefficient of Broken Rotor Bar Motor at 20Hz Zoom-in	Broken Rotor Bar
Coefficient of Bearing Fault Motor at 20Hz Zoom-in	Bearing Fault

Figure 20 Zoom-in extracted features from stator currents at f_s = 20Hz

3.2.3.2   Frequency Spectrum Observation

The extracted features are transformed into frequency spectrum to observe the major characteristic components and their amplitudes in order to help the understanding of later statistical analysis. There are one full scale version of feature spectrum Figure 21 and two zoom-in graphs Figure 22 and Figure 23. The results from three motor conditions are superimposed. The solid blue line represents the broken rotor bar case and the dashed green line and dotted red line represent the healthy case and faulty bearing case respectively. In Figure 21 the spectrums of features from three motors are similar to each other in full vision. The fundamental components locate at 20Hz and take the majority of the signal energy. However, after zoom in, two major differences are found. In Figure 22, the component at inverter frequency of broken rotor bar motor is obviously larger than the other two. As predicted by formula (1) with k =1, there exist a broken rotor bar relevant frequency component at f_s. Hence, it results in larger amplitude of f_s in the broken rotor bar case due to the superimposition. In Figure 23, two prominent characteristic frequencies appear near the inverter frequency at the locations around 19Hz and 20Hz in the broken rotor bar case. The amplitudes of characteristic frequency component are roughly 100 times smaller than the inverter frequency component. These observations are in accord with the prediction made by the theoretical study of broken rotor bar fault in Section 4.1.
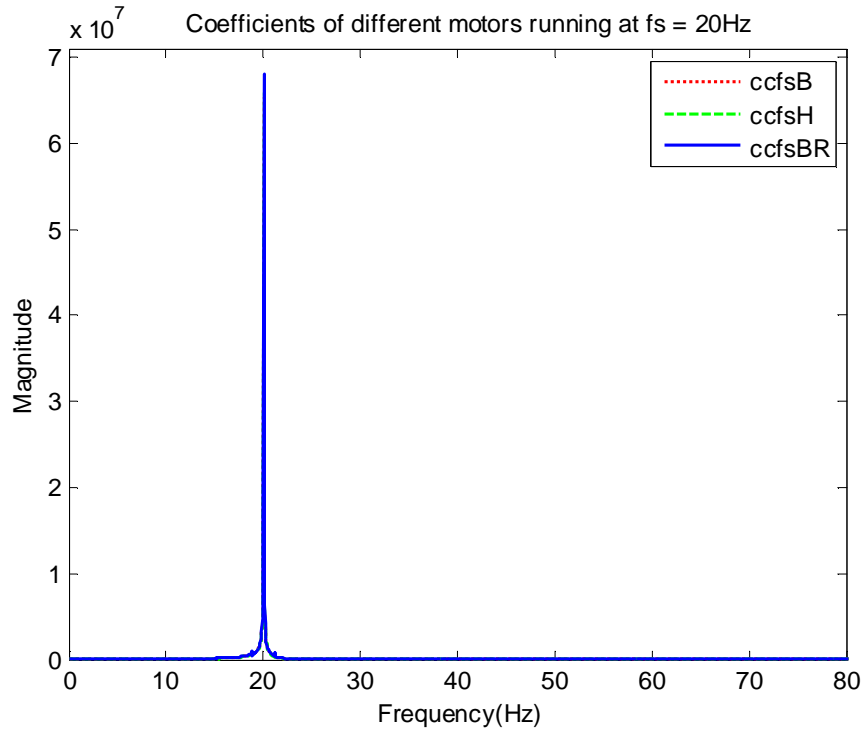
Figure 21 Spectrums of features from stator currents at f_s =20Hz
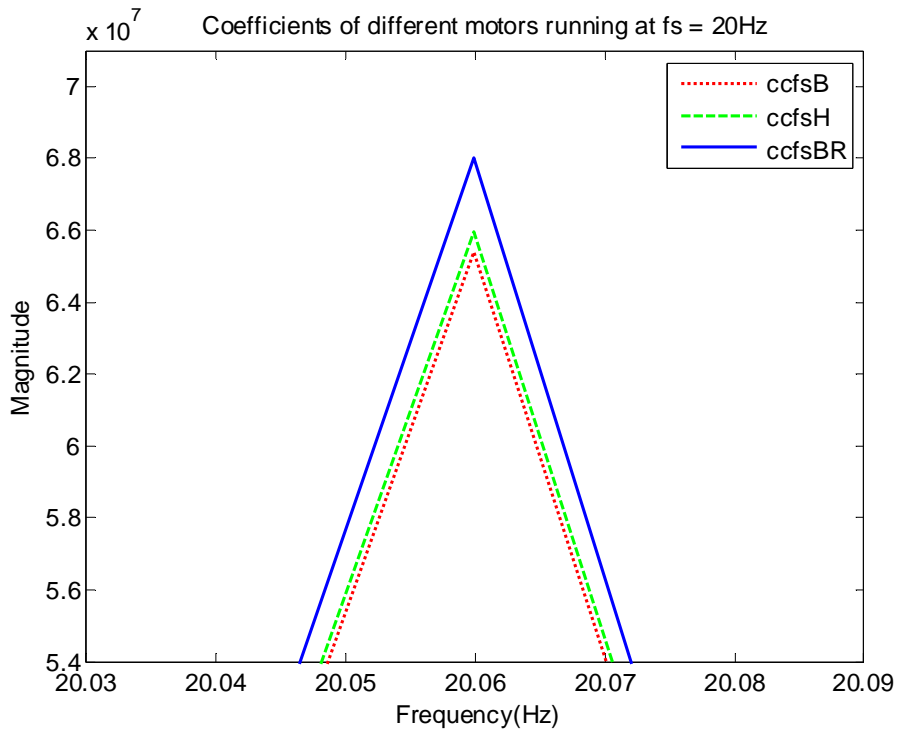

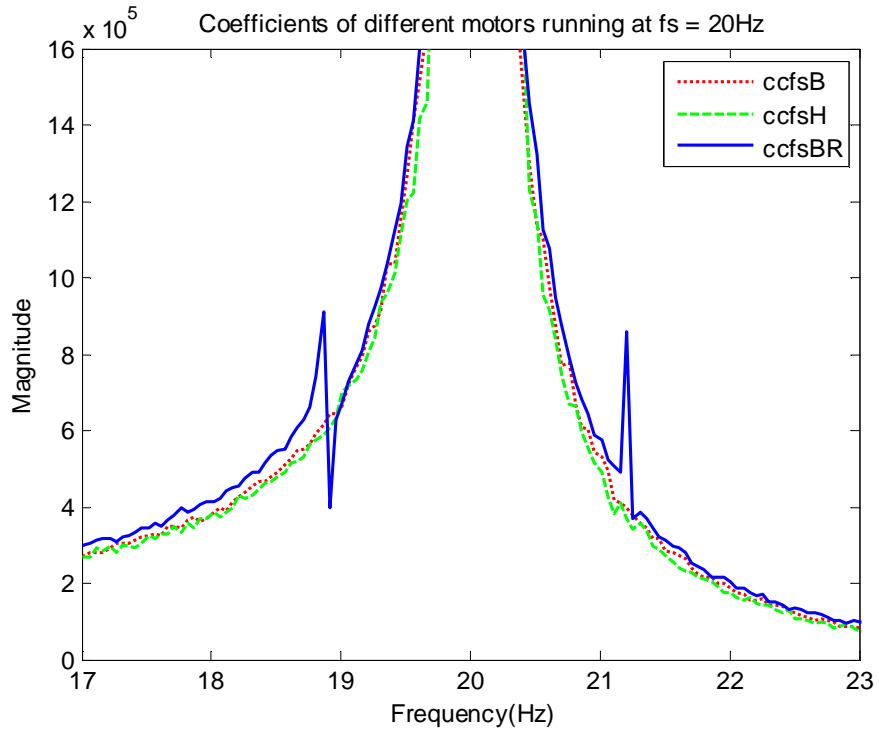Figure 22 Zoom-in spectrums of features from stator currents at f_s =20Hz

Figure 23 Zoom-in spectrums of features from stator currents at f_s =20Hz

3.2.3.3   Statistical Observation

A statistical representation named histogram is used to help a direct statistical observation of the feature data distribution. The x-axis is the segmentation of magnitude and the y-axis is the number of points fall into the corresponding segment. Thus, the surface of histogram is the same for every feature because the number of sampling points of a measurement is the same.

From Figure 24 to Figure 26, it is observed that the data distribution of feature of broken rotor bar fault is different from other two cases in the way of the extended extreme value and smoother distribution around the extreme value. The extended extreme value is mainly contributed by the higher component at inverter frequency f_s which is observed in Figure 25. The smoother coefficient distribution is due to the

existence of extra components which, in this context, are the two broken rotor bar fault

relevant characteristic frequencies locating by the side of inverter frequency. This

observation is consistent with previous prediction in Section 4.1.
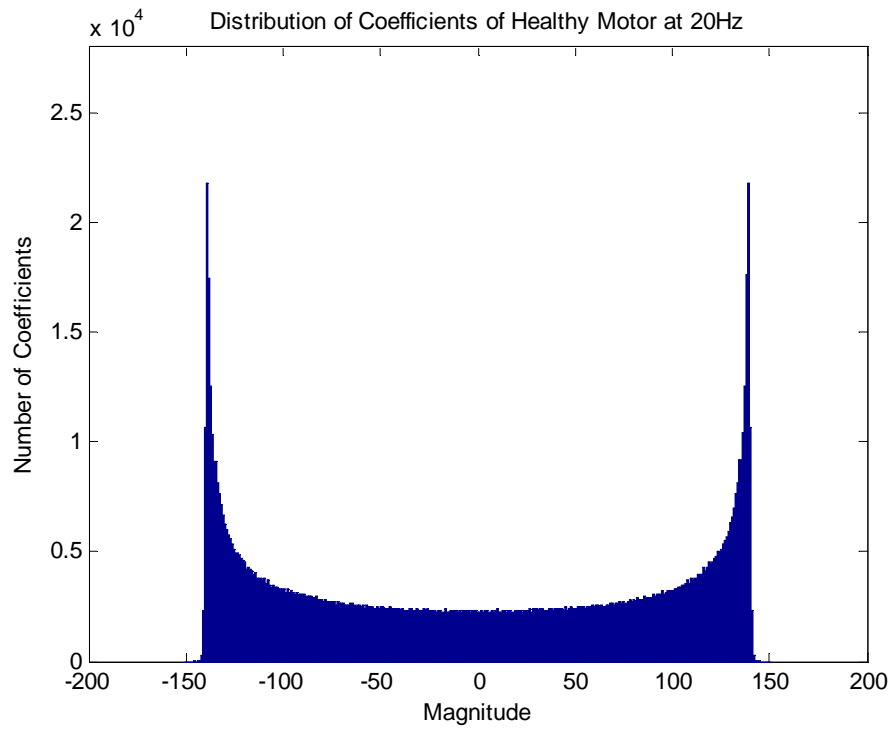
Figure 24 Histogram of healthy motor feature

Figure 25 Histogram of broken rotor bar motor feature

Figure 26 Histogram of bearing fault motor feature

3.2.3.4   Statistic Indices

All sets of data, consisting of five measurements of each operating condition, are put through the proposed method ACWT. Their STD, M and Shannon entropy values at every operating condition are shown in Figure 27, Figure 28 and Figure 31 respectively
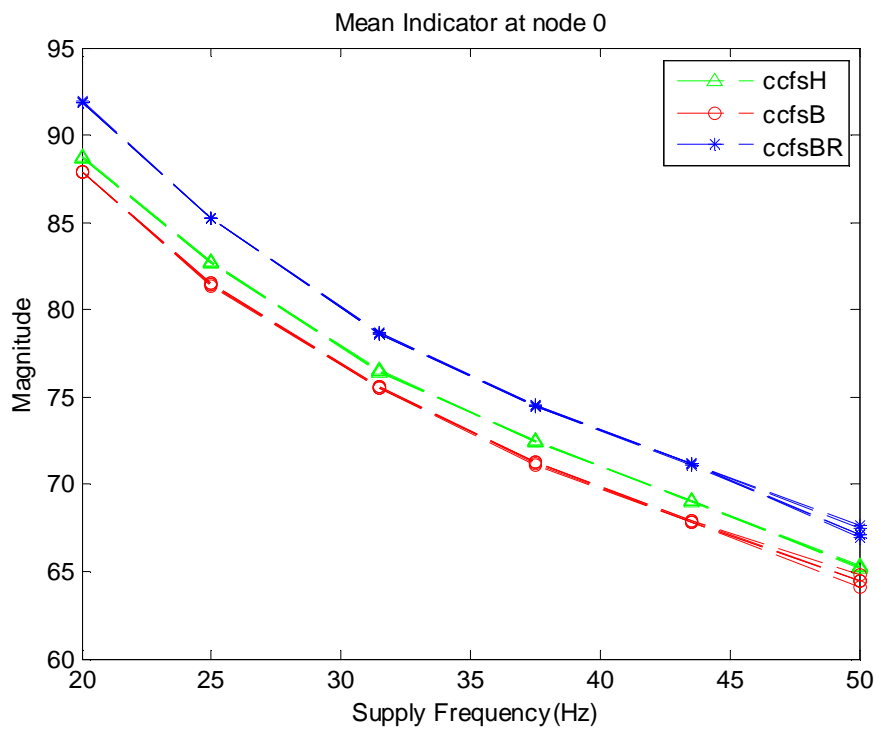
Figure 27 M index from ACWT
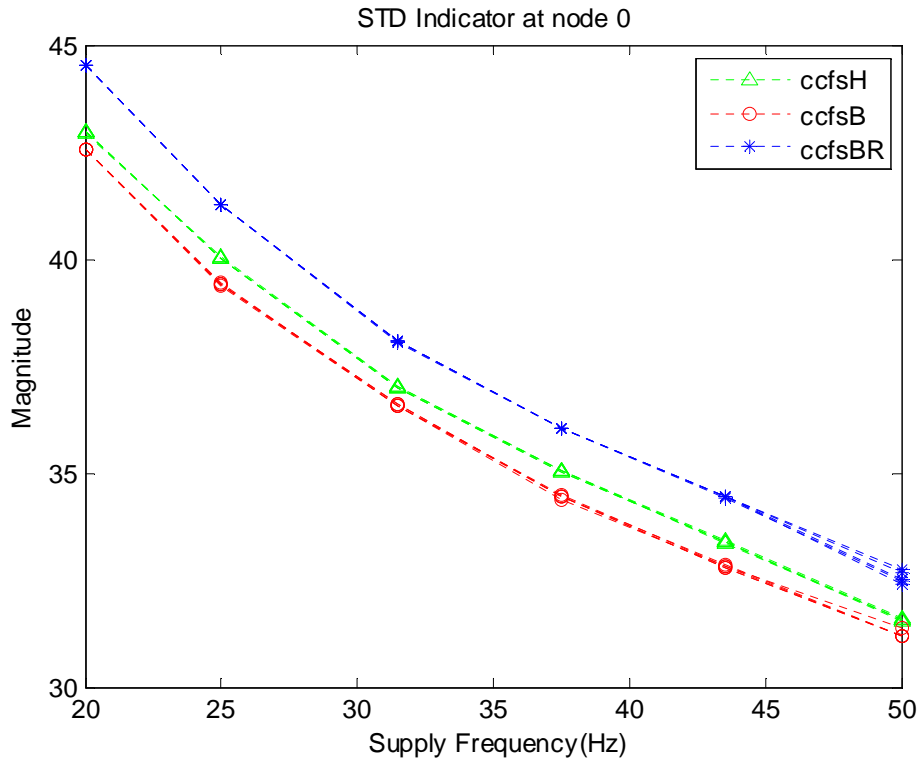
Figure 28 STD index from ACWT

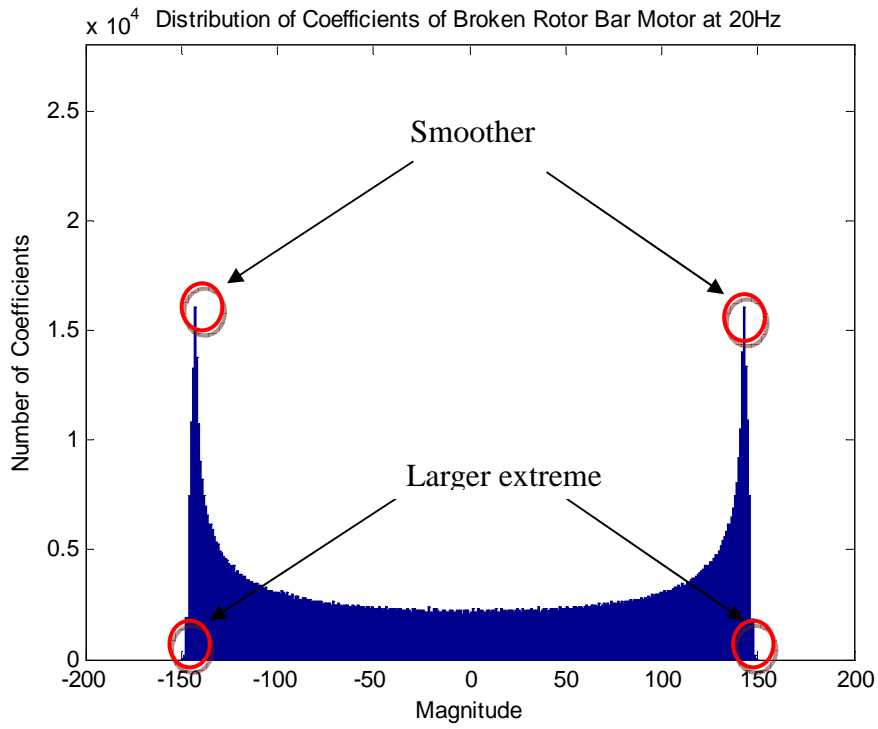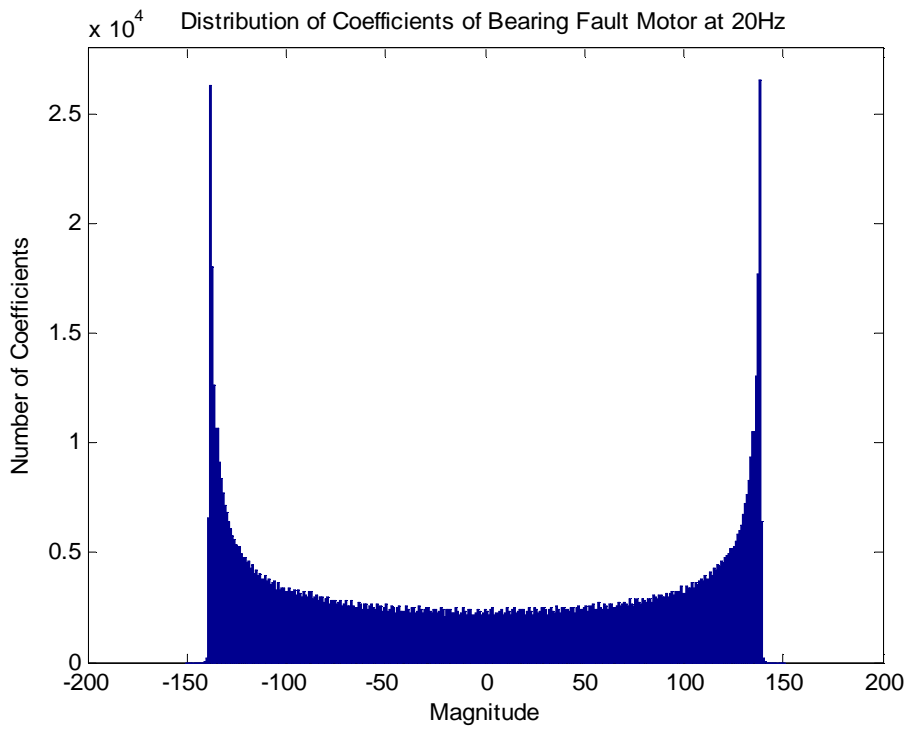As shown in Figure 27 and Figure 28, the STD index and M index of broken rotor bar motor are higher than the other two cases at every operating condition. The difference is obvious and maintained relatively constant throughout the different operating conditions. This constant difference is due to the adjustment of extraction wavelet window along the different inverter frequency. It is the main advantage of this adaptive centered wavelet method. A general threshold for broken rotor bar detection is able to be built for all operating modes. This is so called adaptability to different operating mode. It is also observed that the values of indices decline linearly along the increase of inverter frequency. This is due to the different height of centered wavelet windows. Thus, the baseline needs to be built by training all normal operating conditions. And a predetermined threshold is to be used as a boundary dividing broken

rotor bar fault region and other conditions. The exact threshold value used in our experiment is the healthy condition boundary value after a few measurements. However, it is possible to build in margin to improve the tolerance for errors in measurement in real industry applications and take into consideration of the allowable degree of degeneration of rotor bar before broken up. The specific value of the margin is worthy of studying in the future work.

The ACWT in broken rotor bar detection is compared with another feature extraction technique. The Figure 29 and Figure 30 are the M index and STD index resulting from the method based on Short Fourier transform developed in [16]. This method places a narrow window with fixed wind width around the characteristic frequency to extract the feature. Although, as predicted in Section 4.1, M index and STD index values of broken rotor bar fault are all higher than the other two cases, the distance between them at every operating condition is different. The value of M index increases initially with the increase of inverter frequency to the point of 43.5 Hz and decreases at 50Hz. The STD value of broken rotor bar feature increases linearly along inverter frequency. However, no trend can be observed on the STD values of healthy and faulty bearing cases. At inverter frequency 43.5Hz, the STD value of faulty bearing feature even exceed the healthy one. This brings the difficulty in building a general threshold to detect broken rotor bar fault with merely a priori knowledge of normal conditions. Hence, by examining the STD and M indices, ACWT overtakes the Short Fourier transform based technique in [16] through its better feature extraction result.
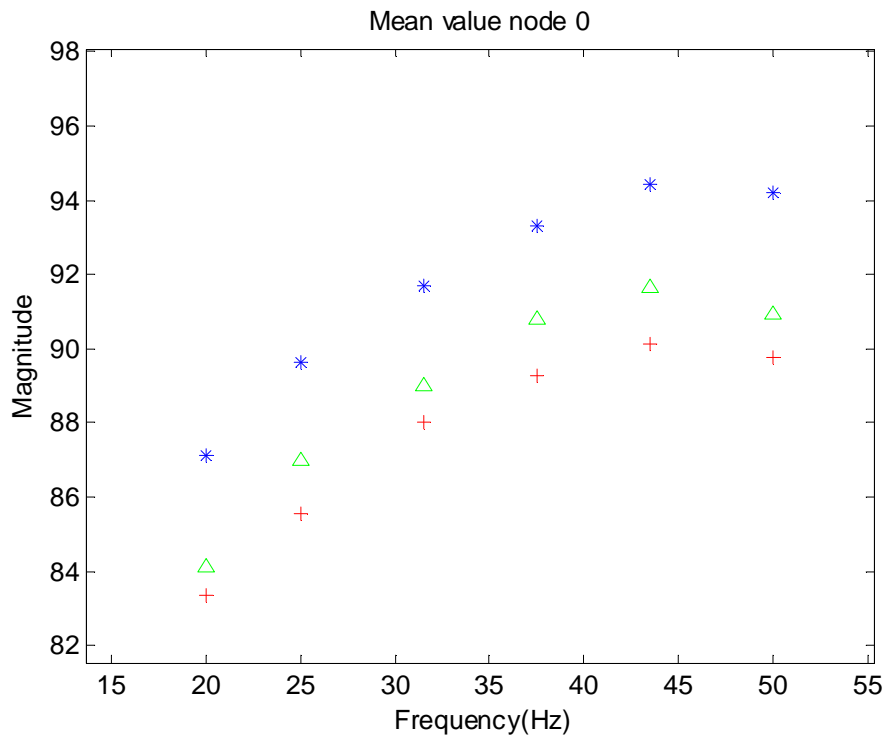
Figure 29 M index from Short Fourier transform
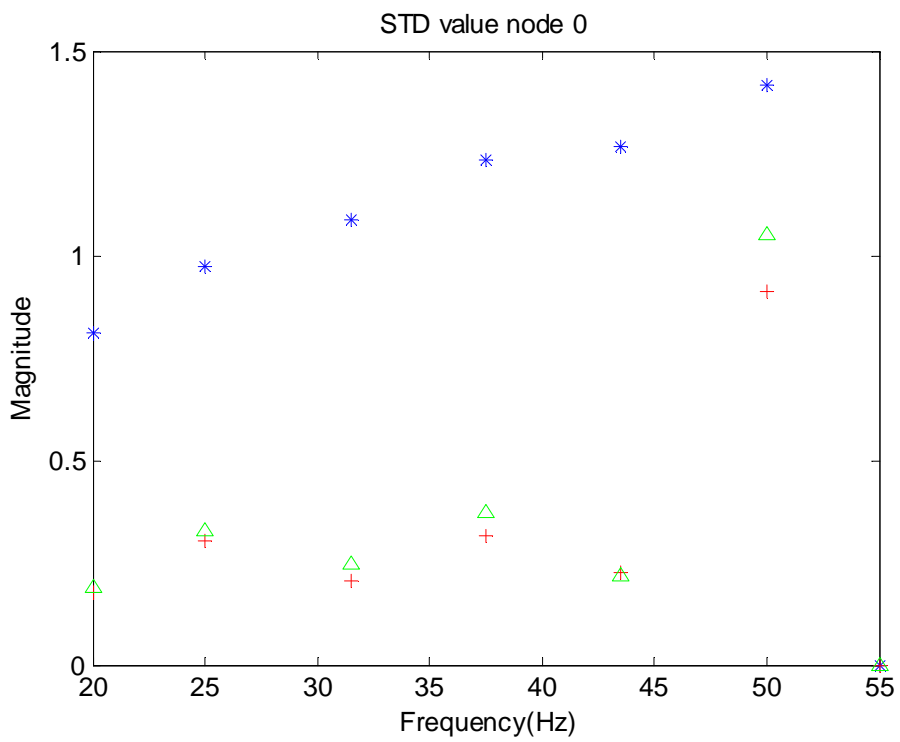
Figure 30 STD index from Short Fourier transform

Next, the third index of feature quantification is studied. The result of Shannon

entropy shown in Figure 31 agrees with the previous prediction. The higher peak value

of inverter frequency and extra components nearby contribute to the certainty of signal;

hence decrease the entropy value of feature in broken rotor bar case. The increase of

entropy values along the inverter frequency is due to the wider window width of

adapted wavelet and lower window height associated. A wider wavelet window

includes more background noise thus increase the randomness of information which

results in higher entropy value for all three cases as inverter frequency increase. Lower

window height reduces the amplitude of centered frequency component after

extraction. As a result, the entropy is increased.
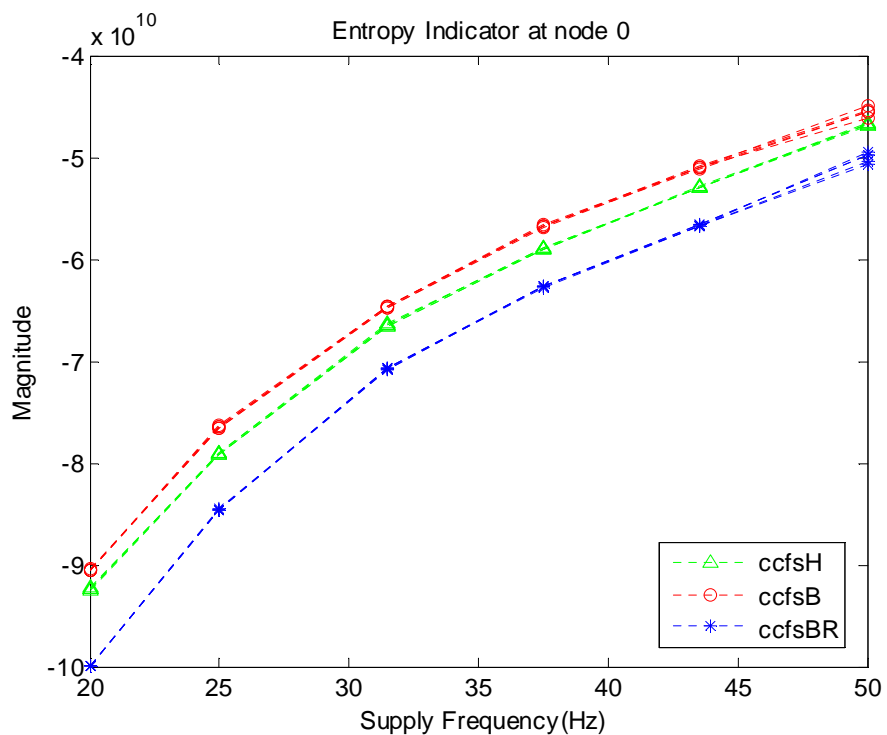
Figure 31 Shannon entropy index from ACWT

After the step of quantification of feature, all statistic indices agree with the theoretical prediction of their performance in broken rotor bar case and other two cases. The broken rotor bar motor can be identified by comparing these statistic values of the extracted feature from stator current to the ones of the healthy motor. The adaptability of ACWT to different motor operating mode is verified experimentally and by comparison with another widely used technique.

Chapter 4

Adaptive Centered Wavelet Technique for Bearing Fault

Detection

Following the success of adaptive centered wavelet technique in the detection of broken rotor bar fault, the similar methodology is applied to detect bearing fault which is the primary cause of induction motor failure in industry.

4.1 Process

A similar process is conducted in bearing fault detection. The major difference resides in the feature extraction stage. Unlike broken rotor bar characteristic frequencies, of which the most significant components exist at two sides of the inverter frequency, the bearing fault characteristic frequencies spread over the entire spectrum and no prominent components are predictable. The magnitude of components depends on the severity of the bearing fault itself as well as the load condition. The more severe fault and/or heavier load lead to larger load variations, which will result in higher amplitude of the characteristic components. As our algorithm is targeted for early fault detection, the lightest load is used in our design. Hence, unlike one wavelet window that is centered around inverter frequency is used in the feature extraction for broken rotor bar fault detection; a set of wavelets are placed over several potential characteristic frequency locations for bearing fault

detection to observe the local conditions. The feature from each wavelet is analyzed separately.

Each wavelet, denoted by the node n, is placed between $|f_s - (n+1)f_o|$ and $|f_s + nf_o|$ in order to cover two nearby bearing fault related frequency components. Table 5.1 lists those chosen centers which are associated with different inverter frequencies:

$$\mathcal{F} = \left(\frac{2n+1}{2}\right) f_o \tag{19}$$

Where

  n   node number

  f_o outer raceway bearing fault vibration characteristic frequency

$\mathcal{F}$ (Hz) f_o (Hz)	1	2	3	4	5	6	7	8	9	10
35.1	52.6	87.7	122.7	157.8	192.9	227.9	263.0	298.0	333.1	368.2
43.8	65.7	109.6	153.4	197.2	241.1	284.9	328.7	372.6	416.4	460.2
55.2	82.8	138.1	193.3	248.5	303.7	359.0	414.2	469.4	524.6	579.9
65.8	98.6	164.4	230.1	295.9	361.6	427.3	493.1	558.8	624.6	690.3
76.3	114.4	190.7	266.9	343.2	419.5	495.7	572.0	648.2	724.5	800.8
87.7	131.5	219.2	306.8	394.5	482.1	569.8	657.5	745.1	832.8	920.4

Table 5 Wavelet placement $\mathcal{F}$

4.2　Result and Discussion

4.2.1　Frequency Spectrum Observation

Because the window widths of wavelets increase with the increasing center frequency, the features extracted in high frequency area have relative large bandwidths. The wider the feature bandwidth is the more unpredictable components are retained in the feature after extraction. In Figure 32, the comparisons are made between the features at node 1 and node 10 of the stator current signal with f_s = 50Hz. It is observed that the feature bandwidths at node 1 and node 10 are around 100Hz and 700Hz respectively. In the feature extraction stage of motor fault detection, the wavelet is designed to target specific characteristic frequencies predicted in Section 3.2.2. Hence, the small wavelet bandwidth is preferred to discriminate the unpredictable or fault irrelevant components around the characteristic frequencies. From this point of view, ACWT manifests its weakness in the feature extraction at high frequency area.
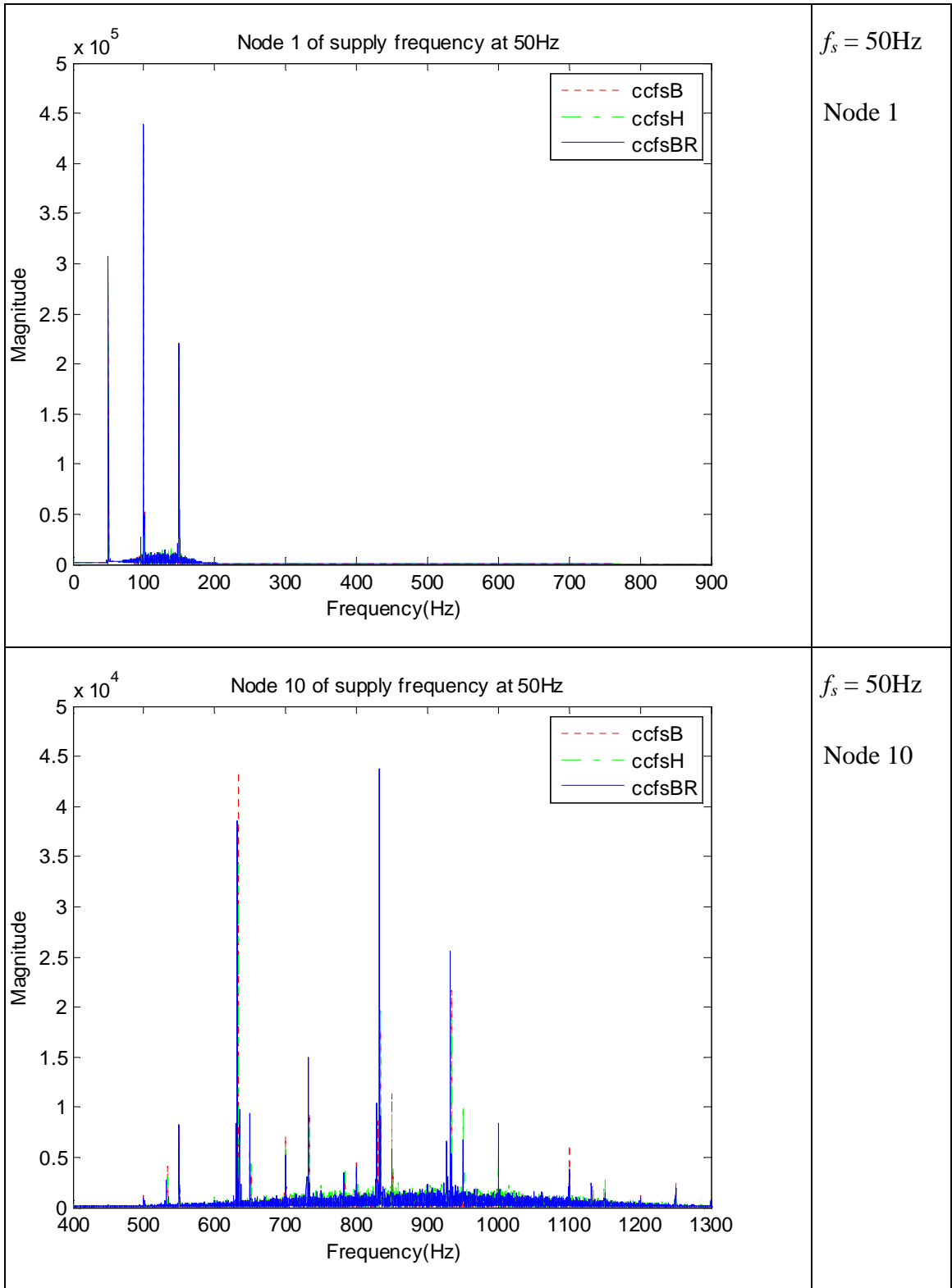
Figure 32 Spectrums of features at node 1 and 10

It is also observed that the difference between healthy motor and bearing fault

motor in stator current exist not only at the characteristic frequencies predicted in

Section 3.2 but also other unpredictable locations.

Firstly, the amplitudes of harmonics of inverter frequency in stator current are different between the different motors. This issue is visualized in frequency spectrum of both stator current signals and extracted features in Figure 33. The frequency spectrum of bearing fault condition is plotted in solid red line on top of the healthy one represented by dashed green line. It is obvious that at harmonics of 40, 100, 120 and 140 Hz, the frequency components are higher in healthy case. This phenomenon is not due to the wavelet transformation but to the nature of stator current in local condition. This is possibly resulted from the installation of motor and/or the disturbance from the connected power system during the measurement. So far, researches have not yet proven the correlation between the motor fault and the resulted modification of the harmonics of inverter frequency in stator current. Hence, the harmonics of inverter frequency are characterized as irrelevant to motor fault condition and are usually excluded in motor fault analysis. By observation, they are of considerable amplitude in low frequency band and become less prominent in the spectrum after the 13th harmonic (ex. 260Hz for f_s = 20Hz). For this reason, it is better to extract the feature locating at middle frequency band which is less affected by the fault irrelevant inverter frequency harmonics
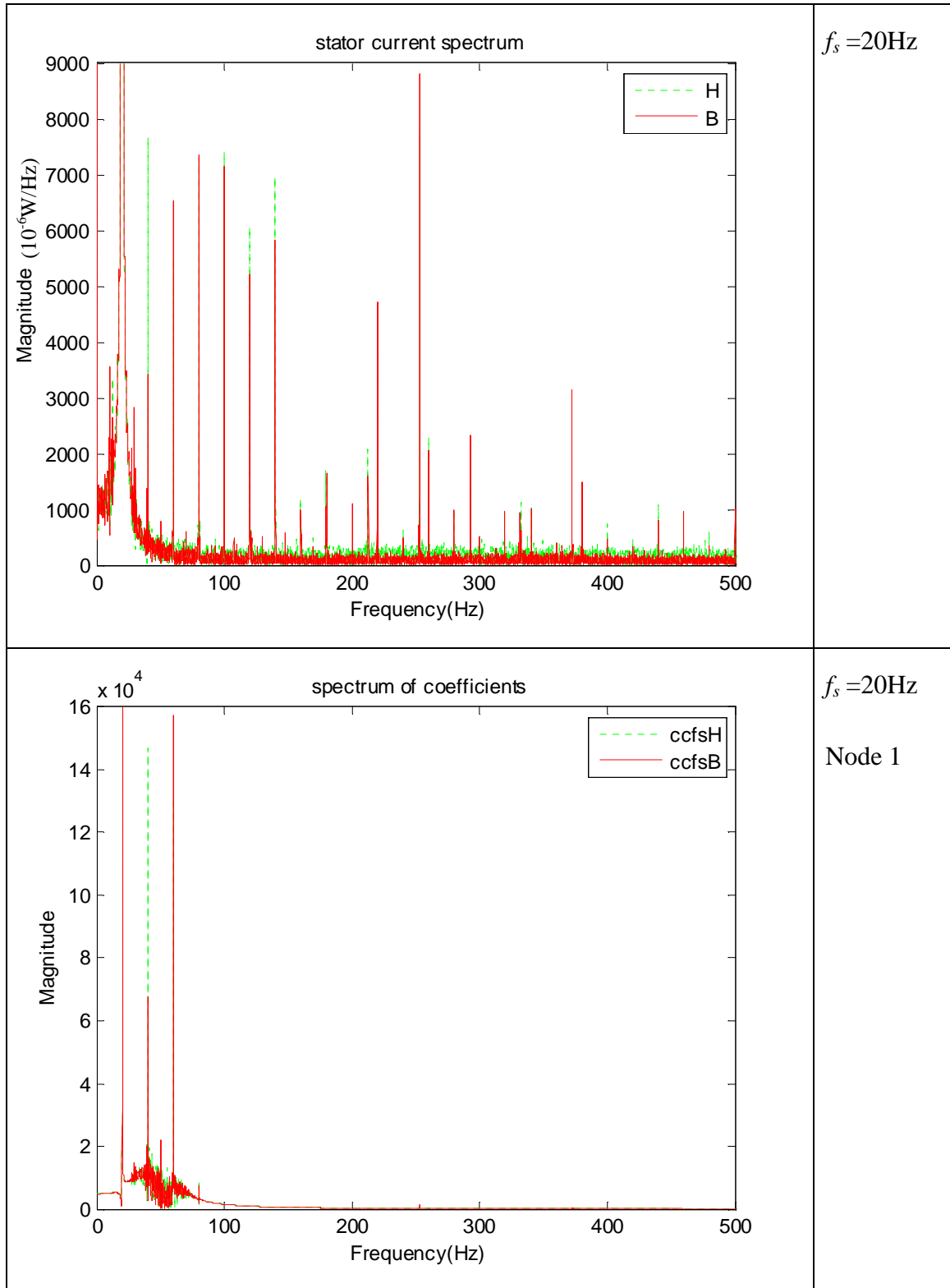
Figure 33 Spectrums of original signal and feature

In addition, from Figure 34, it can be seen that besides inverter frequency harmonics some other unpredictable components present in the original signal and the

extracted feature. They may be introduced by inverter or other factors in the power
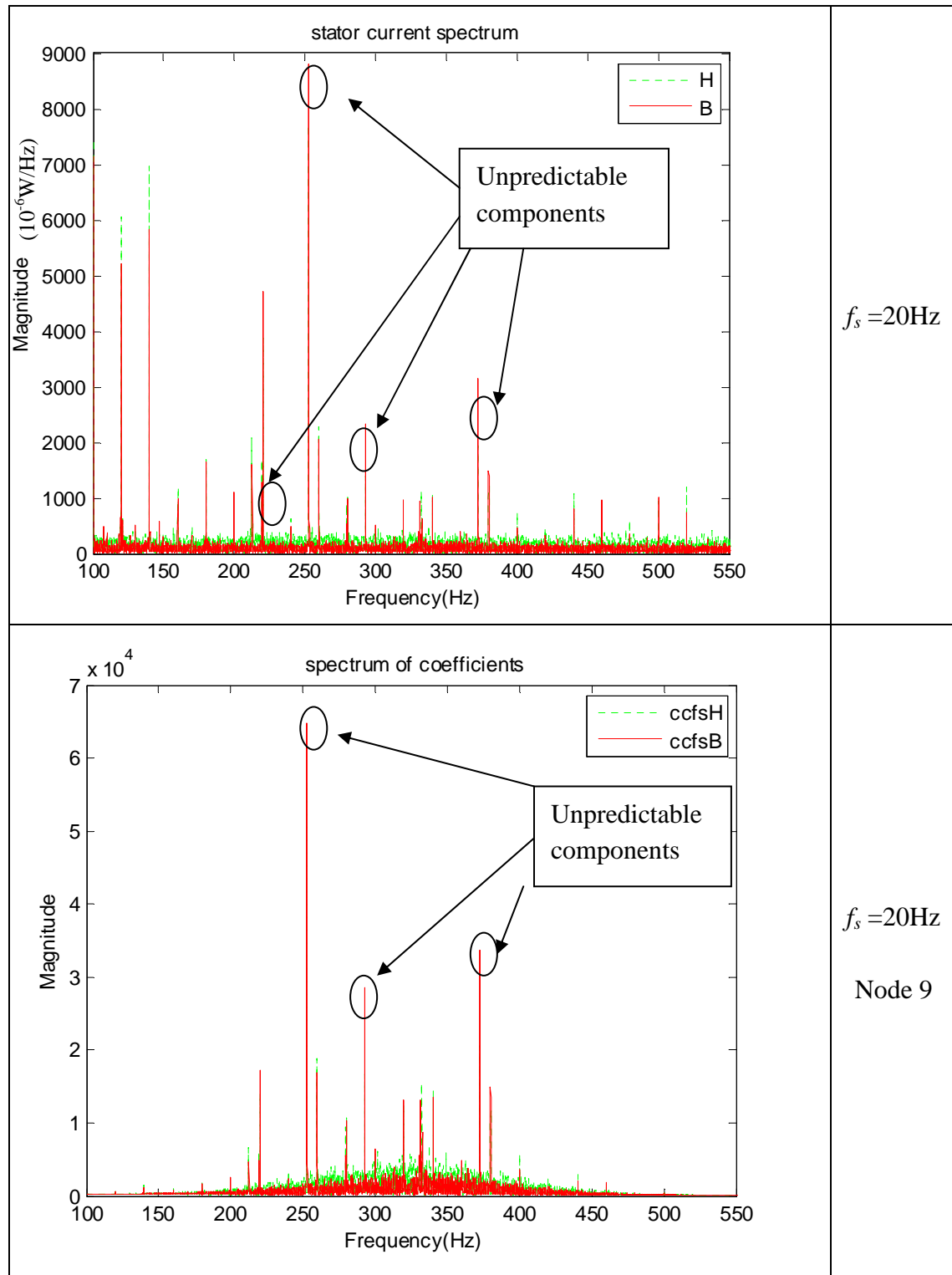
system.

Figure 34 Spectrums of original signal and feature

Based on the direct observation of the stator currents in frequency domain, it is

found that not every bearing fault related characteristic frequency predicted in Section 3.2 appears in stator current spectrum of faulty bearing motor. Some of them with too small amplitude are corrupted by noise and thus not observable in spectrum [5], [18], [19]. The characteristic frequencies are more obvious in middle frequency band such as node 9 where the main harmonics decrease to certain extend. Figure 35 shows the experimental result of bearing fault related characteristic frequency components, which are at the locations around 2Hz smaller than the prediction. This pattern is similar in different operating condition.
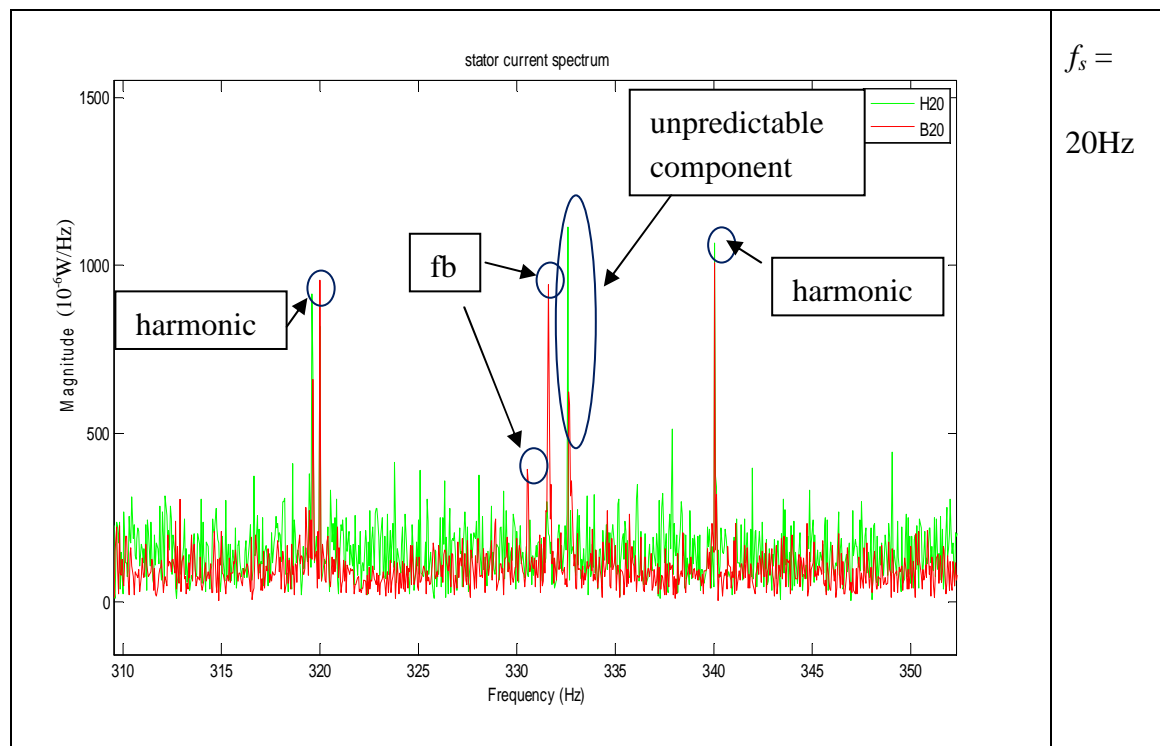

Figure 35 Zoom-in spectrums of original signals around 330Hz

Because the light load is used in experiment, the characteristic components have very low amplitude as compared with main harmonics and even other unpredictable components. This brings difficulty to a reliable bearing fault detection which counts on

the contribution of determined fault-related information in final feature instead of the effect from other unpredictable factors.

4.2.2 Statistic Indices Evaluation

Most STD index values of bearing fault motor features based on ACWT are below the ones of healthy motor in ten nodes at different operating conditions. This implies the existence of bearing fault related information in all nodes [18], [19]. However, in fact, only the bearing fault related features in middle frequency band are of considerable amplitude. Hence, the STD results of lower nodes where the observable fault not included are not convincing. These results may due to other factors such as the variation of harmonics in low frequency band between different motors.

By observation, higher order nodes generate better result in STD. For example, the STD results of features extracted at node 9 and node 1 are shown in Figure 36 and Figure 37. Where the bearing fault related characteristic frequencies are observed within the window of node 9, the STD value is constantly below the other two at all operating modes. In contrast, the consistence along the inverter frequency is violated in low order nodes such as in node 1 shown.
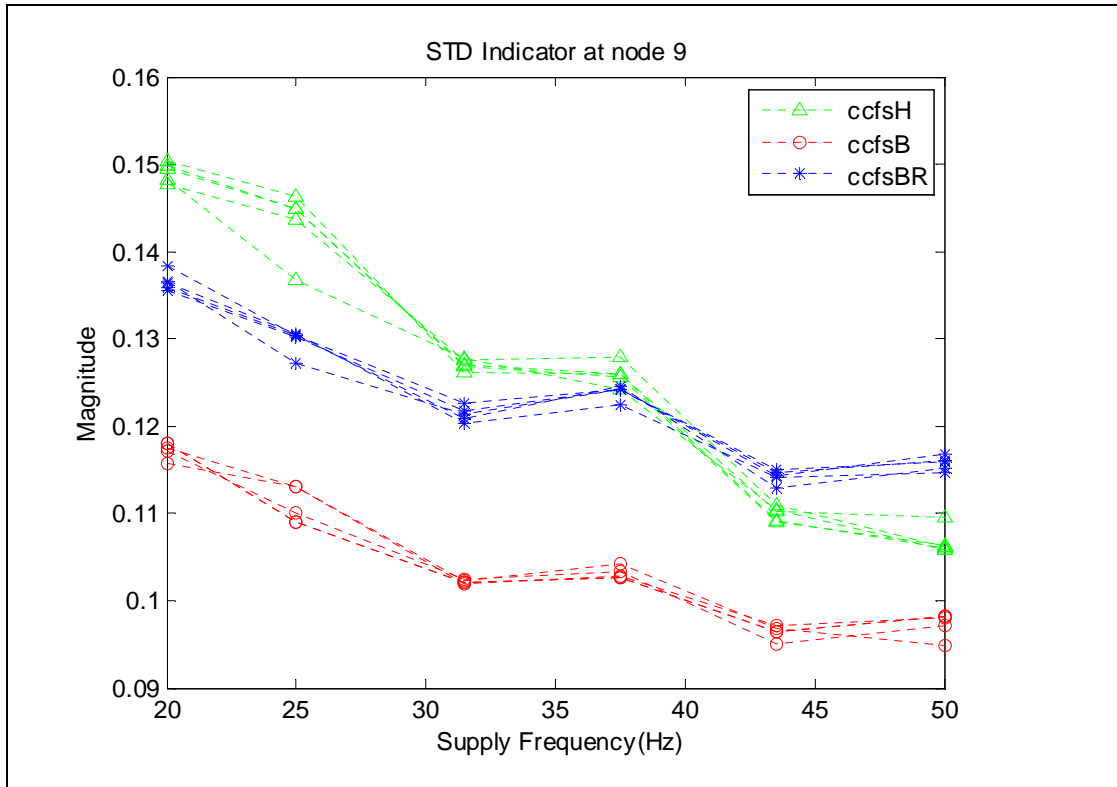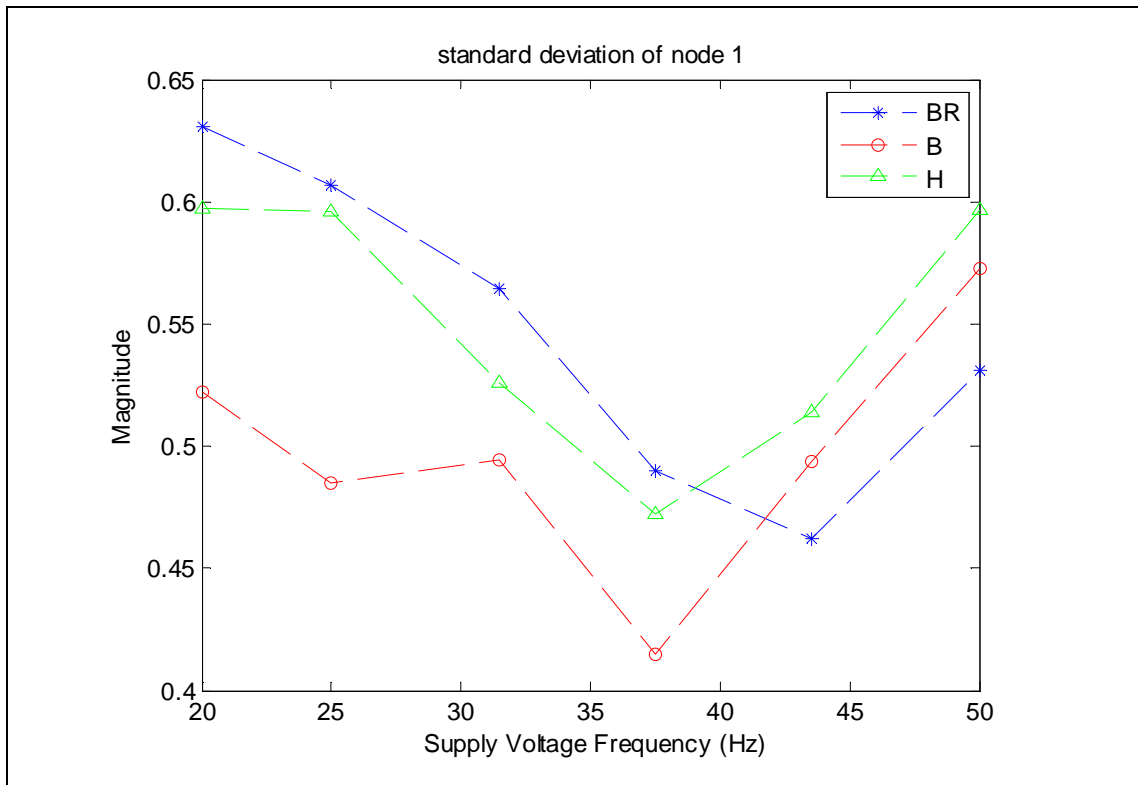
Figure 36 STD index at node 9

Figure 37 STD index at node 1

Shannon entropy reveals a different behavior as compared to STD index. In Figure

38 and Figure 39, Node 2 and Node 9 are used as an example. Node 2 has the entropy

value of bearing fault case beyond the other two cases while Node 9 exhibits the entropy value of bearing fault constantly below which is in accord with the prediction of existence of extra determined components in Node 9. Indeed, in the previous observation of bearing fault spectrum, only the bearing fault related characteristic frequencies within the wavelet window node 9 are observed. Other characteristic frequencies are corrupted by noise and fault irrelevant disturbance presented in low frequency band. This bearing fault related characteristic frequencies are mostly extracted in Node 9 other than Node 2. The entropy index reveals this difference.

The lower entropy value for bearing fault motor at Node 9 agrees with the prediction made before: characteristic frequencies which decrease the uncertainty of information thus decrease the entropy value. Based on the performance of centered wavelet technique on both broken rotor bar and bearing fault detection, it can be concluded that Shannon entropy proves a more reliable statistic measurement of determined fault related information.

However, the wide spread spectrum of feature in high frequency area after extraction reduced the credit of attribution from characteristic frequencies on the final lower entropy value of feature. As can be seen in Figure 34, the feature contains a few harmonics of inverter frequency. Any difference of these motor fault irrelevant components can affect the conclusion.

In conclusion, the reliability of ACWT is less convincing in bearing fault detection compared to broken rotor bar fault detection. This is due to the combined effect of the

non-observable bearing fault feature in low frequency band in our experimental result

and the incapability of wavelet in achieving narrow window width in middle frequency
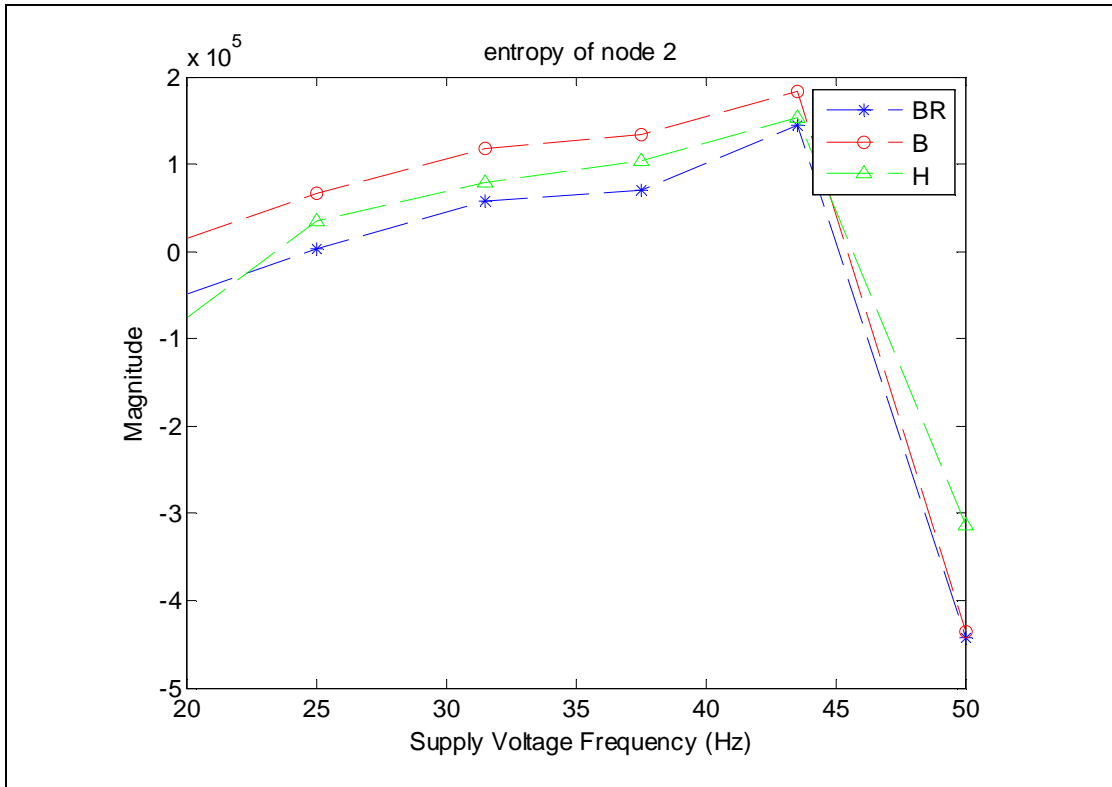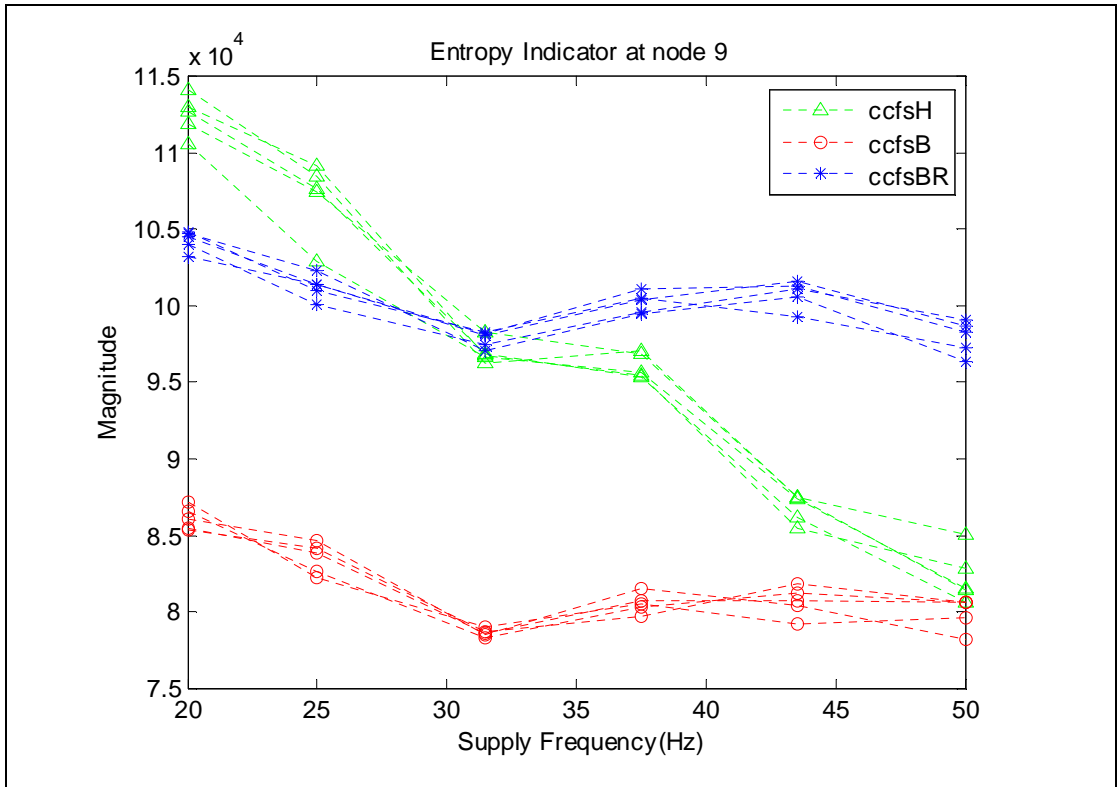
band.

Figure 38 Shannon entropy index at node 2

Figure 39 Shannon entropy index at node 9

Chapter 5

Adaptive Wavelet Packet Technique for Motor Fault Detection

Aiming to maximize the advantage of adaptability of ACWT developed in previous chapters while improve over its shortcoming of wide window width in the high frequency area, adaptive wavelet packet decomposition technique (AWPT) is proposed in this chapter to achieve an adaptive motor fault detection.

There are two main advantages of wavelet packet decomposition (WPD) compared to wavelet analysis: adjustable bandwidth and fast computation. The main challenge is how to deal with the window location and width for feature extraction under different inverter frequencies. The spectrum width of a stator current is determined by its sampling frequency. In WPD, the spectrum is continuously divided into 2 to the desired level imposed by the user [29]. Thus, the fault feature in two different operating modes may locate in different subbands or at different positions within a subband or even in the cross section of two consecutive subbands. This makes the feature node unpredictable or even insignificant. In addition, the inter-relationship between nodes is not maintained. Many people implement neural network to overcome this disadvantage. It uses a big range of fixed nodes from WPT as the inputs of the network, which cover all possible feature locations in different cases. According to this input strategy, the input patterns of the stator current from the same motor condition but under different

f_s are different from each other. Hence, the network needs to memorize all of them as different cases and summarize them into one conclusion of motor condition in the training stage. For example, the motor condition of bearing fault motor with $f_s = 50$Hz cannot be identified although the network has been trained successfully to diagnosis the bearing fault motor under $f_s = 20$Hz. What's more, since the node placement is fixed in WPT, the cases, of which the features reside in the cross sections of nodes, cannot be identified by neural network even in the training stage. These are the limits of the input strategy based on WPT. Hence, for the motor fault detection techniques developed in this thesis as well as the neural network techniques, it is critical to respect the inter-relationship in the feature extraction under various operating modes to achieve a better detection accuracy and efficiency.

The following method aims to achieve a better node placement hence better feature extraction. The overall block diagram of AWPT is presented in the beginning of this section and the details of wavelet packet decomposition, resampling process and statistic indices are illustrated in separate subsections. In Section 5.2, the spectrum observations and the statistic indices evaluations are presented. Finally, a fault region graph is proposed for a visualization of the AWPT results.

5.1 Methodology

The adaptation of wavelet packet to stator currents at difference inverter frequencies is realized by adding a resampling block before the wavelet packet

decomposition Figure 40. The resampling process will change the whole spectrum length in order to adjust the node position and width. Its effect on wavelet packet decomposition will be demonstrated in details in Section 6.1.2.
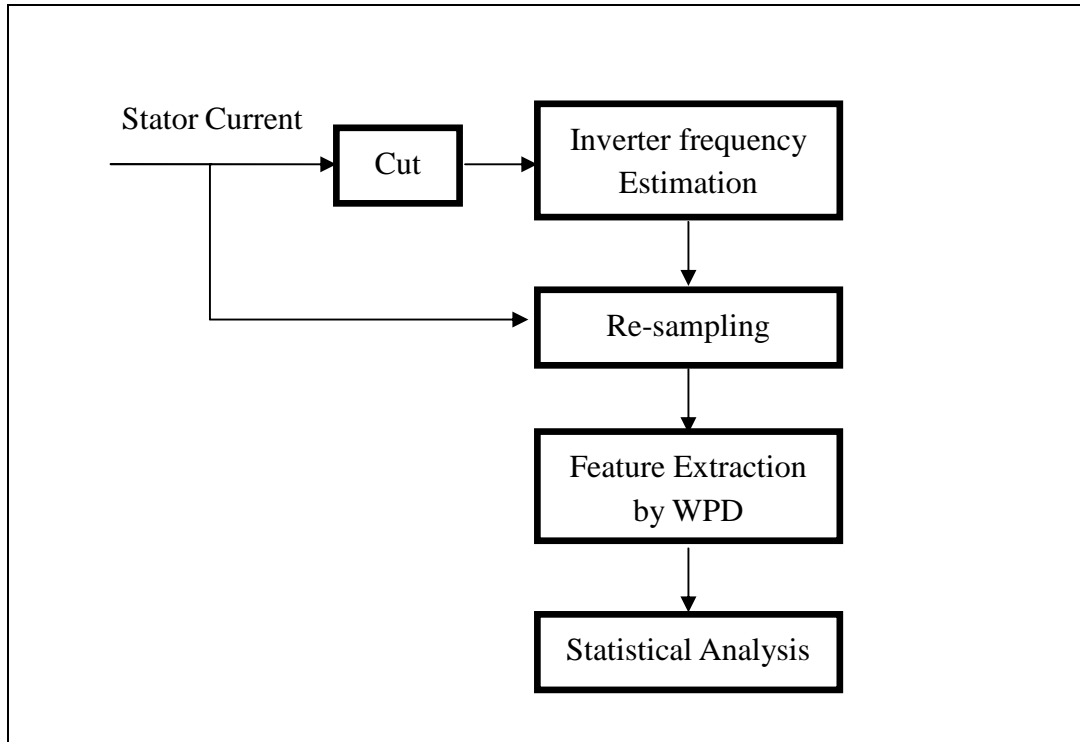
Figure 40 Training stage of AWPT

5.1.1   Wavelet Packet Decomposition

A finer frequency resolution in the middle- or high-frequency band could be achieved via wavelet packet decomposition (WPD). WPD is closely related to multirate filter banks. Subband decomposition of signal using two-band filter banks can be implemented efficiently and conveniently [28]. Daubechies showed that the following equations can be used to numerically obtain wavelet and scaling coefficients

$$\psi_{j,k}(t) = 2^{-j/2}\psi(2^{-j}t - k) \tag{20}$$

The wavelet coefficients for level j can be obtained from scaling coefficients from

level $j - 1$ using

$$\psi_{j,k}(t) = \sum_{n} g_{n-2k} \phi_{j-1,n}(t) \tag{21}$$

$$\langle x, \psi_{j,k} \rangle = \sum_{n} \overline{g_{n-2k}} \langle x, \phi_{j-1,n} \rangle \tag{22}$$

The scaling coefficients for level j can be obtained from the scaling coefficients

from level $j - 1$ using

$$\phi_{j,k}(t) = \sum_{n} h_{n-2k} \phi_{j-1,n}(t) \tag{23}$$

$$\langle x, \phi_{j,k} \rangle = \sum_{n} \overline{h_{n-2k}} \langle x, \phi_{j-1,n} \rangle \tag{24}$$

Where g and h are high-pass and low pass filters, respectively. The procedure can

start by calculating $\langle x, \psi_{1,k} \rangle$ and $\langle x, \phi_{1,k} \rangle$ from $\langle x, \phi_{0,n} \rangle$ using (22), (24) respectively.

Then, the same procedure is used until the level j is reached.

An example of WPD is illustrated in Figure 41 and Figure 42. The frequency

separation obtained by WPD is depicted in Figure 41. As can be seen, the spectrum is

divided into 8 subbands by a 3 level decomposition. The band width is around f/8 where

f is the sampling frequency of the input signal. The wavelet filter bank structure to

accomplish such decomposition is shown in Figure 42.
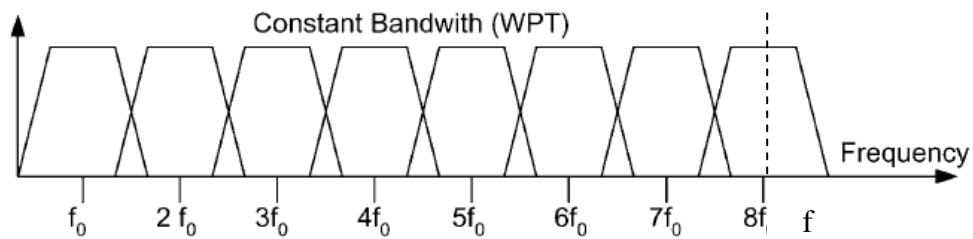
Figure 41 Linear frequency separation
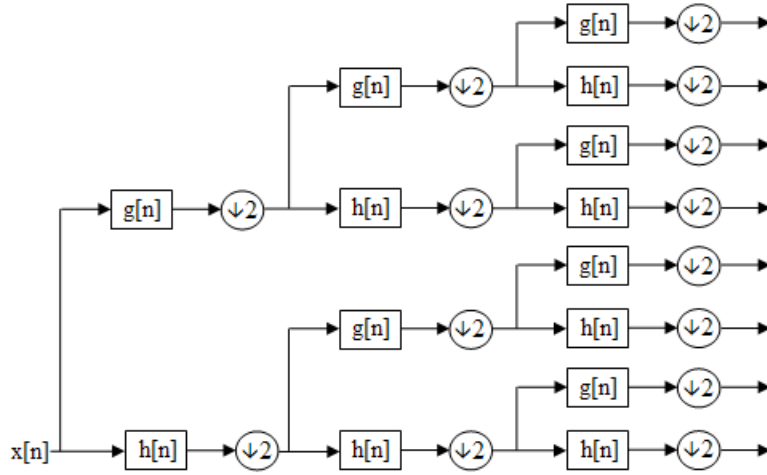
Figure 42 Filter bank structure

The wavelet packet coefficients at any level j+1 can be obtained from coefficients at level j by using equations (25) (26)

$$d_{j+1}^{2p}[k] = d_j^p[k] * \bar{h}[2k] \tag{25}$$

$$d_{j+1}^{2p+1}[k] = d_j^p[k] * \bar{g}[2k] \tag{26}$$

Where

d_0 is the input signal

Thus, subband width and location are determined by sampling rate of signal and level of decomposition.

5.1.2 Resampling

The subband width is expected to be small enough to exclude harmonics of inverter frequency in stator current, which act as unpredictable factors in fault detection around the targeted fault-related characteristic frequencies. This is particularly essential for

detecting bearing fault of which the feature amplitude is weak. Thus, its width should be smaller than f_s. As f_s varies in different operating condition and fault-related features change accordingly, the width is ought to be adapted to this variation to keep the same node covered the same feature under different operating condition. This adaptation is realized by resampling process.

The original signal is sampled at rate of 50 kHz. Thus, the useful spectrum of the discrete signal covers 25 kHz frequency band. Because the information in high frequency band mainly contains the noise and is not of great interest in fault detection. Hence, resampling to lower sampling rate is applicable in this case.

An anti-aliasing FIR filter is first applied during the resampling process to filter out the frequency components above the desired sample rate position in signals. Next, 10 terms on either side of the current sample, x(k), are used to perform the interpolation in order to achieve the least distorted discrete signal in desired sampling rate.

In this work, the sample rate for signals with different inverter frequency is designed as follow:

$$f_R = R \times f_{sampling} \times f_s^*$$
(27)

where

    R   a predetermined constant

The value of R together with the level of decomposition determines the wavelet packet position and bandwidth. In this thesis, R is set to be 5.2×10^{-3} and level of

decomposition is set to be 8 for achieving the best performance. Table 6.1 shows the corresponding bandwidth and fault-related feature nodes for different inverter frequency. Feature Node [8,1] focus on broken rotor bar related information. It covers the broken rotor bar fault related characteristic frequency $f_s(1 - 2s)$. Feature Node [8,48] focus on bearing related information. It covers $|f_s - 10f_0|$ and $|f_s + 9f_0|$ these two bearing fault characteristic frequencies. As can be seen, the width of wavelet window is well adapted to different operating condition. Furthermore, the harmonics of inverter frequency are excluded in feature node [8, 48] so that the extracted information relies more on the bearing condition of a motor. By using these two nodes, the motor rotor bar condition and bearing condition are observed at the same time. They can be analyzed simultaneously in diagnosing the motor condition.

f_s	20Hz	25Hz	31.5Hz	37.5Hz	43.5Hz	50Hz
Sampling Rate (Hz)	5200	6500	8190	9750	11300	13000
Subband Width (Hz)	10.2	12.7	16.0	19.0	22.1	25.4
Feature Node [8,1] (Hz)	10.2~ 20.4	12.7~ 25.4	16.0~ 32.0	19.0~ 38.0	22.1~ 44.2	25.4~ 50.8
Feature Node [8,48] (Hz)	325~ 335.2	406.3~ 418.9	511.9~ 527.9	609.4~ 628.4	706.3~ 728.3	812.5~ 837.9

Table 6 Resampling details

5.1.3 Statistic Index

Both STD index and Shannon entropy are applied on features. In addition, normalization based on packet energy is applied to improve the feature quality.

$$\overline{d_j^p} = \frac{d_j^p}{\left\| d_j^p \right\|} \tag{28}$$

Where

d_j^p feature at node [j,p]

$\overline{d_j^p}$ normalized d_j^p

5.2 Result and Discussion

The features extracted by using AWPT are firstly evaluated in spectrum. The adaptability of AWPT to different operating condition in the step of feature extraction is discussed and compared to the non-adaptive wavelet packet decomposition which is used in other papers [18]-[20]. Later, the performance of different indices is evaluated. At last, by using entropy index, a fault region graph is finally built to achieve the goal of fault detection with a priori knowledge of normal operating conditions.

5.2.1 Frequency Spectrum Observation

The determined fault-related information is effectively extracted by AWPT. This can be observed in the comparison between the frequency spectrum of feature d_8^{48} and original signal spectrum of the 20Hz signal in Figure 43. The harmonics at 320Hz and 340Hz are all excluded after the extraction whereas broken rotor bar related feature and bearing fault-related features around predicted location 330Hz are conserved. However, an unpredictable component at frequency 333Hz in healthy motor and bearing fault motor remains after extraction.

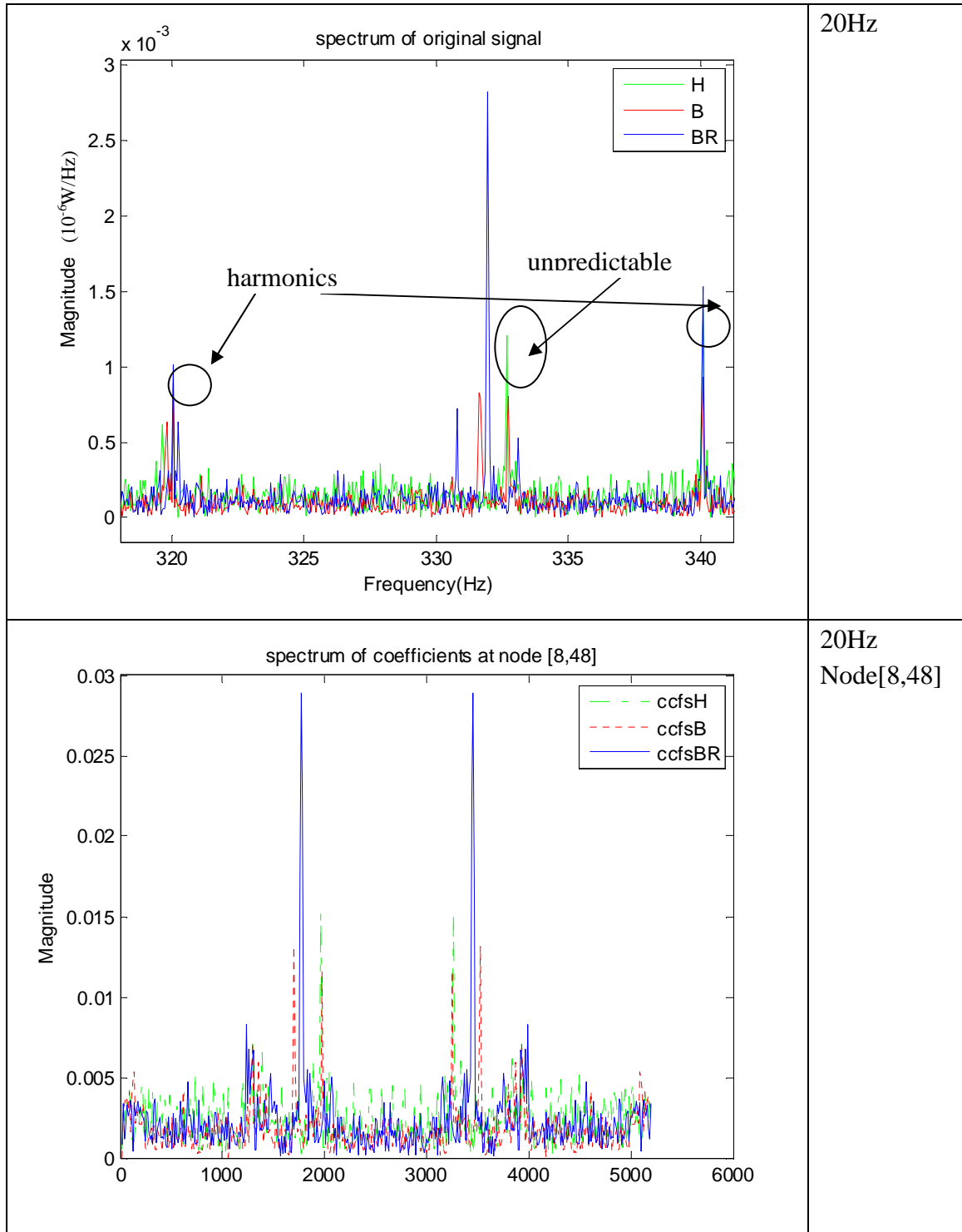|	20Hz
spectrum of original signal	
spectrum of coefficients at node [8,48]	20Hz Node[8,48]

Figure 43 Spectrums of original signals and d_8^{48} features by AWPT

Figure 44 shows the frequency spectrums of the re-sampled stator current of 50Hz

inverter frequency and its feature d_8^1. Although the original spectrum pattern is not

conserved in this case after extraction, the essential difference between the broken rotor

bar fault and other two cased are remained.

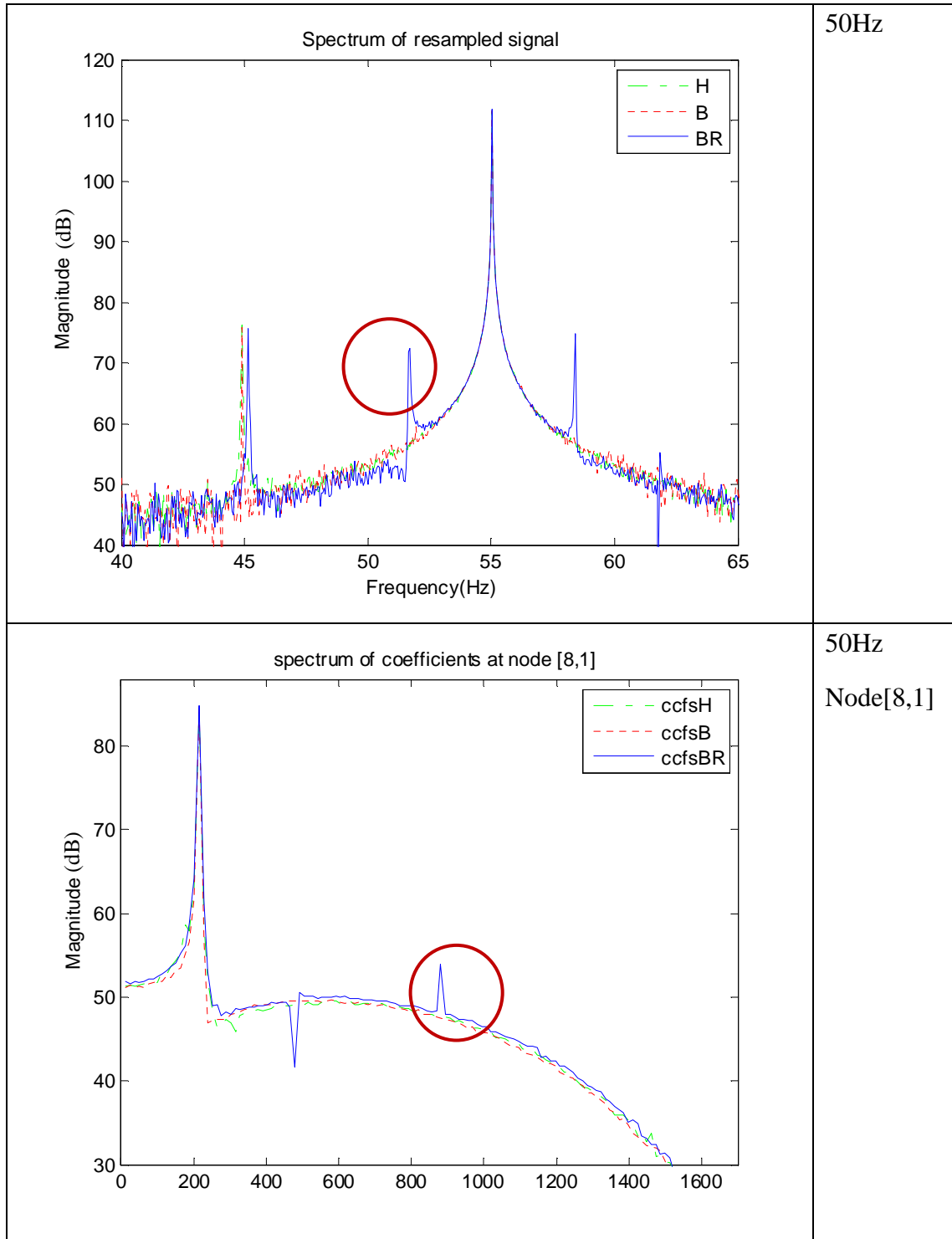| | 50Hz |
	50Hz
	Node[8,1]

Figure 44 Spectrums of original signals and d_8^1 features by AWPT

In Figure 45, the similar layouts of spectrum of feature d_8^{48} are found in different

operating conditions in AWPT. This result proves the success of the method in

associating same node at same feature from motors running under different inverter frequency. The node [8,48] extracts the feature around 520Hz from 31.5Hz signal and the feature around 825Hz from 50Hz signal. A comparison with traditional non-adaptive wavelet packet decomposition is given in Figure 46. With the constant sampling rate of 5200 and 3 level decomposition, the node [8, 48] always focus on frequency band around 330Hz regardless of different operating condition. Thus, as can be seen in the upper graph, for inverter frequency not equal to 20Hz, the feature extracted at node [8,48] is not related to predicted fault feature. Moreover, although the fault-related frequency band can be found, such as node [8,121] for 50Hz inverter frequency current shown in the second graph, the extracted pattern does not conserve the similar layout for different operating conditions as compared with the ones by AWPT shown in Figure 45. Hence, AWPT overtakes the traditional WPT in term of the adaptability of feature extraction to different operating conditions.

	31.5Hz Node[8,48]
 spectrum of coefficients at node [8,48]	
 spectrum of coefficients at node [8,48]	50Hz Node[8,48]
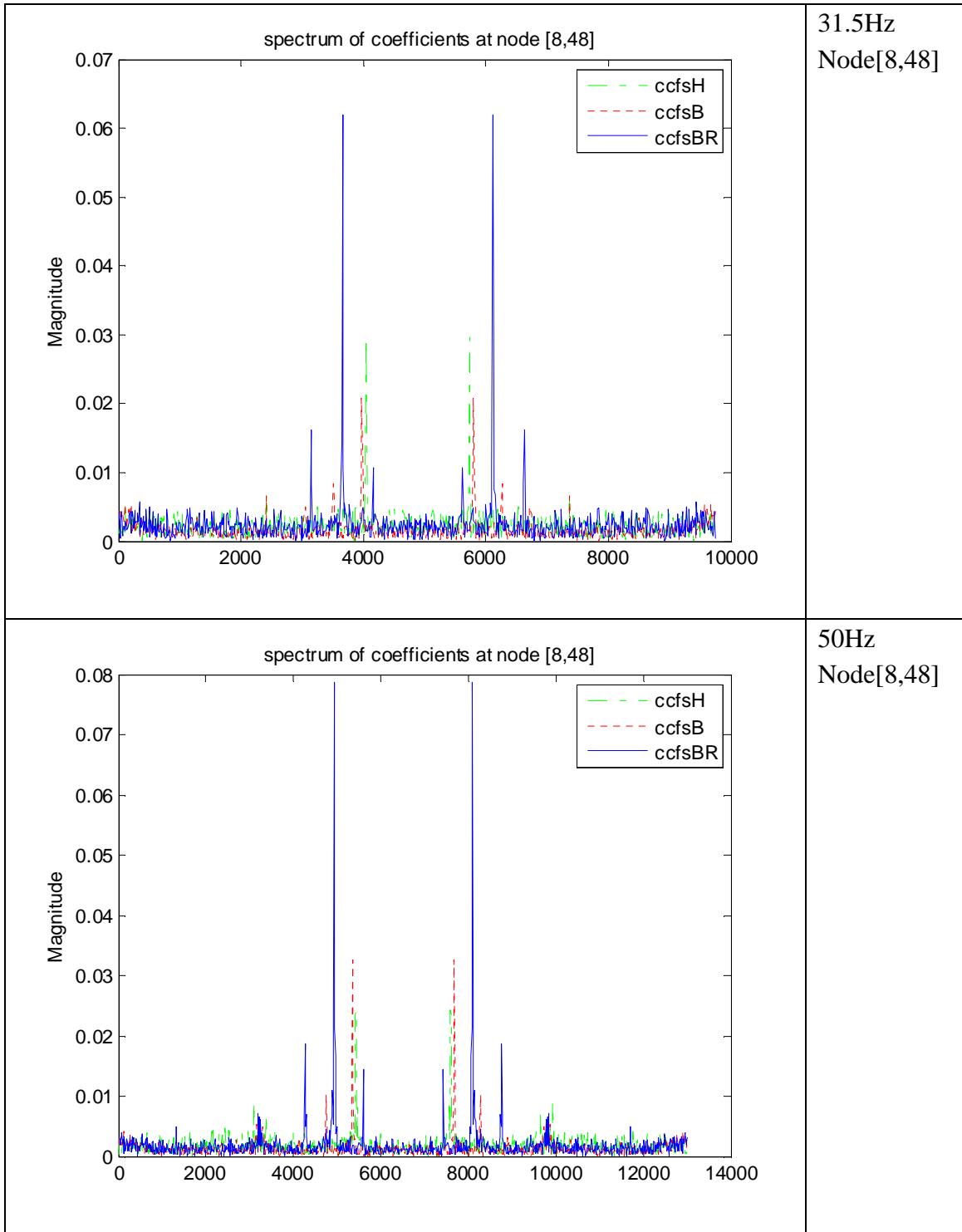
Figure 45 Spectrums of d_8^{48} features at different f_s by AWPT

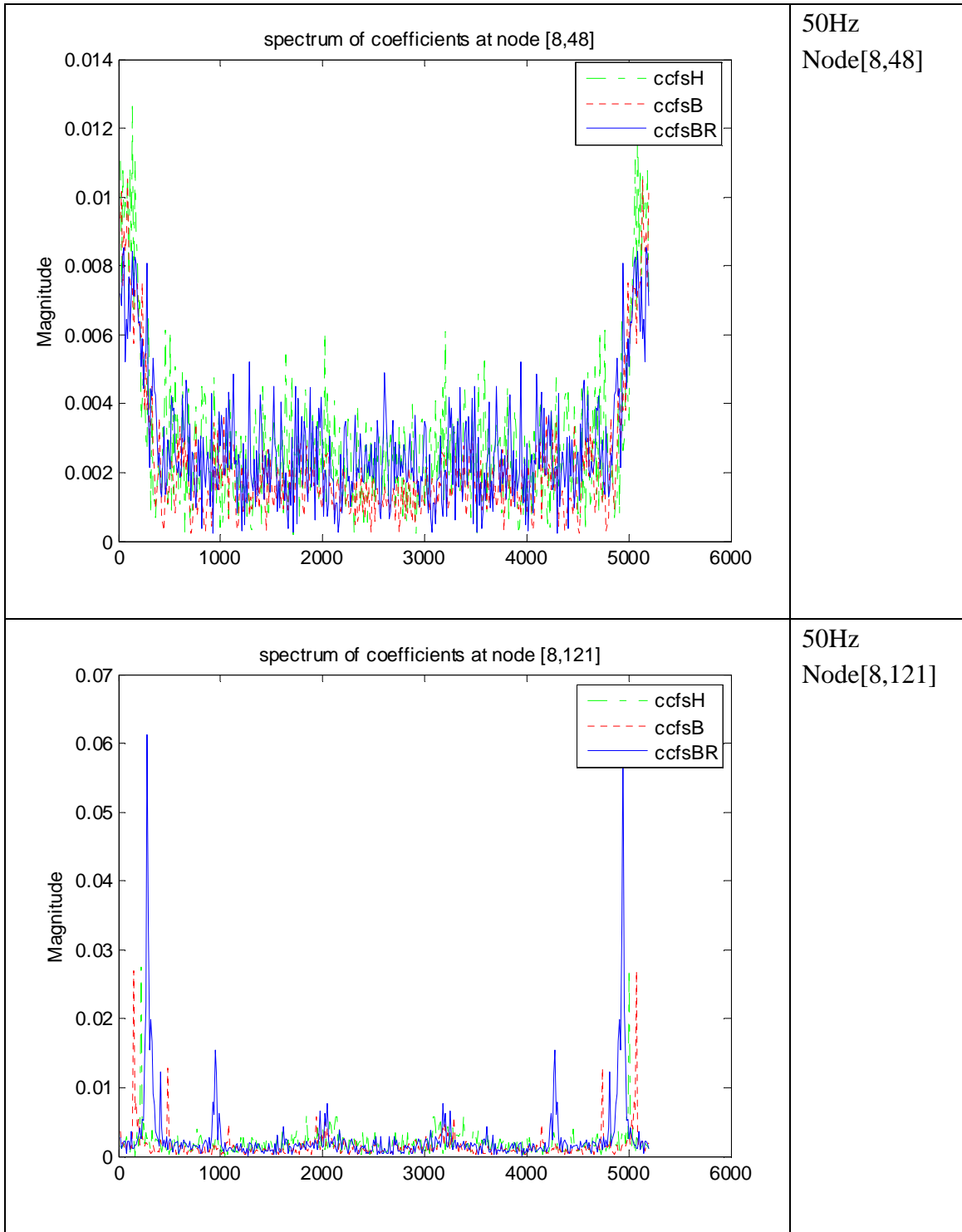|	
	50Hz Node[8,48]
	50Hz Node[8,121]

Figure 46 Spectrums of features by traditional WPD

The similar layouts of feature d_8^1 are also found in different operating conditions as shown in Figure 47.
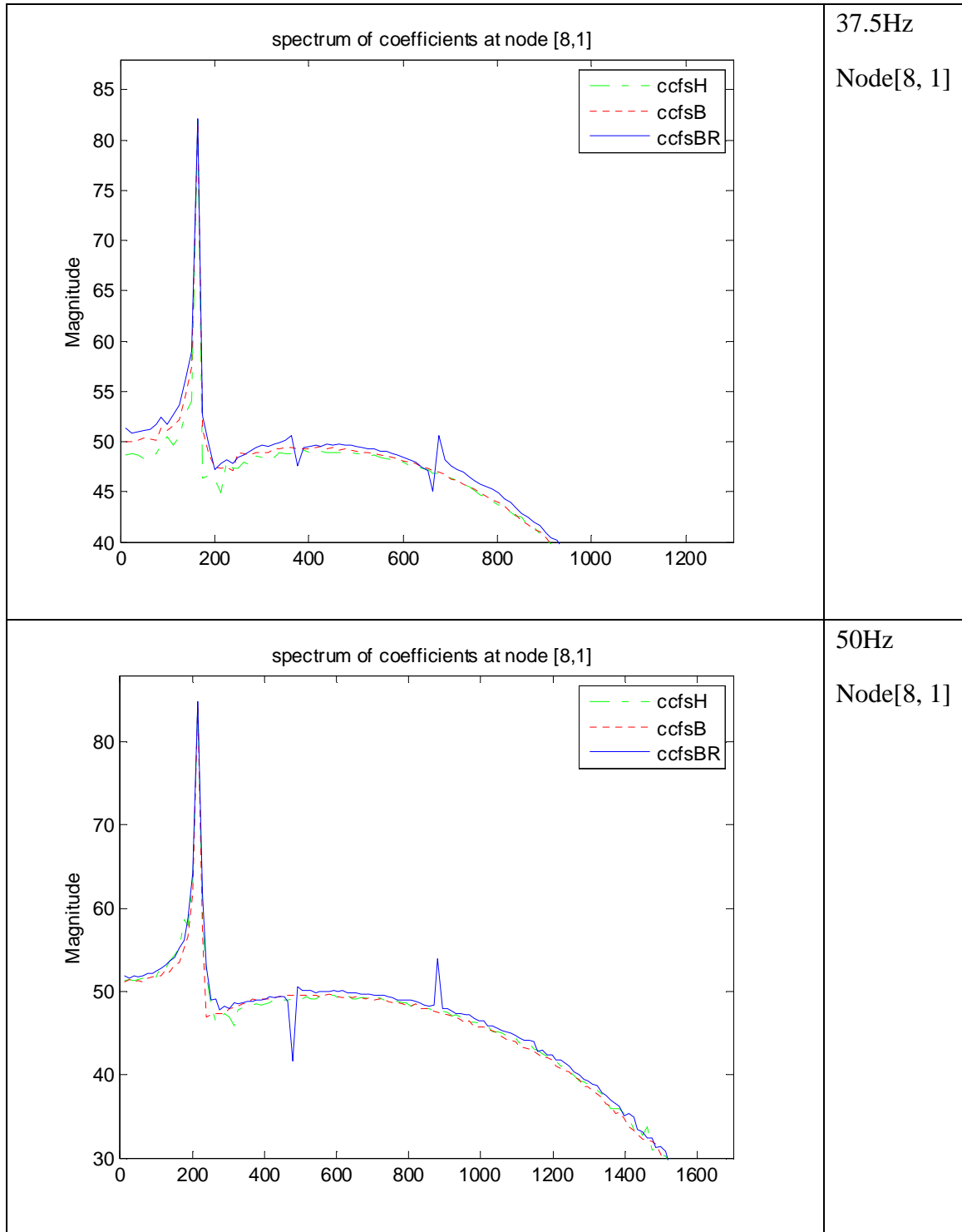
| | 37.5Hz Node[8, 1] |
| | 50Hz Node[8, 1] |

Figure 47 Spectrums of d_8^1 features at different f_s by AWPT

The bearing fault related feature is enhanced by normalization using packet energy

(28). The spectrums of d_8^{48} and $\overline{d_8^{48}}$ of stator current with 31.5Hz inverter frequency

are compared in Figure 48. Indeed, the bearing fault characteristic frequencies at the

predicted positions become more obvious in faulty bearing case after the normalization.

In contrast, as can be seen in Figure 49 , the broken rotor bar related feature d_8^1 in three

cases remains almost the same after normalization except the change of the amplitude

of the whole spectrums.
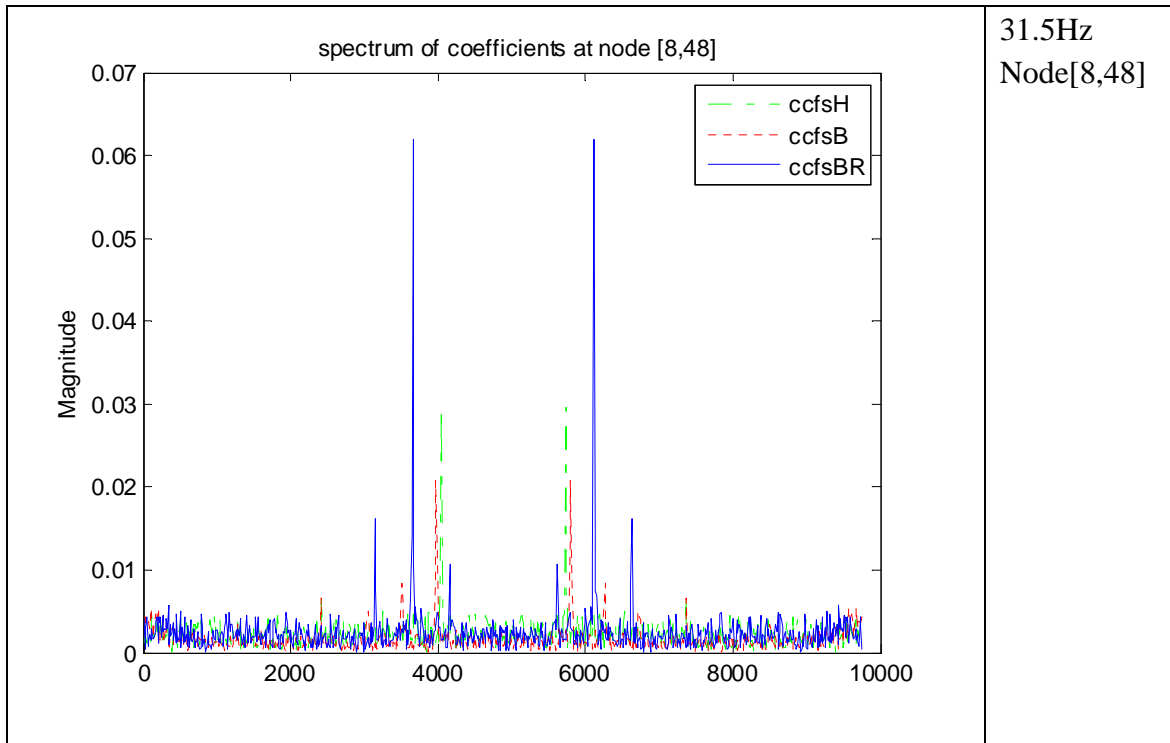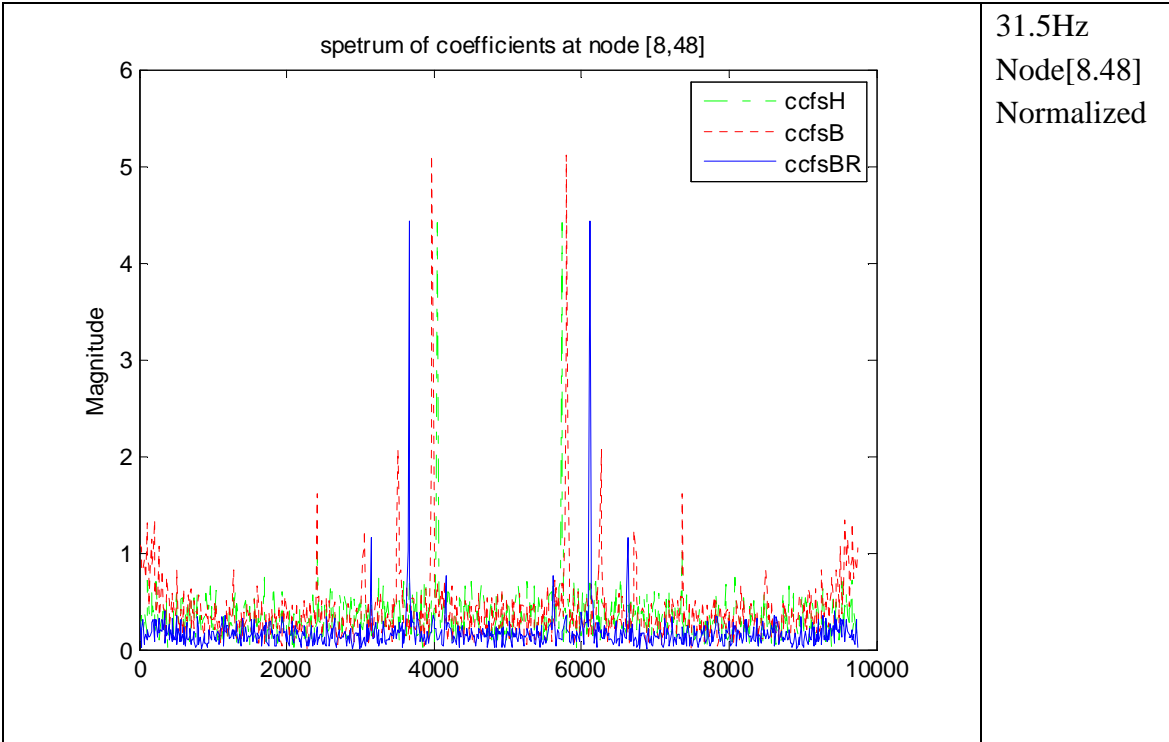
	31.5Hz Node[8,48]

| | 31.5Hz Node[8.48] Normalized |

Figure 48 Spectrums of features d_8^{48} and normalized features $\overline{d_8^{48}}$
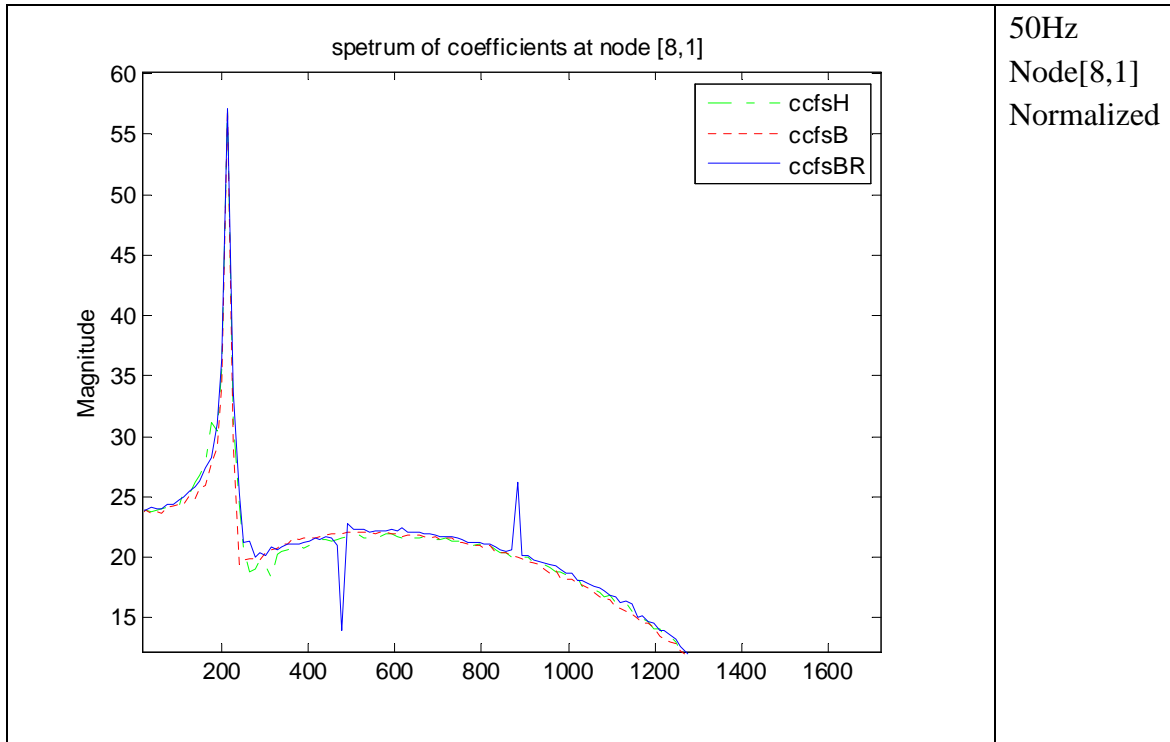
| | 50Hz Node[8,1] |

Figure 49 Spectrums of features d_8^1 and normalized features $\overline{d_8^1}$

5.2.2   Statistic Indices Evaluation
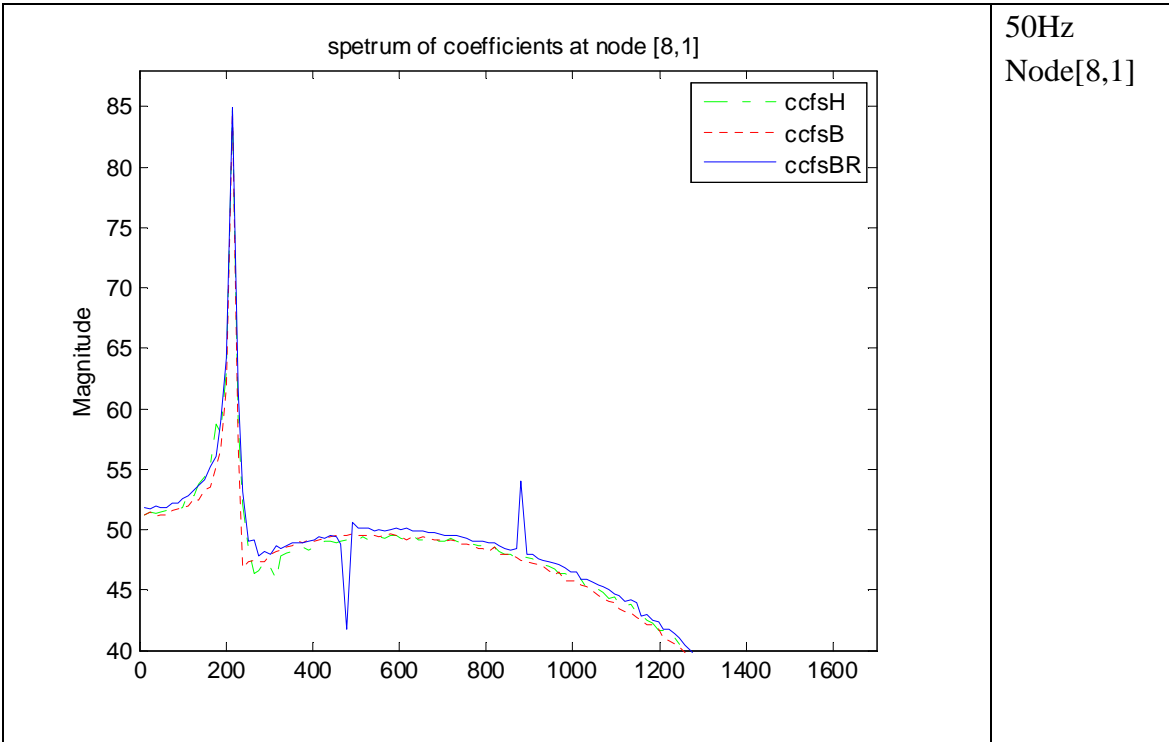
STD and Shannon entropy are applied to quantify the features in node [8,1] and node [8,48] directly after the extraction. Node [8,1] contains broken rotor bar related feature d_8^1 whereas node [8,48] contains bearing fault related feature d_8^{48}. The results are shown in Figure 50 and Figure 51. As can be seen, their interrelationship agrees with the previous predictions. It is also observed that Shannon entropy gives a better separation of data in node [8,48] which is associated with bearing fault feature. As early as in the bearing fault detection in Chapter 5, Shannon entropy has proven its better predictability of fault feature as compared to STD. Hence, from this point on, the Shannon entropy is accepted as a general statistic index in evaluating the features.
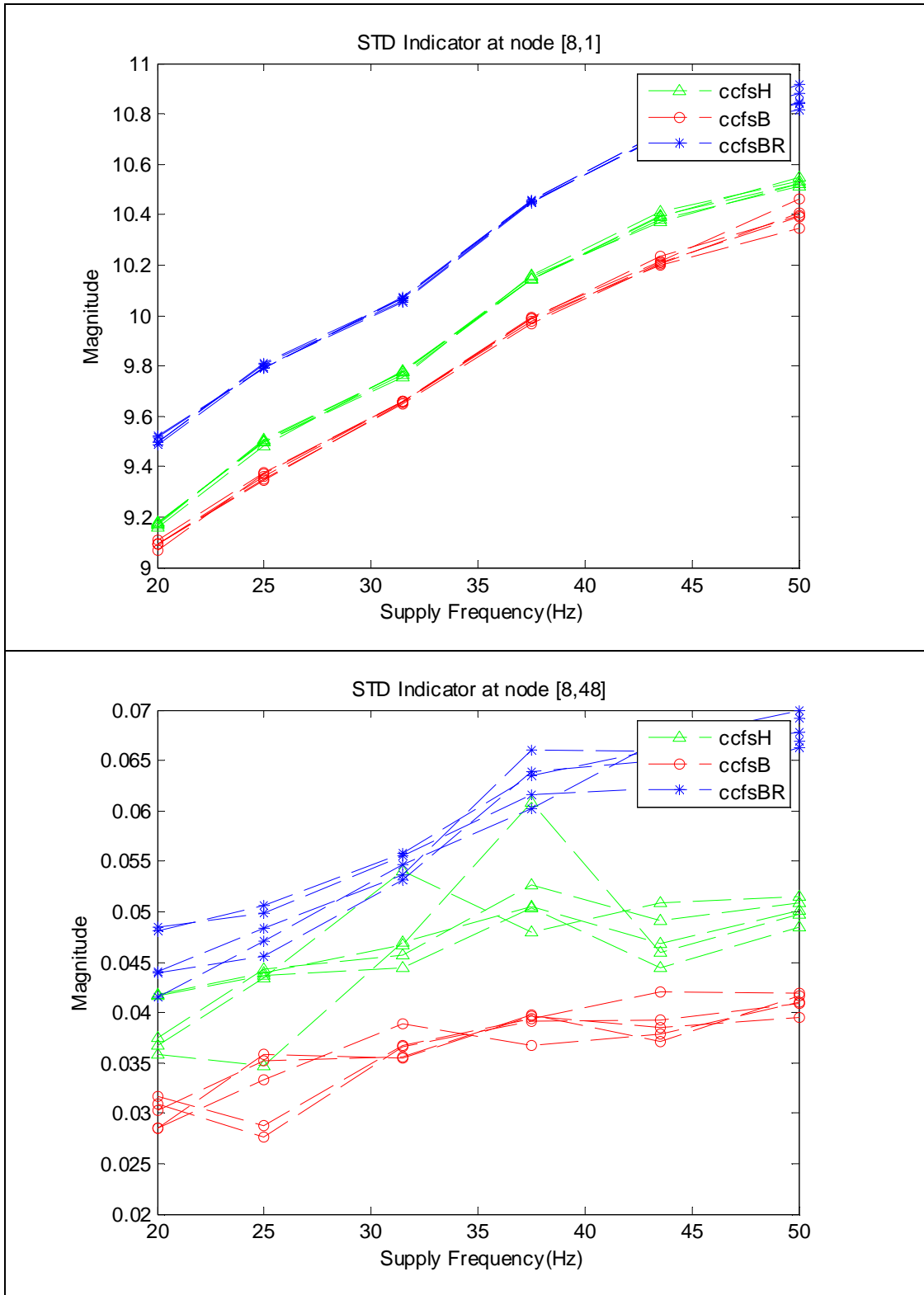
Figure 50 STD index at node [8,1] and node [8,48]
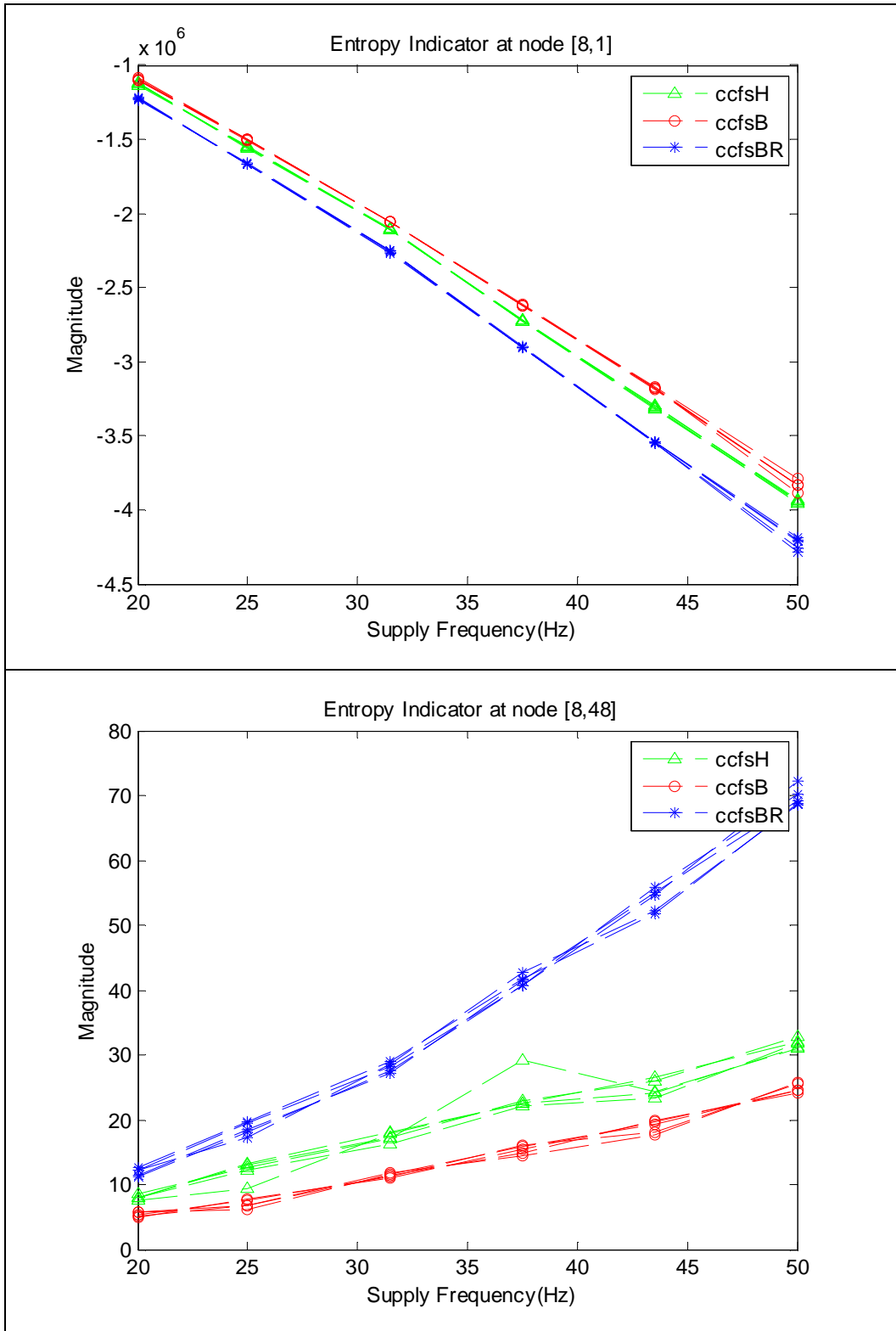
Figure 51 Entropy index at node [8,1] and node [8,48]

The entropy of the normalized feature at node [8,1], denoted by $E\left(\overline{d_8^1}\right)$, measures

the Shannon entropy of feature around the inverter frequency. It is observed in Figure

52 that the $E\left(\overline{d_8^1}\right)$ of broken rotor bar motor is much lower than the ones in both healthy and bearing fault motors. And the relative position is kept nearly constant throughout the different inverter frequencies. This is similar to the result obtained in section 4.2 by ACWT. This observation agrees with the previous prediction and result.
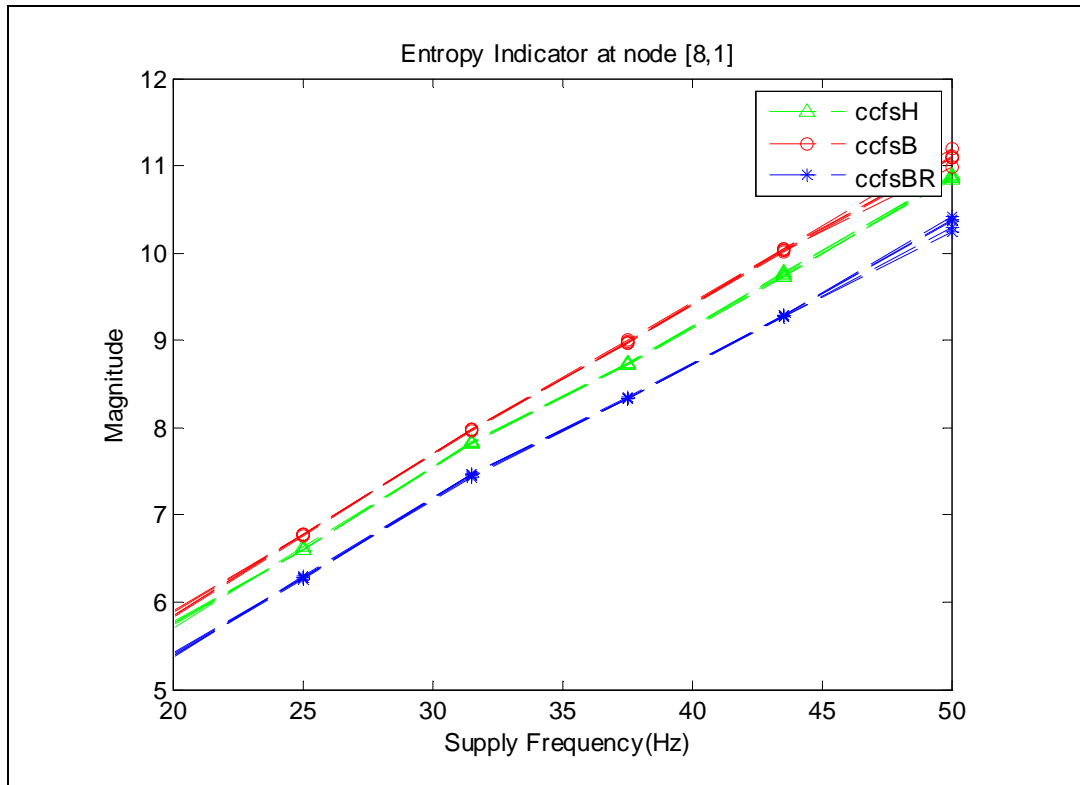
Figure 52 Shannon entropy index at node [8,1]

In addition, the linear relationship between inverter frequency and entropy magnitude is observed in all three cases. After the linear regression, the slope and the offset for three motors are found. It can be deduced that the position of entropy value of broken rotor bar fault becomes further below the healthy motor with the increase of inverter frequency. Thus, the detection accuracy is better for motors in higher operating frequency.

Condition	Healthy	Bearing Fault	Broken Rotor Bar
Slope	0.1697	0.1745	0.1631
Offset	2.3881	2.4189	2.2088

Table 7 Slope and offset after linear regression

The good linear behavior of $E\left(\overline{d_8^1}\right)$ along the inverter frequency and the similar slope between three cases make the compression of feature to one bench mark possible. For the purpose of condition monitoring, the slope of $E\left(\overline{d_8^1}\right)$ of healthy motor, which is obtained in training stage, is used to compress all data to one benchmark, which is the $E\left(\overline{d_8^1}\right)$ of lowest operating frequency of healthy motor (20Hz in this study). The final entropy value of node [8,1] is calculated by equation (29). And the result is shown in Figure 53.

$$\mathbb{E}\left(\overline{d_8^1}, f_s\right) = E\left(\overline{d_8^1}, f_s\right) - \alpha \times (f_s - f_{sl}) \tag{29}$$

Where

f_{sl} is the lowest operating frequency of motor

f_s is the estimated inverter frequency of signal

α is the slope found in training stage of healthy motor
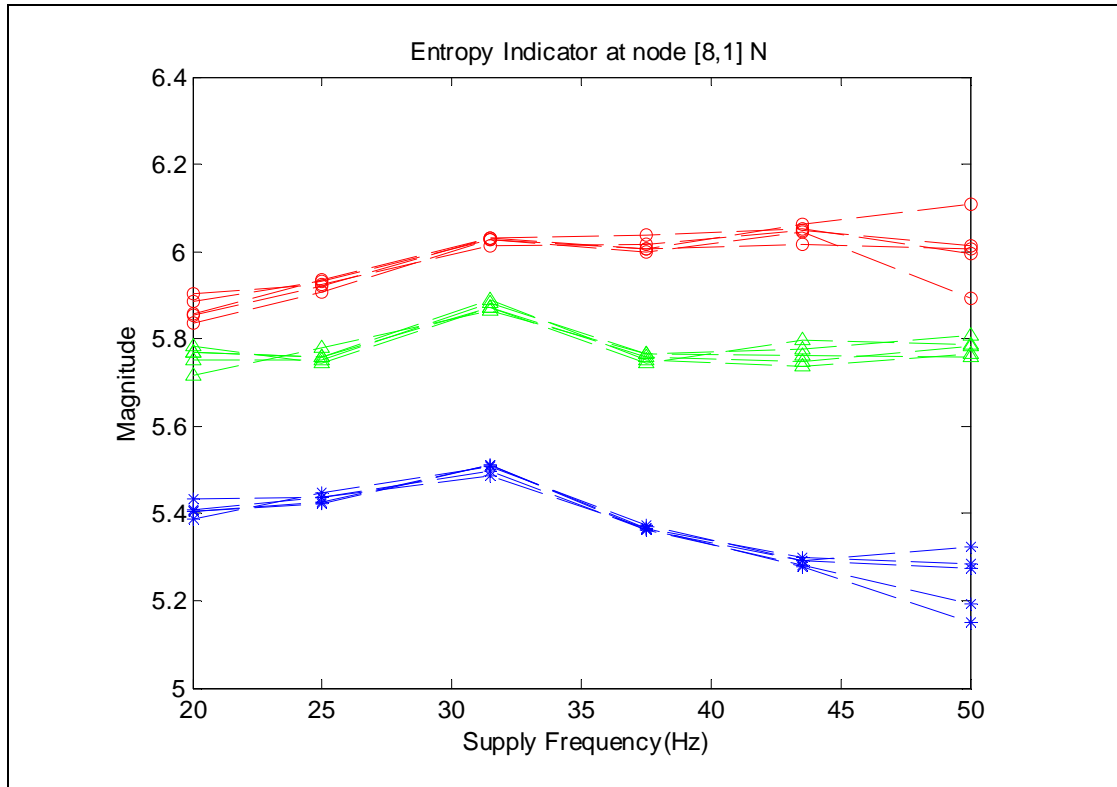
Figure 53 Entropy index at node [8,1] after linear regression

By using only the healthy motor stator current, the baseline can be built to detect broken rotor bar fault, of which the entropy is below the healthy case. The lower the $E\left(\overline{d_8^1}\right)$ the higher the possibility of broken rotor bar fault is. However, the hard threshold is to be established based on experience such as the motor type and working environment. In the scope of the present thesis, the lower boundary of $E\left(\overline{d_8^1}\right)$ in normal conditions after a few measurements is used as the baseline to detect broken rotor bar fault.

Figure 54 shows the entropy of the normalized feature at node [8,48], denoted by $E\left(\overline{d_8^{48}}\right)$, It is observed that $E\left(\overline{d_8^{48}}\right)$ of bearing fault motor is much lower than the ones in both healthy and broken rotor bar motors. This observation is in accord with the previous prediction. Compared with the non-normalized result in Figure 51, the

normalized result has a better consistence of separation distance between three cases at different inverter frequency whereas the separation distance in non-normalized case grows along the inverter frequency.
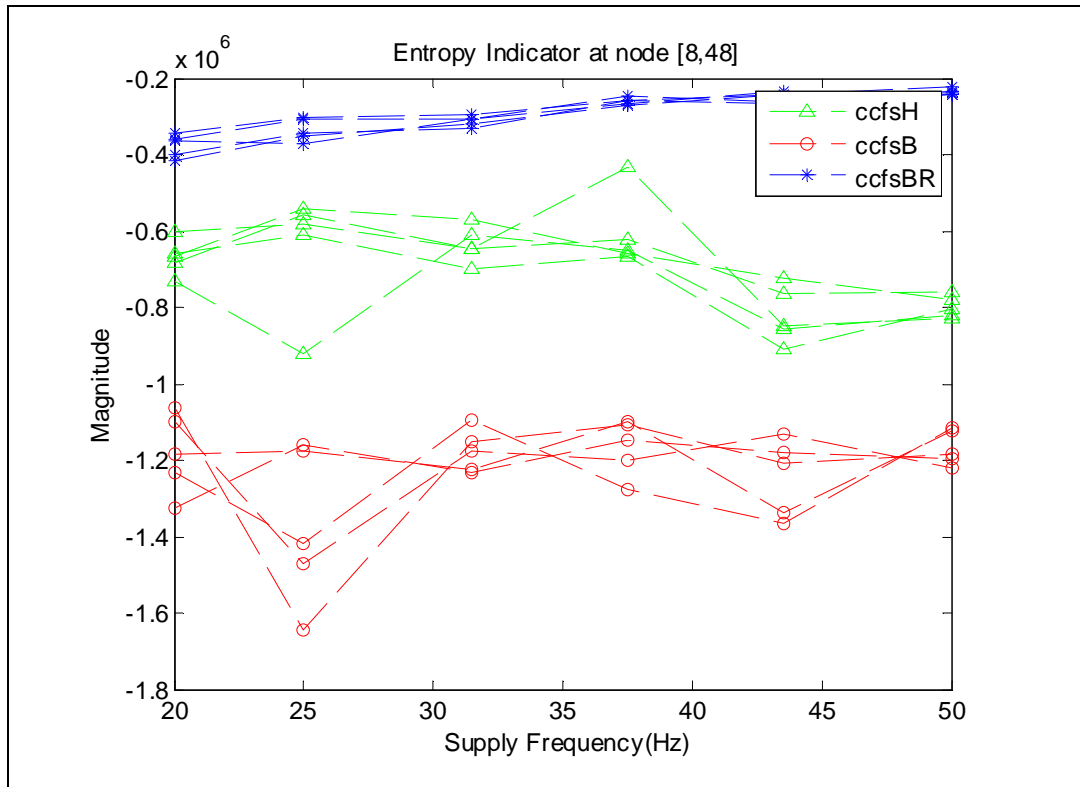
Figure 54 Entropy index at node [8,48] after linear regression

Different from the entropy behavior in node [8,1], the $E\left(\overline{d_8^{48}}\right)$ is relatively constant along the inverter frequency. It can be directly used to compress the bearing fault feature into one dimension. It is also found that in high operating frequency the deviation of entropy between different measurements is smaller than the one in low operating frequency. The smaller $E\left(\overline{d_8^{48}}\right)$ compared the baseline, the higher the possibility of bearing fault is.

5.2.3 Fault Detection Graph

Since each feature can be compressed into one dimension, a two-dimensional fault detection graph can be obtained through integrating these two features as shown in Figure 55. Different from many other researcher's classification methodologies of motor conditions [21][22][30], this graph has determined regions for motor conditions which makes the prediction of specific motor fault from a priori knowledge of healthy condition possible. The principle idea is that many motor faults add characteristic frequency components into stator current, such as broken rotor bar fault and bearing fault. By focusing on specific frequency bands, where relatively prominent components of specific fault reside, the determined fault-related features can be extracted and finally evaluated by statistic index such as Shannon entropy. This fault-related feature always decreases the entropy value as compared with the feature extracted from the same frequency band of the normal operating conditions. In Figure 55, Node [8, 1] focus on the frequency band around inverter frequency while Node [8,48] focus on the frequency band around the position of 9th order characteristic frequency of bearing fault. The training takes normal operating conditions as many as possible. And the lower bounds of the training results in these two nodes are used as boundaries to divide this graph into four regions: healthy region, broken rotor bar region, bearing fault region and other abnormal region, as illustrated in Figure 55. It is predicted that broken rotor bar fault will result in lower entropy in Node [8, 1] as compared to normal operation conditions while bearing fault will result in lower

entropy in Node [8,48]. If a signal's indices are lower in both nodes than normal condition, it implies that extra components existing in the two targeted frequency bands. Hence, an unidentified abnormal condition occurs. In subsequent testing stage, a motor, whose indices fall in one specific region, is diagnosed to be of this specific condition. Finally, a reliable and adaptive motor fault detection is achieved with a priori knowledge of normal operating conditions. In the fault detection graph, different color represents different operating mode. It is observed a good consistence of the results from the same motor but different operating mode. A good separation is also observed for stator currents from different motor conditions which proves the reliability and adaptability of AWPT based on our experimental data.
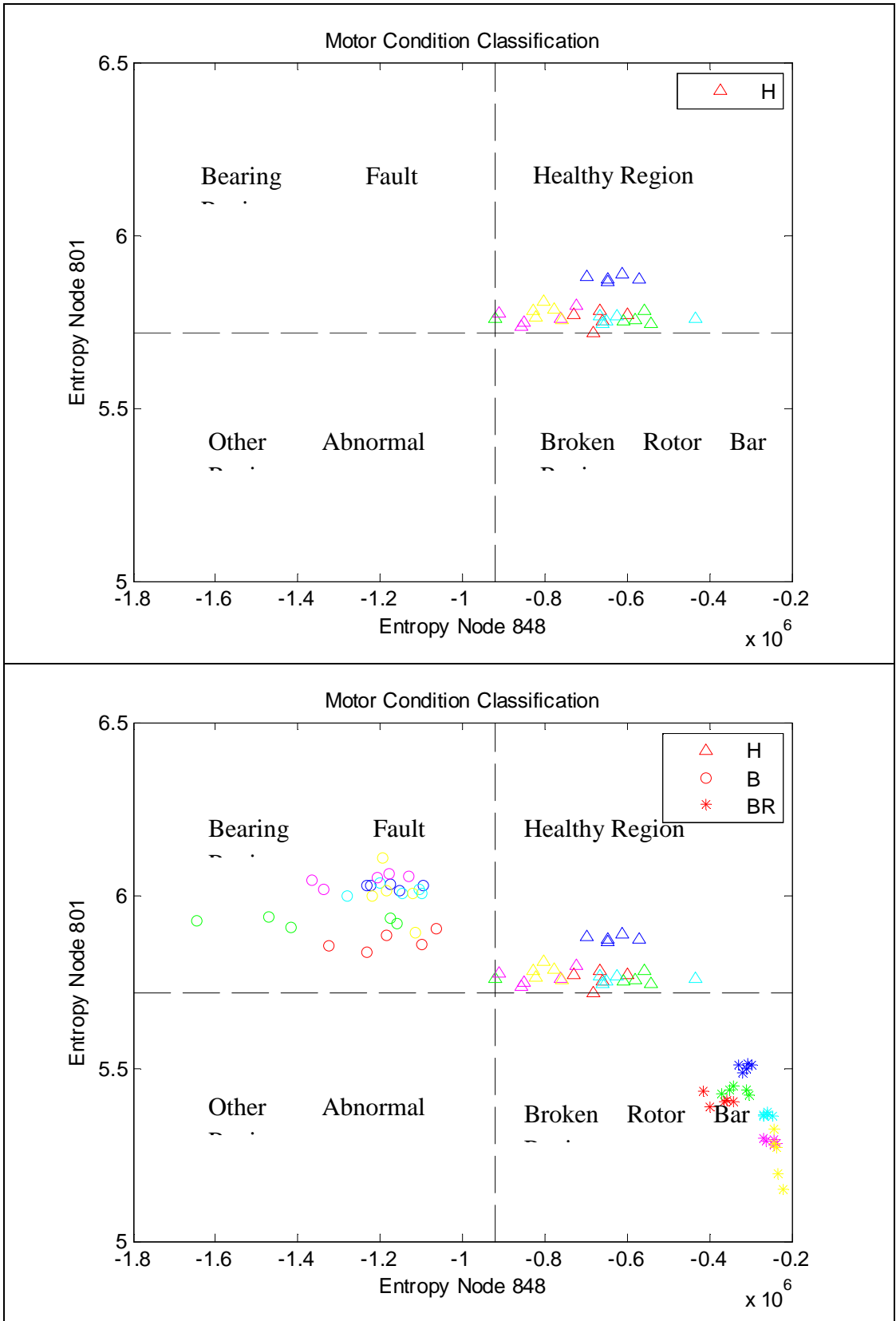
Figure 55 Fault detection graph

Chapter 6

Conclusion

6.1   Outcomes

In the framework of the present thesis, the motor broken rotor bar fault and bearing fault have been studied in details both theoretically and numerically. Based on the investigation of physical natures of the three laboratory motors (one normal, one with broken rotor bar and one with faulty bearing), the stator current features of the faults measured on the laboratory motors have been predicted through the theoretical analysis. By using the real time measurement data of stator current from the laboratory motors, these predictions have been verified numerically. Although the fault-related features can be observed directly on frequency spectrum by FFT, the good feature extraction strategy and quantification method developed in the present thesis surely improve the reliability and provide convenience of fault detection, especially for the purpose of online application. The candidate has proposed two techniques in the present thesis, ACWT and ACPT, to achieve an adaptive feature extraction for motors running under different inverter frequencies. ACWT's capability of reliable detection of broken rotor bar fault under various operation conditions has been verified. Compared with the result based on the method of Short Fourier transform [16], ACWT has demonstrated a better adaptability for various operating conditions. On top of the success of ACWT on broken rotor bar fault detection, ACWT has been further extended its performance for

bearing fault detection. However, ACWT has revealed its weakness in bearing fault detection for two reasons. The features of bearing fault generated on the laboratory motor only appear at certain positions instead of all as predicted in theoretical studies. In addition, the window size of AWCT for bearing fault feature extraction is too large to focus only on determined fault-related features. It includes other unpredictable components from stator current after extraction. Hence, the reliability of ACWT is less-convincing in bearing fault detection. In order to improve on the shortcoming of ACWT, another method named AWPT has been proposed to narrow down the window size of extraction while maintaining the adaptability in various operating modes. Unlike the traditional methods of wavelet packet decomposition, AWPT is able to focus on specific fault features and extract them robustly irrespective of different inverter frequencies.

In terms of feature quantification, several statistic indices have been studied in the thesis. Their capability of quantifying fault features has been demonstrated. After several comparisons and discussions, Shannon entropy has been chosen to be used as a general index for its great predictability of fault features and its consistent performance in different operating conditions.

Finally, the goal of motor fault detection under various operating conditions based on prior knowledge of normal operating condition has been achieved by AWPT with Shannon entropy index. During the training stage, stator currents of normal operating conditions have been collected to build a fault detection graph. The extraction of

broken rotor bar related feature is chosen to be around the inverter frequency while the one of bearing fault related feature is determined based on the number of bearing balls and the motor slip estimated in normal operating condition. Shannon entropy values of these two features from healthy motor are used to define four motor condition regions in the fault detection graph: healthy region, bearing fault region, broken rotor bar fault region and other abnormal region. In the subsequent testing stage, the motor condition has been determined by the region where it falls inside this graph based on its feature values. The experimental result has proved the adaptability and reliability for motor condition monitoring and fault detection of the proposed method.

6.2   Future Work

In the motor fault detection graph, the division of motor condition regions makes use of lower bound of Shannon entropy values of normal operating conditions in each feature. In Figure 55 it is observed that there exists certain deviation of feature locations in different measurements of the same motor. Hence, the use of lower bound of limited measurements may result in misclassification of a normal operating condition into faulty regions. As can be seen, there exist obvious separations between normal conditions and faulty conditions. Thus, it is possible to build in margins to improve the tolerance for errors in measurement. The specific values of the margins are worthy of further study.

In addition, in the present thesis the severity of motor fault has not been

addressed. For example, the broken rotor bar fault is made by drilling a hole on one bar in our experiment. The cases of more broken bars have not yet been established. The interest of studying fault severity is for the better prediction of the transient change of motor condition in real cases in order to achieve early fault detection. Hence, in the future work, more laboratory models are recommended to be built for the study of the severity in each kind of motor faults.

In the present thesis, only broken rotor bar fault and bearing fault have been targeted in motor fault detection under various operating conditions. There is some potential for AWPT to be extended to other types of motor faults in order to become a more generally accepted motor fault technique. Thus, more types of faults are expected to be established on laboratory motors in future research.

References

[1] Siyambalapitiya, D.J.T.; McLaren, P.G.;"Reliability improvement and economic benefits of online monitoring systems for large induction machines," *Industry Applications, IEEE Transactions on* , vol.26, no.6, pp.1018-1025, Nov/Dec 1990

[2] El Hachemi Benbouzid, M.; "A review of induction motors signature analysis as a medium for faults detection," *Industrial Electronics, IEEE Transactions on* , vol.47, no.5, pp.984-993, Oct 2000

[3] Nandi, S.; Toliyat, H.A.; Xiaodong Li; "Condition monitoring and fault diagnosis of electrical motors-a review," *Energy Conversion, IEEE Transactions on* , vol.20, no.4, pp. 719- 729, Dec. 2005

[4] Bikfalvi, P.; Imecs, M.; "Rotor Fault Detection in Induction Machines: Methods and Techniques - State-of-the-Art," *Automation, Quality and Testing, Robotics, 2006 IEEE International Conference on* , vol.1, no., pp.199-204, 25-28 May 2006

[5] Schoen, R.R.; Habetler, T.G.; Kamran, F.; Bartheld, R.G.; "Motor bearing damage detection using stator current monitoring," *Industry Applications Society Annual Meeting, 1994., Conference Record of the 1994 IEEE* , vol., no., pp.110-116 vol.1, 2-6 Oct 1994

[6] Kliman, G. B., "Methods of motor current signature analysis," *Elec. Mach Power Syst* , vol. 20, no. 5, pp.463-474, Sept 1992

[7] Benbouzid, M.E.H.; Vieira, M.; Theys, C.; "Induction motors' faults detection and localization using stator current advanced signal processing techniques," *Power Electronics, IEEE Transactions on* , vol.14, no.1, pp.14-22, Jan 1999

[8] S. Berry, R. Belmans., "How to track rolling element bearing health with vibration signature analysis," Sound and Vibration 25 (11)(1991) 133_/139.

[9] J. R. Cameron, W. T. Thomson, and A. B. Dow, "Vibration and current monitoring for detecting airgap eccentricity in large induction motors," Proc. Inst. Elect. Eng. B, vol. 133, no. 3, pp. 155–163, May 1986.

[10] H. A. Toliyat and T. A. Lipo, "Transient analysis of cage induction machines under stator, rotor bar and end ring faults," IEEE Trans. Energy Convers., vol. 10, no. 2, pp. 241–247, Jun. 1995.

[11] J. Penman and A. Stavrou, "Broken rotor bars: Their effect on the transient performance of induction machines," in Proc. IEEE Electric Power Applications, vol. 143, Nov. 1996, pp. 449–457.

[12] Chen Yiguang; Zhang Hongxia; Shen Yonghuan; "Method of EMD and ZOOM-FFT to detect the broken bars fault in induction motor," *Electrical Machines and Systems (ICEMS), 2010 International Conference on* , vol., no., pp.1387-1391, 10-13 Oct. 2010

[13] Wang Hongxi; Yang Weidong; , "Rotor bar fault feature extraction of induction motor base on FFT and MUSIC," *Mechatronic Science, Electric Engineering and Computer (MEC), 2011 International Conference on* , vol., no., pp.126-129, 19-22 Aug. 2011

[14] A. Menacer, M. S. Nait-Said, A. H. Benakcha, S. Drid, "Stator current analysis of incipient fault into asynchronous motor rotor bars using Fourier Fast Transform," Electrical Engineering, vol. 55, no. 5-6, 2004, 122-130

[15] Boashash, B.,"Time-frequency signal analysis," in Advances in Spectrum Analysis and Array Processing, S. Haykin, Ed. Engelwood Cliffs, NJ: Prentice-Hall, 1990, pp. 418-517

[16] Yazici, B.; Kliman, G.B.; "An adaptive statistical time-frequency method for detection of broken bars and bearing faults in motors using stator current," Industry Applications, IEEE Transactions on , vol.35, no.2, pp.442-452, Mar/Apr 1999

[17] Paul S. Addison, "The Illustrated Wavelet Transform Handbook", *Institute of Physics*, 2002

[18] Zhongming Ye; Bin Wu; Sadeghian, A.; "Current signature analysis of induction motor mechanical faults by wavelet packet decomposition," *Industrial Electronics, IEEE Transactions on* , vol.50, no.6, pp. 1217- 1228, Dec. 2003

[19] Lau, E.C.C.; Ngan, H.W.; "Detection of Motor Bearing Outer Raceway Defect by Wavelet Packet Transformed Motor Current Signature Analysis," *Instrumentation and Measurement, IEEE Transactions on* , vol.59, no.10, pp.2683-2690, Oct. 2010

[20] Eren, L.; Devaney, M.J.; "Bearing damage detection via wavelet packet decomposition of the stator current," *Instrumentation and Measurement, IEEE Transactions on* , vol.53, no.2, pp. 431-436, April 2004

[21] Xin Wen; Brown, D.; Honghai Liu; Qizheng Liao; Shimin Wei; , "Motor Fault Diagnosis Based on Wavelet Energy and Immune Neural Network," *Measuring Technology and Mechatronics Automation, 2009. ICMTMA '09. International Conference on* , vol.2, no., pp.648-652, 11-12 April 2009

[22] Bo Hu; Wen-hua Tao; Bo Cui; Yi-tong Bai; Xu Yin; , "Wavelet neural network based fault diagnosis of asynchronous motor," *Control and Decision Conference, 2009. CCDC '09. Chinese* , vol., no., pp.3260-3263, 17-19 June 2009

[23] Filippetti, F.; Franceschini, G.; Tassoni, C.; Vas, P.; , "AI techniques in induction machines diagnosis including the speed ripple effect," *Industry Applications Conference, 1996. Thirty-First IAS Annual Meeting, IAS '96., Conference Record of the 1996 IEEE* , vol.1, no., pp.655-662 vol.1, 6-10 Oct 1996

[24] Hirvonen, R.,"On-line condition monitoring of defects in squirrel cage motors," *in Proc. 1994 Int. Conf. Electrical Machines,* vol. 2, Paris, France, pp.267-272"

[25] ___, "Report of Large Motor Reliability Survey of Industrial and Commercial Installations, Part I," *Industry Applications, IEEE Transactions on* , vol.IA-21, no.4, pp.853-864, July 1985

[26] Blodt, M.; Granjon, P.; Raison, B.; Rostaing, G.; "Models for Bearing Damage Detection in Induction Motor Using Stator Current Monitoring," *Industrial Electronics, IEEE Transactions on,* vol.55, no.4, April. 2008

[27] Gray, R.M., "Entropy and Information Theory", *Springer-Verlag,* 1991

[28] Coifman, R.R.; M.V. Wickerhauser (1992), "Entropy-based Algorithms for best basis selection," IEEE Trans. on Inf. Theory, vol. 38, 2, pp. 713-718.

[29] Vetterli, M.; Herley, C.; , "Wavelets and filter banks: theory and design," *Signal Processing, IEEE Transactions on* , vol.40, no.9, pp.2207-2232, Sep 1992

[30] Cao Zhitong; Fang Jiazhong; Chen Hongpingn; He Guoguang; Ritchie, E.; , "Support vector machine used to diagnose the fault of rotor broken bars of induction motors," *Electrical Machines and Systems, 2003. ICEMS 2003. Sixth International Conference on* , vol.2, no., pp. 891- 894 vol.2, 9-11 Nov. 2003

Appendix A

Parameters for Induction Motor

Power	1.1kW
Voltage	230/400V
Current	4.5/2.6A
Frequency	50Hz
Speed	1410rpm
Pole	2

Annotation for Data "090407Healthy_load10_Inverter"

Inverter Frequency	Voltage(V)	Current(A)	Angular Speed(rpm)
20Hz	39.00	1.787	585
25Hz	48.81	2.238	732
31.5Hz	61.86	2.837	922
37.5Hz	73.92	3.391	1099
43.5Hz	85.82	3.938	1275
50Hz	98.46	4.517	1465

Annotation for Data "090407BrokenBar_Inverter_load10"

Inverter Frequency	Voltage(V)	Current(A)	Angular Speed(rpm)
20Hz	39.20	1.800	582
25Hz	49.10	2.254	729
31.5Hz	62.20	2.850	920
37.5Hz	74.05	3.400	1094
43.5Hz	86.20	3.900	1271
50Hz	99.05	4.550	1461

Annotation for Data "090408Bearing_load10_Inverter"

Inverter Frequency	Voltage(V)	Current(A)	Angular Speed(rpm)
20Hz	39.26	1.800	584
25Hz	49.37	2.265	731
31.5Hz	62.42	2.860	922
37.5Hz	74.38	3.410	1098
43.5Hz	86.45	3.960	1274
50Hz	99.92	4.590	1464

Calculation of load

$$Load = \frac{S_s - S_m}{S_s - S_r} \times 100\%$$
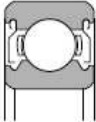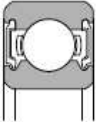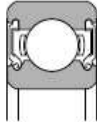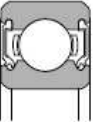
Where:

  Load   Output power as a % of rated power

  Sm   Measured speed in rpm

  Ss   Synchronous speed in rpm

  Sr   Nameplate full-load speed

Appendix B

1. Bearing Design and Features, Seal/Shield Bearing Types and Selection

Table 1 Bearing design and futures

Type, code no.		Shield type	Seal type		
		Non-contact type ZZ	Non-contact type LLB	Contact type LLU	Low torque type LLH
Construction		• Metal shield plate is affixed to outside ring; inner ring incorporates a V-groove and labyrinth clearance.	• Outer ring incorporates synthetic rubber molded to a steel plate; seal edge is aligned with V-groove along inner ring surface with labyrinth clearance.	• Outer ring incorporates synthetic rubber molded to a steel plate; seal edge contacts V-groove along inner ring surface.	• Basic construction the same as LU type, but specially designed lip on edge of seal prevents penetration by foreign matter; low torque construction.
Performance comparison	Torque	Very Low	Very Low	Medium	Low
	Dust proofing	Good	Very Good	Best	Excellent
	Water proofing	Poor	Poor	Very good	Good
	High speed capacity	Same as open type	Same as open type	Limited by contact seals	Better than LLU-type
	Allowable temp.range ❶	Depends on lubricant	-25 ℃～120 ℃	-25 ℃～110 ℃	-25 ℃～120 ℃

❶ Please consult **NTN** Engineering about applications which exceed the allowable temperature range of products listed on this table.
Note : This chart lists double shielded and double sealed bearings, but single shielded (Z) and single sealed (LB, LU, LH) are also available.
Grease lubrication should be used with single shielded and single sealed bearings.